Photocatalytic Efficiency of Nanocrystalline TiO_2 Doped with Additives

Kornkanok Uboncholakat

A Thesis Submitted in Partial Fulfillment of the Requirements for the Degree of

Master of Engineering in Materials Engineering

Prince of Songkla University

2008

Thesis Title Photocatalytic Efficiency of Nanocrystalline TiO_2 Doped with Additives

Author Miss Kornkanok Ubonchonlakat

Major Program Materials Engineering

Major Advisor

……..

(Assoc. Prof. Dr. Lek Sikong)

Co-advisor

……..

(Assoc. Prof. Kalayanee Kooptarnond)

…….....

(Assoc. Prof. Dr. Sumpun Wongnawa)

Examining Committee

……..…….....Chairperson

(Assist. Prof. Dr. Sutham Niyomwas)

……..……..…… Committee

(Assoc. Prof. Dr. Lek Sikong)

…… Committee

(Assoc. Prof. Kalayanee Kooptarnond)

…… Committee

(Assoc. Prof. Dr. Sumpun Wongnawa)

…… Committee

(Dr. Anob Kantacha)

The Graduate School, Prince of Songkla University, has approved this as partial fulfillment of the requirements for the Master of Engineering Degree in Materials Engineering

……

(Assoc. Prof. Dr. Krerkchai Thongnoo)

Dean of Graduate School

Thesis Title	Photocatalytic Efficiency of Nanocrystalline TiO_2 Doped with Additives
Author	Miss Kornkanok Ubonchonlakat
Major Program	Materials Engineering
Acaemic Year	2007

ABSTRACT

The aim of this research is to investigate the influene of calcinations temperature and dopants (Ag and MWNTs) on the phase transformation of TiO_2, crystallite size, specific surface area, absorbed wavelength of light, band gap energy, photocatalytic reaction and hydrophilic property. Pure TiO_2 and TiO_2 composite powders and films were prepared by sol-gel method. The films were coated on ceramic tile substrate by a spin coater. The synthesized products were characterized by XRD, SEM, DTA, EDS, FT-IR, BET and AFM. The photocatalytic activities of thin films were carried out by means of the degradation of methylene blue solution with 49 cm^2 film surface area irradiated by UV light of 4.77 mW/ cm^2 intensity. The hydrophilic property of the film was also investigated in terms of a contact angle of water droplet on the film surface under UV or fluorescent light irradiation. The results show that both calcinations temperature and Ag or MWNTs dopant have an influence on phase transformation of TiO_2, crystallite size, specific surface area, absorbed wavelength of light, band gap energy, photocatalytic reaction and hydrophilic property of the TiO_2 catalysts. Calcination at the temperature of 500^oC seems to give the high degree of crystallinity of anatase phase with the smallest crystallite size and the highest specific surface area resulting in the highest rate of photocatalytic reaction and super hydrophilic property. The more amounts of Ag or MWNTs doped leads to shift the absorbed wavelength to be longer and band gap energy to be narrower.

The photocatalytic reaction of the film may be expressed as an exponential rate equation of $R = 1.00\ e^{-kt}$. It was found that the photocatalytic efficiency of the films can be ranked as $1Ag/TiO_2$ > $1Ag/1MWNTs/TiO_2$ > pure TiO_2 ≥ $1MWNTs/TiO_2$. The contact angles of $1Ag/TiO_2$, $1MWNTs/TiO_2$ and $1Ag/1MWNTs/TiO_2$ films were found to be zero degrees leading to super hydrophilicity after irradiation by UV light for 15 minutes and less than 10 degree after irradiation by fluorescent light for 15 minutes.

ชื่อวิทยานิพนธ์ ประสิทธิภาพปฏิกิริยาโฟโตคะตะไลติกของไทเทเนียมไดออกไซด์ที่โด๊ปด้วยสารเติม

ผู้เขียน นางสาว กรกนก อุบลชลเขต

สาขาวิชา วิศวกรรมวัสดุ

ปีการศึกษา 2550

บทคัดย่อ

จุดมุ่งหมายของงานวิจัยนี้คือ การศึกษาอิทธิพลของอุณหภูมิแคลไซเนชันและสารโด๊ป (Ag และ MWNTs) ต่อสมบัติการเปลี่ยนเฟสของไทเทเนียมไดออกไซด์ ขนาดผลึก พื้นที่ผิวจำเพาะ ความยาวคลื่นแสงที่ดูดซับ ช่องว่างพลังงาน ปฏิกิริยาโฟโตคะตะไลติก และสมบัติไฮโดรฟิลิก อนุภาคผงและฟิล์มของไทเทเนียมไดออกไซด์บริสุทธิ์ และไทเทเนียมไดออกไซด์ที่โด๊ปด้วยสาร เตรียมโดยวิธีโซล-เจล ฟิล์มจะถูกเคลือบไปบนผิวของกระเบื้องเซรามิกซ์ด้วยเครื่องเคลือบแบบหมุนปั่น การตรวจคุณลักษณะเฉพาะของสารสังเคราะห์จะตรวจสอบด้วยเทคนิค XRD, SEM, DTA, EDS, FT-IR, BET และ AFM ศึกษาปฏิกิริยาโฟโตคะตะไลติก ในการสลายสารเมทิลลีนบลูโดยใช้พื้นที่ผิว 49 ตารางเซนติเมตร ภายใต้ความเข้มของรังสียูวี 4.77 มิลลิวัตต์ต่อตารางเซนติเมตร นอกจากนี้สมบัติไฮโดรฟิลิกของฟิล์มยังถูกศึกษาในเทอมของค่ามุมสัมผัสของหยดน้ำบนฟิล์ม ที่มีการฉายยูวี หรือฟลูออเรสเซนต์เป็นเวลาต่างๆ

จากผลการศึกษาพบว่าทั้งอุณหภูมิแคลไซเนชันและสารโด๊ป Ag หรือ MWNTs มีอิทธิพลต่อสมบัติการเปลี่ยนเฟส ขนาดผลึก พื้นที่ผิวจำเพาะ ความยาวคลื่นแสงที่ดูดซับ ช่องว่างของพลังงาน ปฏิกิริยาโฟโตคะตะไลติก และสมบัติ ไฮโดรฟิลิก ของฟิล์ม ไทเทเนียมไดออกไซด์ การแคลไซเนชันที่อุณหภูมิ 500 องศาเซลเซียส ดูเหมือนว่าจะทำให้ได้เฟสอนาเทสที่มีความเป็นผลึกสูง มีขนาดผลึกเล็กที่สุด และมีพื้นที่ผิวมากที่สุดซึ่งจะส่งผลทำให้อัตราการเกิด ปฏิกิริยาโฟโตคะตะไลติกมีค่าสูงสุด และเป็นฟิล์มที่มีสมบัติเป็นซูปเปอร์ ไฮโดรฟิลิก ปริมาณของ Ag หรือ MWNTs ที่มากขึ้นทำให้ดูดซับความยาวคลื่นแสงที่ยาวขึ้น และทำให้ช่องว่างของพลังงานแคบลง

อัตราการเกิดปฏิกิริยาโฟโตคะตะไลติกของฟิล์มไทเทเนียมไดออกไซด์อาจแสดงด้วยสมการเอ็กโพเนเชียลดังนี้ $R = 1.00\ e^{-kt}$ ประสิทธิภาพของไทเทเนียมไดออกไซด์ของฟิล์มสามารถเรียงจากสูงไปต่ำดังนี้ $1Ag/TiO_2 > 1Ag/1MWNTs/TiO_2 >$ pure $TiO_2 \geq 1MWNTs/TiO_2$ ค่ามุมสัมผัสของฟิล์ม $1Ag/TiO_2$, $1MWNTs/TiO_2$ และ $1Ag/1MWNTs/TiO_2$ มีค่าเป็นศูนย์องศา ซึ่งจะแสดงถึงสมบัติซูปเปอร์ไฮโดรฟิลิก หลังจากฉายยูวีเป็นเวลา 15 นาที ในขณะที่มีค่าต่ำกว่า 10 องศา เมื่ออยู่ภายใต้แสงฟลูออเรสเซนต์เป็นเวลา 15 นาที

ACKNOWLEDGEMENTS

The author would like to express greatest gratitude to her advisor, Associate Professor Dr. Lek Sikong and co-advisor, Associate Professor, Kalyanee Kooptarnond and Associate Professor Dr. Sumpun Wongnawa for their invaluable suggestions in this study.

The author would like to thank NANOTEC Center of Excellence at Prince of Songkla University and National Research Council of Thailand (NRCT) and the Department of Mining and Materials Engineering, Faculty of Engineering, Prince of Songkla University for their financial support.

The author also would like to thank my parents and my friends for their encouragement.

Kornkanok Uboncholakat

CONTENTS

Subject **Page**

LIST OF TABLE

LIST OF FIGURES

LIST OF ABBREVIATIONS AND SYMBOLS

A	Anatase phase
Å	Angstrom
Ag	Silver
Am	Amorphous phase
BET	Surface area/pore size measurement
c	velocity of light (3×10^8 m/s)
C	The concentration of methylene blue after treatment for t hours
C_0	Initial concentration of methylene blue
DTA	Differential thermal analyzer
e-	Electron
E_g	Energy band gap
EDS	Energy dispersive x-ray spectroscopy
FT-IR	Fourier-transformed infrared spectrophotometer
h	Plank's constant (6.67×10^{-34} j.s.)
h	Hour
h^+	Hole
k	kinetics rate constant (h^{-1})
MWNTs	Multi walled carbon nanotube
nm	Nanometer (10^{-9} m)
R	Rutile phase
SEM	Scanning electron microscope
TiO_2	Titanium dioxide
XRD	X-ray diffraction
Z	Zircon
λ	Wavelength

CHAPTER 1

Introduction

1.1 Introduction

Titanium dioxide (TiO_2) is an excellent photocatalyst. It is widely used as a photocatalyst because it is relatively highly efficient, cheap, non-toxic, chemically and biologically inert and photo stable.

In recent year, titanium dioxide photocatalysis has been used for the treatment of waste water, sterilization/antimicrobial, water splitting, solar energy application, self-cleaning, and environmental applications. These are three froms of TiO_2 sush as anatase (E_g~3.23eV), brookite and rutile (E_g~3.02eV). The crystal structures of anatase, brookite and rutile are tetragonal, orthorhombic and tetragonal, respectively (Wells, 1975). The major phases used as photocatalyst are anatase and rutile. Brookite phase can not be used in industry because its instability at room temperature (Kim and Chung, 2001).

TiO_2 in the anatase phase has been used as an excellent photocatalyst for photodecomposition and solar energy conversion due to its high photoactivity. Rutile phase has lower band gap energy than the anatase phase affected to the recombination of activated electron from conduction band to valance band. However in a room illuminated by visible or fluorescent light, the photocatalytic activity of rutile phase seems to be better than anatase phase because rutile phase has a lower band gap energy than that of the anatase phase so that electron from valence band is easily to be exited to conduction band (Tsuji et al., 2003) as shown in Figure 1.1. Generally, in other cases, an anatase/rutile mixture demonstrates better photocatalytic activity than it does in single phase (Tanaka and Mario, 1991). Other factors, such as preparation process, crystallite size and anatase–rutile ratio seem to have an effect on the activities. The effective way to improve the TiO_2 photocatalytic activities is to introduce metal ions into TiO_2 (Sonawane and Dongare, 2006) because it produce to a large surface area and prevent the electron-hole pairs to recombine rapidly after excitation. Many works introduced ions or compounds, such as V^{5+} (Hou et al., 2005), Se^{2+} (Nguyen et al., 2005), N^{5+} (Shifu et al., 2005), Pt^{4+} (Zhang et al., 2005), Fe^{3+} (Yu

et al., 2006), C (Li et al., 2005), ZnS (Xiaodan et al., 2006) and Ag^{1+} (Liu et al., 2003) etc., into TiO_2.

Normally, TiO_2 powders are used for wastewater treatment in industry but the separation and removal of TiO_2 powders from water are difficult. Several previous researches have shown that TiO_2 film was coated on many kinds of substrates such as glass, (Sonawane Dongare, 2006) stainless steel(Wu et al., 2006) and polymer in order to recycle them more easily. (Langlet et al., 2003)

Although in Japan and United States of America, TiO_2 are widely used for many applications with a rapid growth rate, there are few researches on TiO_2 in Thailand. In order to strengthen the knowledge of TiO_2 photocatalysis, Thai researchers should play attention on this issue. Many paper suggested that the photocatalytic efficiency can be improved by doping with additives such as metal or non-metal ions. Among the additives used for enhancing photocatalytic activity Ag seems to be the most challenge as well as MWNTs. Therefore, the aim of this study is to investigate the effect of calcinations temperature and dopants i.e. Ag and MWNTs on the photocatalytic efficiency and hydrophilic property of the composite films. Pure TiO_2, Ag/TiO_2, $MWNTs/TiO_2$, and $Ag/MWNTs/TiO_2$ powders and also the thin films were prepared by sol-gel method and coated on ceramic tile substrates by spin coating process.

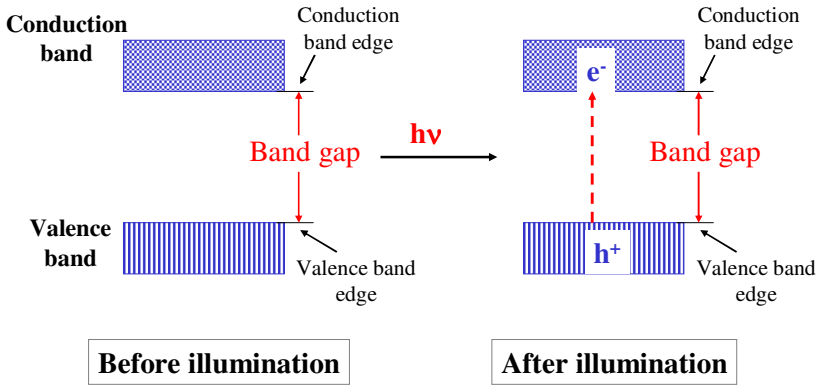

Figure 1.1 Photocatalyst mechanism (www.export-japan.com)

1.2 Objectives

Objectives of the research are the following,

1. To study the effect of time, wave length and calcinations temperature on morphology and crystal structure of titanium dioxide.
2. To study the effect of Ag and MWNTs doping into titanium dioxide on the photocatalytic efficiency and hydrophilic property.

1.3 Scope of research work

Pure TiO_2, Ag/TiO_2, $MWNTs/TiO_2$, and $Ag/MWNTs/TiO_2$ powders and thin films were prepared by sol-gel method. The xerogel of TiO_2 and TiO_2 composite were coated on ceramic tile substrate by a spin coater with the speed of 1500 rpm. The calcinations temperature was varied as 400 ^{o}C-800^{o}C for making powders and 400 ^{o}C-600 ^{o}C for making films. Amount of Ag and MWNTs additives were in range of 0.5-5 mol%Ag and 0.1-1 wt%MWNTs respectively.

CHAPTER 2

Theory and Literature Review

2.1 Physical and Chemical Properties of Titanium Dioxide

Titanium (Ti) is chemical elements in the periodic table which has an atomic number "22" and 47.9 g/mol atomic weight. Titanium occurs in many forms naturally such as ilmenite(Fe TiO_2), rutile (tetragonal TiO_2), anatase (tetragonal TiO_2), brookite (rhombic TiO_2), perovskite ($CaTiO_3$), sphene ($CaTiSiO_5$) and geikielite ($MgTiO_3$). TiO_2 has high tensile strength, light weight and high corrosion resistance. Properties of titanium are shown in Table 2.1.

Titanium dioxide is a semiconductor and primarily occurs in three phases anatase, brookite and rutile. All these three crystal structures are built up of TiO_6 octahedral but in different ways. In rutile (tetragonal), two opposing edges of each octahedron are shared to form linear chains along the [0 0 1] direction, and the TiO_6 chains are linked to each other via corner connection. Anatase has no corner sharing but has four edges shared per octahedron. The crystal structure of anatase (tetragonal) can be viewed as zigzag chains of the octahedra linked together through the edge sharing. On the other hand, the octahedral shares both edges and corners and forms an orthorhombic structure of brookite. Anatase and brookite are thermodynamically metastable with respect to rutile, and anatase, brookite and rutile have the density of 3.90, 4.13 and 4.27 g/cm^3, respectively. (Li and Ishigaki, 2004). Further property and structural data of three TiO_2 forms are shown in Table 2.2. and Figure 2.1, respectively.

Among the three difference structures, brookite phase can not be used in the industry because of its instability at room temperature. The anatase phase has high photocatalytic and photo stability. It has advantages for photocatalytic materials such as purification environments; water purification, air purification, degradation of organic compound and killing bacteria. The rutile phase can be used as outdoor pigment because of its well light resistance and high reflective index. Also the most important function of titanium dioxide powder is for providing whiteness products such as paints, plastics, paper, ink, fibers, food and cosmetics (Siddiguey et al. 2008).

Table2.1 Properties of titanium (Clark, 1968, Kirk and Othmer, 1985)

Property	Value
Melting point, °C	1668±5
Boiling point, °C	3260
Density, g/cm^3	
α phase at 20 °C	4.507
β phase at 885 °C	4.35
Thermal conductivity at 25 °C, W/(m·K)	21.9
Electrical resistivity at 20 °C, nΩ·m	420
Magnetic susceptibility, mks	180 x 10^{-6}
Modulus of elasticity, GPa	
Tension	*Ca.* 101
Compression	103
Shear	44
Metallic radius (Å)	1.47
Entropy S° 298 (cal/deg/mol)	7.33
E° (M^{2+} /M) volts, 25 °C	-1.63
E° (M^{3+} /M^{2+}) volts, 25 °C	-0.37
Heat of atomization (kcal/g·atom)	112.6

Table 2.2. Properties of the three phases of titanium dioxide

	Anatase	Brookite	Rutile
Density (g/cm^3)	3.90	4.13	4.27
Hardness (Mohs'scale)	5.5-6.0	5.5-6.0	6.0-6.5
Melting Point (°C)	Change to rutile	Change to rutile	1,840±10
Entropy $S^o_{298.16}$ (cal/deg/m)	11.93	-	12.01
Refractive Index	n_ω 2.5612	n_α 2.5831	n_ω 2.6124
(25 °C) (λ = 5893 Å)	n_ε 2.4880	n_β 2.5843	n_ε 2.8993
		n_γ 2.7004	
Dielectric Constant	ε = 48	ε = 78	ε_{av}≈110
	(powder)		ε_{II} = 180
			at 3x10^5 c/s 25 °C
			$\varepsilon_\perp$ = 89
			at 3x10^5 c/s 25 °C

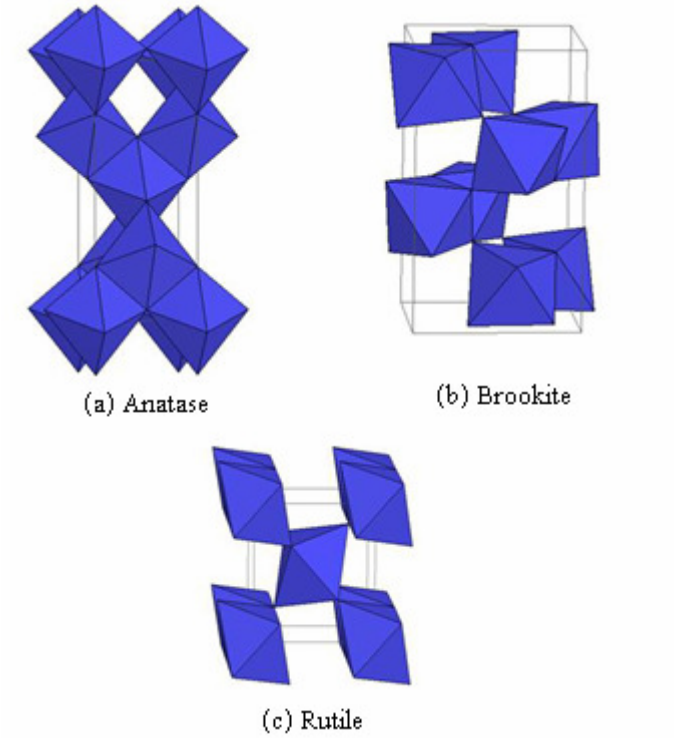

Figure2.1 Three crystal structures of titanium dioxide; (a) anatase, (b) brookite and (c) rutile. (http://ruby.cororado.edu)

Titanium dioxide can be synthesized by various processes such as precipitation (Kim et al. 1999), chemical vapor deposition (Ding et al., 2000), hydrothermal method (Yang et al., 2001), glycothermal method (Iwamoto et al., 2000) and metal-organic chemical vapor deposition (MOCVD) (Kuo et al., 2007). Another common technique that can result in extremely high surface area is sol-gel method (Rengaraj and Li, 2006). Usually, titanium dioxide powder prepared from commercial inorganic compounds such as titanium isopropoxide(TIPP), titanium tetrachloride ($TiCl_4$) and titanium disulfate ($Ti(SO_4)_2$)(Hu et al., 2003; Hsing and Lin, 2006).

2.2 Sol-Gel Process

The sol-gel process is a wet-chemical technique for the fabrication of materials (typically a metal oxide) starting from a chemical solution containing colloidal precursors (sol). Typical precursors are metal alkoxides and metal chlorides, which undergo hydrolysis and polycondensation reactions to form a colloid, a system composed of solid particles (size ranging

from 1 nm to 1 μm) suspened in a solvent. The sol evolves then towards the formation of an inorganic network containing a liquid phase (gel) shown in Figure 2.2 (Michael, 2006).

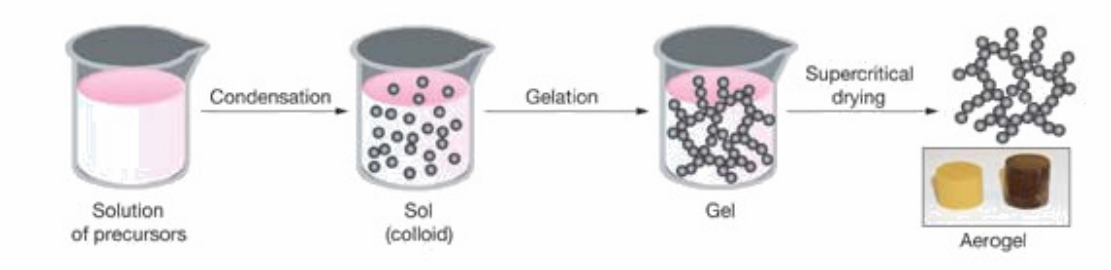

Figure2.2 The sol-gel principle (www.cmls.llnl.gov)

The reaction in sol-gel processes has three reactions which are hydrolysis, water condensation and alcohol condensation as shown in the equation below. Several important factors have effect on the reaction of sol-gel processes such as pH, ratio of water and metal, catalyst, and temperature.

Hydrolysis:	$M\text{-}O\text{-}R + H_2O \rightarrow M\text{-}OH + R\text{-}OH$
Water condensation:	$M\text{-}OH + OH\text{-}M \rightarrow M\text{-}O\text{-}M + H_2O$
Alcohol condensation:	$M\text{-}O\text{-}R + HO \rightarrow M\text{-}O\text{-}M + R\text{-}OH$

Hsiang and Lin (2006) have studied the effect of aging on crystalline phases, crystallite sizes and agglomeration of TiO_2 gels which investigated by using thermogravimetry (TG), differential thermal analysis (DTA), X-ray diffraction (XRD), BET specific surface area analyzer and transmission electron microscopy (TEM). The activation energies of anatase crystallite growth for aged and unaged gels were calculated to determine and explain the growth mechanism. The TiO_2 gel was prepared by adding $TiCl_4$ to NH_4OH solution at pH 9. After precipitation, the gels were aged in a boiling solution. The powders were annealed in air at temperatures between 600 and 650 ˚C for a different period of time. TiO_2 aging treatment decreased the number of hydroxyl ions existing in the anatase, resulting in downing the rate of surface area reduction and decreasing the amount of agglomeration after calcinations. The activation energy values for crystallite growth in samples with aging treatment were greater than that found in unaged samples. In nanocrystalline anatase samples without aging treatment, the

oriented attachment controlled the crystallite growth. However, grain boundary diffusion controlled the crystallite growth for nanocrystalline anatase samples with aging treatment.

Hu, et al. (2003) prepared TiO_2 powder from the $TiCl_4$ precursor precipitate under different pH values by adding aqueous ammonia. First, $TiCl_4$ was dissolved in an aqueous solution consisting of isopropanol and HCl. The ratio of H_2O and isopropanol was 1:3 in molar ratio. It has shown very clear and transparent without any precipitate. The powders were then heated at different temperatures for 2 hours. It was found that the crystallite size decrease with a decrease in pH value about 3. The critical particle size for anatase-rutile transformation is about 15 nm. The beginning and ending temperatures for anatase-rutile transition increase with the increasing of synthesized pH value.

The sol precursor can be either deposited on a substrate to form a film by dip-coating or spin-coating, cast into a suitable container with the desired shape such as a monolithic ceramics, glasses, fibers, membranes, or used to synthesize powders. The sol-gel processing shown in Figure2.3 offers many advantages such as a cheap, homogeneous multicomponent oxide and low-temperature technique that allows for the fine control on the product such as chemical composition, even though small quantities of dopants, (organic dyes and rare earth metals) introduced in the sol and ends up in the final product finely dispersed (Suresh, 1998). It can be used in ceramics manufacturing processes, as an investment casting material, or as a means of producing very thin films of metal oxides for various purposes. Sol-gel derived materials have diverse applications in optics, electronics, solar cell, photcatalytic, sensors, and separation. Many previous works have prepared titanium dioxide powder and thin film by sol-gel method with good properties.

Yoon et al. (2006) prepared TiO_2 by sol-gel process and titanium isopropoxide (Ti $[OCH\ (CH_3)_2]_4$) and isopropyl alcohol were used as a precursor and a solvent, respectively. After 10 min stirring of the mixture, water and nitric acid were added and stirred at 80 ˚C for 8 h. In case of a solution with acetyl acetone, AcAc was added with isopropyl alcohol as a reaction controller and the mixture was stirred for 30 min. The final reaction took place with the aid of nitric acid at room temperature. In presence of AcAc, Ti $(i\text{-}PrO)_3$ AcAc precursor was formed

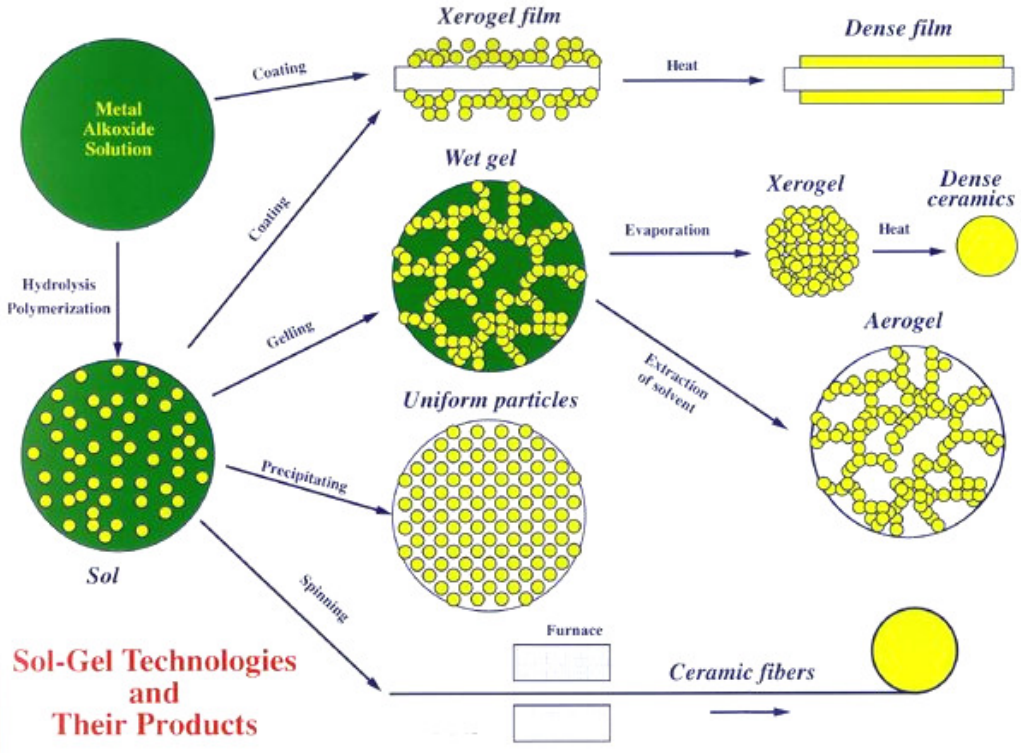

Figure2.3 Schematic illustration of sol-gel processing (www.chemat.com)

acetic acid displaced two isopropoxide ligands to form the alkoxide chelate $Ti(iPrO)_2(CH3COO)_2$. Both solutions with and without AcAc were coated on the glass substrates via spin coating at room temperature, being subject to post-deposition heat treatment at various temperatures. The result found the formation of the anatase phase in the thin films using AcAc was initiated at 300 ˚C while the anatase phase in the thin films without using AcAc began to appear at 100 ˚C. Surface roughness of the TiO_2 films using and without using AcAc ranged from 0.414 to 3.08 nm and from 3.72 to 5.35 nm, respectively. Photocatalytic decomposition rate examined by methylene blue solution showed 80% at 400 ˚C and 88% at 600 ˚C for the TiO_2 thin films using AcAc. On the other hand, the photocatalytic decomposition rate of the TiO_2 thin films without using AcAc showed 80% at 100 ˚C and 97% at 400 ˚C, respectively. At the temperature above 400 ˚C, the photocatalytic activity decreased due to the appearance of the rutile phase. Comparison between the TiO_2 thin films showing the maximum photocatalytic activity revealed that the TiO_2 thin film without using AcAc showed 10% higher photocatalytic decomposition rate from the initial 10 to 120 min as compared with the TiO_2 thin film using AcAc, which was closely related to the formation of the anatase phase and the surface roughness.

Hou et al. (2006) prepared TiO_2 films by the sol–gel method. The sol was a mixture of tetrabutylorthotitanate (Ti (OBu) $_4$), ethanol, acetylacetonate (AcAc), H_2O and HNO_3 in a molar ratio of 1: 18: 0.5: 2: 0.2. Three layers of gel were dip-coated on each glass substrate. Each layer was annealed to 450 ^oC at a rate of 1.5 ^oC /min for 30 min. A metal vapor vacuum arc (MEVVA) ion implanter was used to perform the implantation of V^+ ions at 40 kV. The fluences of implanted V+ ions were chosen as 3 x 10^{15}, 6 x 10^{15}, 1 x 10^{16}, 3 x 10^{16} and 6 x 10^{16} ions/cm^2. After the implantation, TiO_2 films were annealed at 450 ^oC for 4.5 h. The result was found that V^+ ion implantation can produce high-efficient and visible-light-sensitive TiO_2 films. The photocatalytic effect of V^+ion implanted TiO_2 films depends strongly on the amount of implanted ions and the annealing process. The catalytic efficiency of V^+ ion implanted TiO_2 films with visible light excitation has an optimum value for an implantation fluency of 1 x 10^{16} ions/cm^2.

Neppolian et al. (2008) prepared nano-size TiO_2 photocatalysts by sol-gel and ultrasonic-assisted sol-gel methods using two different sources of ultrasonicator, i.e., a bath type and tip type. The physicochemical characteristics of the catalysts were investigated by BET, XRD and TEM analyses and the photocatalytic properties of the TiO_2 catalysts prepared by three different methods were compared. It was synthesized by using titanium tetra isopropoxide (TTIP) as a precursor. The ratio of water and TTIP was 175 for sol-gel and 35 for the ultrasonic-assisted methods. The catalysts were kept for 20 h for slow hydrolysis at room temperature, dried at ambient temperatures for 12 h and calcined at the temperature 500 ^oC in a furnace under the continuous flow of air for 3 h. Among the three different methods, TiO_2 photocatalysts prepared by ultrasonic (tip-US) assisted sol-gel possessed the smallest particle size, highest surface area and highest pore-volume than the catalysts prepared by the other two methods. 4-Chlorophenol was used as a pollutant to observe the photocatalytic degradation ability of the prepared photocatalysts and the TiO_2 catalysts prepared by the bath-US ultrasonic-assisted sol-gel method were shown to be the most highly active. This is due to their high surface area and high pore-diameter. This study clearly demonstrates the importance and advantages of ultrasonication in the modification and improvement of the photocatalytic properties of mesoporous nano-size TiO_2 particles.

Sonawane et al. (2004) prepared thin films of iron (Fe) doped titanium dioxide (Fe/TiO_2) by using the titanium tetraisopropoxide (1.77 g) that was hydrolyzed with 100 ml of water and the resulting titanium hydroxide was washed thoroughly to remove alcohol formed during the hydrolysis. To this precipitate, 20 ml of aqueous H_2O_2 (15%) was added slowly and allowed to dissolve the precipitate completely. During dissolution, 85 ml of distilled water was added to this solution to avoid immediate dense gel formation. Various amounts of 10% PEG solution was added to get PEG containing sol. Then 0.1M iron (Fe) solution (0.1M solution prepared by dissolving 0.404 g $Fe(NO_3)_3 \cdot 9H_2O$ in 100 ml distilled water) was added into this sol to prepare the PEG and Fe containing TiO_2 sol. The above diluted titanium peroxide sol was allowed to stand for 4–5 h to form a viscous sol. Following this method the sols containing different concentrations of Fe such as 0, 1, 2, 4 wt. % were prepared. This result has shown the increasing in concentration of PEG increases the number and size of the pores on surface of the film when the films are subjected to heat treatment. The adsorbed hydroxyl content of such porous films was found to increase with amount of PEG added and addition of Fe into the sol lowers the crystallization temperature as well as phase transition temperature. Photocatalytic properties of the surface modified and Fe ion doped TiO_2 catalyst was investigated by degradation of methyl orange in sunlight. It was found that the films prepared with 0.6 g PEG containing 2% $Fe–TiO_2$ and 4% Fe/TiO_2 have shown excellent photo-catalytic activity after the heat treatment at 450 ˚C, up to 95% of methyl orange can be decomposed in sunlight within 3–4 h by using these catalysts.

Guan (2005) prepared the TiO_2/SiO_2 composite films by sol-gel method by using 1 mole of tetraethylorthosilicate (TEOS, 1 mole) in 20 mole of ethanol is hydrolyzed containing 0.2 mol HCl for 1 h used as TEOS precursor solution. Then 1 mole of tetrabutylorthotitanate (TBOT) is dissolved in a solution of 58 mole of ethanol used as TBOT precursor solution. Then TEOS and various amounts of TBOT precursor solution were mixed together and further quantities of HCl catalyst are added (TBOT/HCl = 1:0.5 in molar ratio). The content in mol% of SiO_2 is varied from 0 to 50%, respectively. The coatings were prepared by a dip-coating method, dried at 200 ^{o}C for 30 min and then heat-treated in air. The temperature is elevated slowly to 650 ^{o}C for 1 h. This research has investigated the relationship between hydrophilicity, photocatalysis and the self-cleaning effect. It was shown that the TiO_2/SiO_2 surface has more hydrophilic activity

and photocatalytic activities from adding different amount of SiO_2. It was the synergetic effect of hydrophilicity and photocatalysis that improved and maintained the self-cleaning effect. SiO_2 addition increases the acidity which results in the increase of the hydroxyl content in the composite films; with the consequence that the hydrophilicity and photocatalytic activity were increased during UV irradiation thus enhanced the self-cleaning effect.

Sonawane and Dongare (2006) synthesized thin films of Au/TiO_2 on glass substrates which had been prepared by sol–gel and dip coating methods using titanium hydroxide precipitate formed then dissolved in 10 ml H_2O_2 (15%). This sol was diluted with water as per requirement and allowed to stand for few hours. The gold colloidal solution used for doping was prepared by reduction of $HAuCl_4$ with a reducing agent, $NaBH_4$. The Au/TiO_2 sol prepared by this method started to form viscous liquid after 1–3 h. The liquid after attaining the particular viscosity range of 140–2800 cps was used for deposition of thin films on soda-lime glass. As the viscosity of sol used for deposition of thin film increases the film thickness has increased also. Thin film photo-catalyst prepared was characterized by various techniques such as UV–vis, TG-DTA, XRD, ICP-OES and TEM. This result found the films were modified by addition colloidal Au solution in titanium peroxide sol to increase the photoresponse of TiO_2 in visible light. By addition of 1–2% Au the absorption wavelength of TiO_2 was shifted from 340 nm in UV to 450 nm in visible region. The increased in photoresponse was tested by photocatalytic decomposition of aqueous solution of phenol in sunlight. Doping 1–2% Au into TiO_2 improved the photocatalytic activity by 2–2.3 times than undoped. The catalyst was very stable and it can be used for several times with no much changes in an efficiency for long term used.

Tsuji et al. (2006) investigated on improvement of photocatalytic properties under fluorescent light of anatase-type titanium oxide film by using silver negative-ion implantation. The anatase films were prepared in a sol–gel method on a glass plate with a commercial sol material by spin-coating and baking at 500 ^{o}C for 30 min. Typical thickness of films was about 500 nm. Silver negative ions were implanted to these films at 30 keV with a dose in $1.5x10^{16}$ ions/cm^2. For forming Ag nanoparticles and recovering ion-induced defects, the implanted samples were annealed at temperature in a range of 400–600 ^{o}C. The photocatalytic activity test was investigated by degradation of methylene blue solution under fluorescent light.

All of the samples showed the improvement of photocatalytic efficiency in methylene blue decomposition under the normal fluorescent light, 1.6 times higher than that of a rutile crystal catalyst.

2.3 Spin coating process

Spin coating has been used for several applications of thin films. Spin Coating involves the acceleration of a liquid puddle on a rotating substrate. The coating material is deposited in the center of the substrate either manually or by a robotic arm. The physics behind spin coating involve a balance between centrifugal forces controlled by spin speed and viscous forces which are determined by solvent viscosity. The film-forming process is primarily driven by two independent parameters which are viscosity and spin speed.

These charts represent general trends for the various process parameters shown in Figure2.4. For most materials, the final film thickness will be inversed proportional to the spin speed and spin time. Final thickness will be also somewhat proportional to the exhaust volume although uniformity will suffer if the exhaust flow is too high since turbulence will cause non uniform drying of the film during the spin process. Spin coating has been used for several applications of thin films as follows.

Tsuji et al. (2005) investigated improvement of photocatalytic properties of anatase-type TiO_2 with negative ion-implantation by sol–gel method and spin-coated on a glass. TiO_2 film has thickness about 500 nm. The Ag implanted samples were subsequently annealed at temperatures of 300–600 ^{o}C for 1 h in Ar gas. Photocatalytic efficiencies were evaluated by a method of decolorizing methylene blue (MB) solution with implanted samples under irradiation of a fluorescent light (9600 LUX in visible light and 2.7 l W/cm^2 in ultra violet light) in dark box for 19h. The result shown, almost all of the samples made an improvement on photocatalytic properties in methylene blue decomposition under the normal fluorescent light.

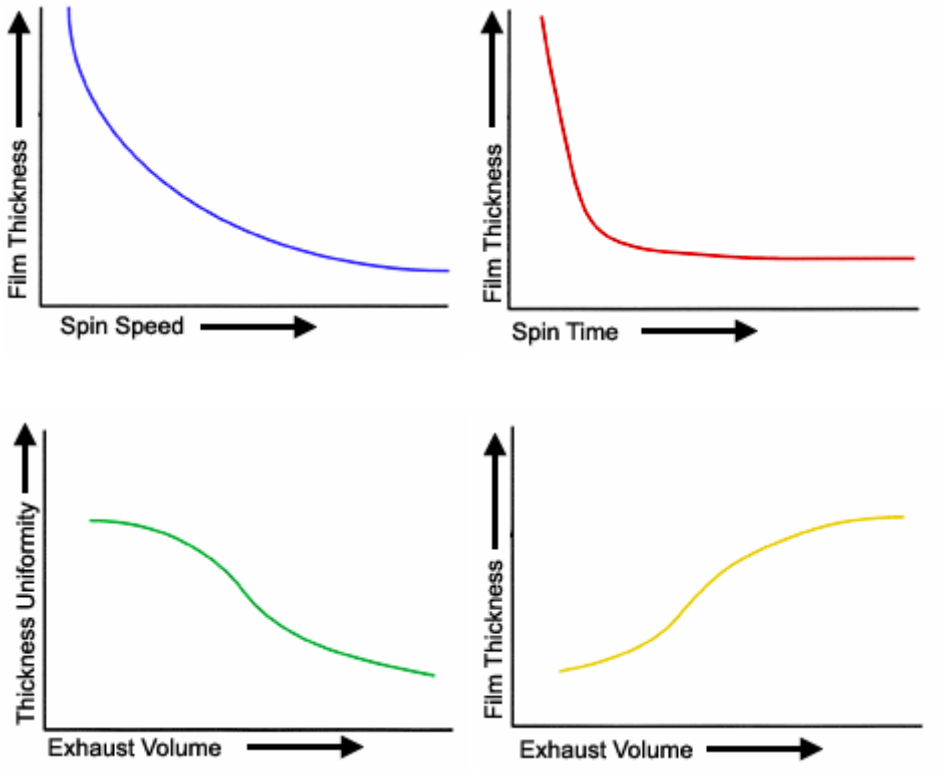

Figure2.4 Process trend charts (www.cpmt.org)

Guo et al. (2005) investigated porous TiO_2 thin film by spin-coating on glass substrates from a sol-gel solution containing titanium alkoxide as precursor. TTIP (1.25 ml) was added to a solution made up of 10 ml ethanol and 0.3 ml HCl at room temperature. After 1 h of stirring, a given volume of water and a different molecular weight of PEG (HO (CH_2CH_2O) nH) (1 mol % of the TTIP) at 200, 600, 1000, 2000 and 6000, respectively for increasing the surface area and changing the properties of thin film to hydrophilic and then coating on Pyrex glass by spin coating with a rate of 2000 rpm and calcination at 550 ^{o}C for 1 h in air. The result showed that, the photocatalytic activity of the TiO_2 thin films as evaluated by the decomposition of methyl orange was increased when the PEG molecular weight increased.

2.4 Photocatalytic process

The primary photocatalytic process occurs upon irradiation of a semiconductor catalyst. A semiconductor is characterized by electronic band structure in which the highest occupied energy band, called valence band (VB), and the lower empty band called conduction

band (CB) which are separated by a band gap and the band gap also defines wavelength sensitivity of the semiconductor to irradiation. When photon of energy is higher or equal to the band gap, energy was absorbed by a semiconductor particle, an electron from valence band is promoted to the conduction band with simultaneous generation of an electronic vacancy or "hole" (h^+) in valence band. Figure2.5 shows the primary steps in the photocatalytic mechanism (Hoffmann, et al. 1995)

(1) Formation of charge carriers by photon.
(2) Charge carriers recombination to liberate heat.
(3) Initiation of an oxidative pathway by a valence-band hole.
(4) Initiation of reductive pathway by a conduction-band electron
(5) Further reaction such as hydrolysis or reaction with active oxygen species and photocatalytic reaction to yield mineralization products.
(6) Trapping of conduction band electron in a dangling surficial bond to yield Ti(III)
(7) Trapping of a valence band hole at a surficial titanol group.

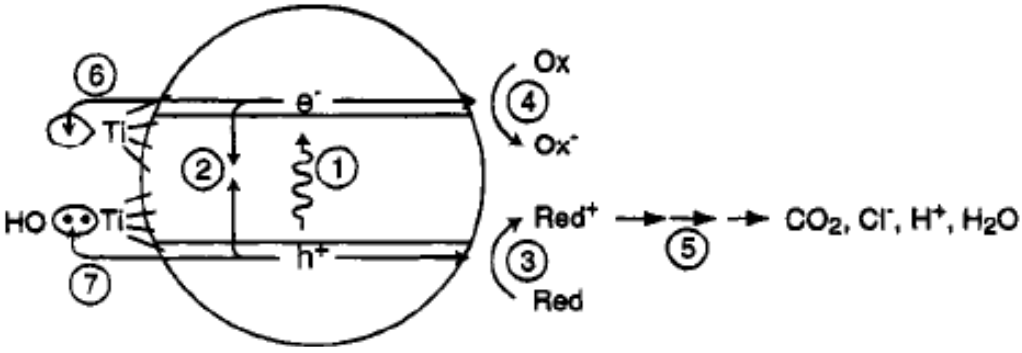

Figure2.5 Primary steps in the photocatalytic mechanism (Hoffmann et al. 1995).

Recently year, photocatalytic process has been used in many applications such as dye sensitized solar cells (Lee et al., 2007), self cleaning (Madaeni and Ghaemi, 2007), sterilization, waste water treatment (Yuan et al., 2007) and sensor (Su and Chang, 2008) as follows.

Su and Chang (2008) studied low-humidity sensors which were fabricated by the in situ photopolymerization of polypyrrole/Ag/TiO_2 nanoparticles (PPy/Ag/TiO_2 NPs) composite thin films on a quartz-crystal microbalance (QCM). The characterizations of the thin films were analyzed by scanning electron microscopy (SEM) and atomic force microscopy (AFM). The result was shown that the sensor was highly sensitive especially to low humidity with acceptable linearity, a fast response time and well reversibility. Therefore, the PPy/Ag/50 wt% TiO_2 NPs composite material combined with QCM can be reliable for measuring trace of humidity.

Usui et al. (2004) studied the effect of addition of nanoparticles into a dye-sensitized solar cells (DSCs) ionic liquid electrolyte. The dispersion of CNTs resulted in a substantial increase in their viscosity and electrical conductivity increased as well. Notable effects were obtained in photocurrent density and voltage measurements of the DSC assembled with them. Energy conversion efficiency of them was significantly improved and increased compared with a DSC using a bare ionic liquid electrolyte.

Yuan et al. (2007) prepared titanium dioxide and loaded on activated carbon fibers (ACF) with different surface areas. Their surface properties and photodegradations of wastewater from paper mill have been investigated. TiO_2 powder distributed on ACF in the form of small clusters, and its surface element state changed after UV irradiation. After TiO_2 was loaded on ACF, the surface area of supported catalysts (TiO_2/ACF) decreased, but the pore structure of ACF remained well. The photodegradation results showed that an increase in surface area favored high COD removal for paper mill effluents; the best COD removal was obtained only by using TiO_2/ACF with moderate surface area and pore structure for organic molecules from the effluents, and its photocatalytic activity was higher than suspended P25 and without any decline when used repeatedly.

Colpini et al. (2008) prepared TiO_2 catalysts by the sol-gel method from two different alkoxide precursors; titanium (IV) tetrabutoxide and titanium (IV) isopropoxide, called TiO_2-TBOTC and TiO_2-IPOTC, respectively. The catalysts were used in the photocatalytic discoloration and degradation of textile dye C.I. reactive orange-122 aqueous solutions. The discoloration percentages were calculated by using the equation given below:

$$\text{Discoloration (\%)} = \frac{Co - C}{Co} \times 100 \quad (2.1)$$

TiO_2-TBOTC discolored dye solutions 100% in 40 min with maximum TOC reduction of 65.8%, in contrast to TiO_2-IPOTC, which required 20 min of reaction and yielded maximum TOC reduction of 27.7%. Photocatalyst TiO_2-TBOTC was more efficient than TiO_2-IPOTC.

Evans and Sheel (2007) described an innovative method to achieve highly photoactive and antibacterial titania thin films on stainless steel by a novel combination of flame-assisted CVD (FACVD); to deposit silica, and thermal APCVD; to deposit titania. The comparison was done by considering the chemical and structural characteristics, and photocatalytic activities of thin films of titania deposited onto stainless steel using APCVD from two different precursors, TTIP and $TiCl_4$. For TTIP film growth the deposition temperatures were varied from 450–650 °C and for $TiCl_4$ from 550–650 °C. Films deposited from TTIP were anatase whereas those deposited from $TiCl_4$ (in conjunction with ethyl acetate) were rutile. FACVD was used to deposit SiO_2 layers of different thickness. The presence of the SiO_2 layers rendered films from both precursors to be anatase. The photoactivity of the films varied considerably, with those deposited directly onto stainless steel showing the lowest activity. The presence of a SiO_2 layer improved the photoactivity of the films, with the thickest SiO_2 layer giving the best performance. It was found that SiO_2 layers acted as barriers to the deleterious effects of cation diffusion from the stainless steel substrate. Initial studies indicated the films to be biocidally effective against *E. coli* with a 100% killing (6 log reduction) in less than 3 h.

Maness et al (1999) presented the appellation of photocatalyst in terms of mechanism of death of *Escherichia coli* K-12 cells. TiO_2 photocatalyst can disinfect or kill the cell of *Escherichia coli* K-12 because it disrupted of the cell membrane and the cell wall of *Escherichia coli* K-12. The result showed that TiO_2 can kill *Escherichia coli* K-12 about 77-93%.

Priya and Madras (2005) prepared nanosize TiO_2 by the solution combustion method and degradation of various phenols was investigated. The postulated mechanism of

degradation of multi-substituted phenol was shown in Figure2.6. The photocatalytic degradation of seven multi-substituted phenols was investigated. The organics degraded to 10% of the original concentration within 1 h of degradation. The rate of degradation followed the order: 4-chloro,3-methylphenol > 2-chloro,4-methylphenol > 4- chloro,2-nitrophenol > 4-chloro,2-methylphenol > 2-chloro,4- nitropheno l ~ 4-chloro,3-nitrophenol > 4-methyl,2-nitrophenol. Chloromethylphenols degraded faster than chloronitrophenols due to the ring deactivating characteristic of nitro group for hydroxyl radical attack.

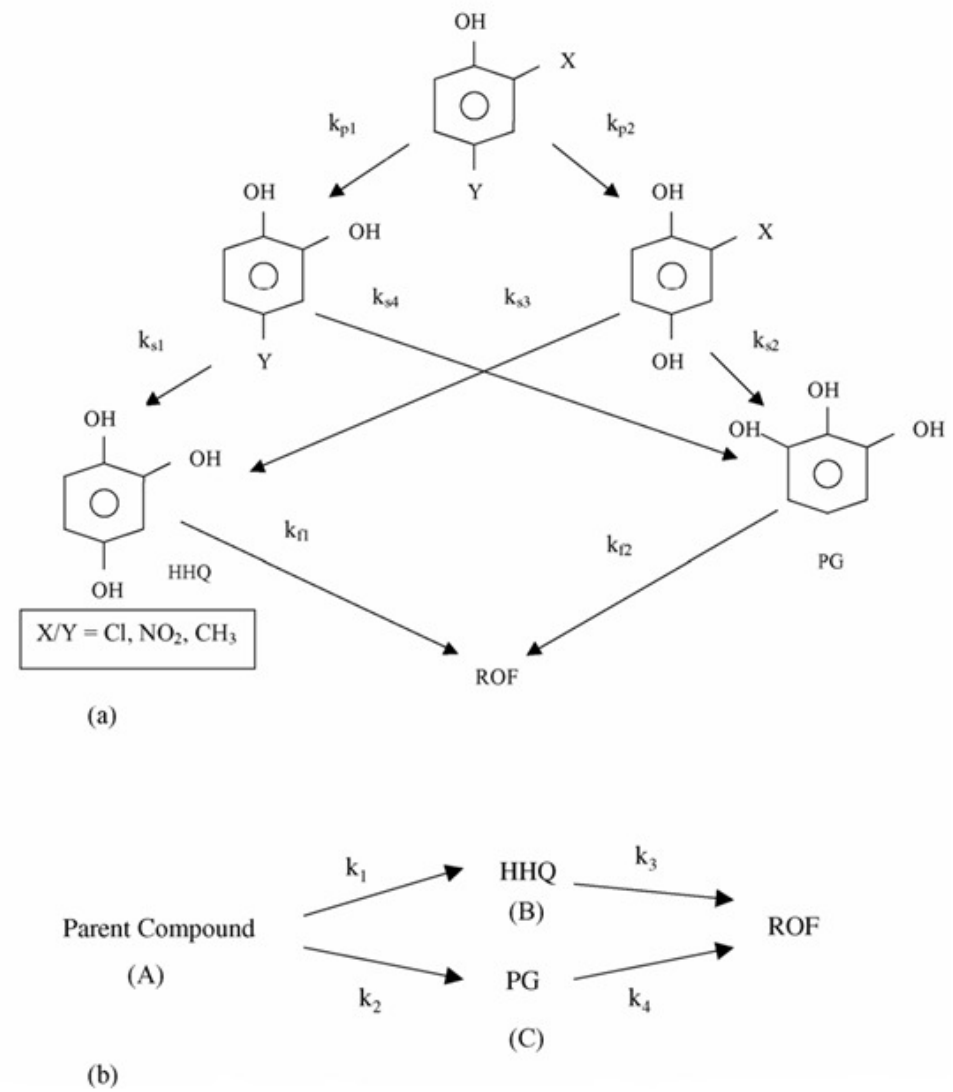

Figure2.6. (a) Postulated mechanism for the degradation of multi-substituted phenols

(b) Simplified mechanism to determine the kinetics

The efficiency of TiO_2 photocatalytic is low for its application. Other factors, such as preparation process, crystallite size and anatase–rutile ratio seem to have an effect on the activity. The effective way to improve the TiO_2 photocatalytic activity is to introduce metal ions into TiO_2. Because, the accepted mechanism to explain the enhancement is the formation of shallow charge trapping on the surface of TiO_2 nanoparticles due to the replacement of Ti^{4+} by metal ions. Ganerally, the initial process for heterogeneous photocatalysis of organic and inorganic compounds by semiconductors is the generation of electron–hole pairs in the semiconductor particles (Legrini et al., 1993). When photon of light, of sufficient energy ($E \geq E_{bg}$) strikes a TiO_2 particle, the energy of the photon is absorbed and used to promote an electron (e^-) from the valence band to the conduction band. This movement of an electron leaves a hole (h^+) in the valence band. These species (h^+ and e^-) produced by the absorption of light, can either recombine or they migrate to the surface of the TiO_2 particle where they can react with other species at the interface. The holes can directly oxidise organic species adsorbed onto the TiO_2 particle or can increase hydroxyl radicals ($OH^{\bullet}$) by reacting with water or OH^-. These highly reactive hydroxyl radicals then attack organic compounds present at or near the surface (Mills et al., 1993). It is necessary that the electrons promoted to the conduction band be removed rapidly from the TiO_2 to prevent recombination with the holes and allow the mechanism to continue. Usually the electrons are passed on to molecular oxygen at the interface. Many works introduced metal ions, such as Fe^{3+} (Wu et al., 2006), Pt^{4+} (Coleman et al., 2005) V^{5+}(Hong and Kang, 2005), MWCNT (Eswaramoorthi and Hwang, 2007) Ag^+ (Chang et al., 2006) etc., into TiO_2 in order to enhance the photocatalytic activity due to the following factors such as crystallite size decreased to nano-scaled particles having the large surface areas and the increase in surface hydroxyl content to prevent electron-hole recombination.

Many researchers have the studied the behavior of introduced metal ions into TiO as follows. Chao et al. (2003) prepared powder and thin film of titanium dioxide photocatalyst by doping with Ag by sol–gel process. They also investigated the effect of silver doping on the phase transformation and grain growth. The powder was prepared from tetrabutyl orthotitanate and acetylacetone into ethyl alcohol at room temperature. After stirring for 30 min, certain amounts of water and nitric acid were added into the solution. The TiO_2 sol was dried at 100 ^oC in air for several days to get TiO_2 xerogel and calcined at different temperatures for 30

min to get TiO_2 powders. The Ag doped TiO_2 were prepared by adding silver nitrate solution into the TiO_2 sol with nitric acid as a stabilizer. The Ag concentration studied were 2, 4, 6, 8, 10 mol%, respectively. TiO_2 films were prepared by the dip-coating process on glass substrates. Characteristics of film and powder determine by XRD, TEM, SEM, DSC-TG, HRTEM and SEM. It was found that temperature calcinations and Ag content effect to crystallite size, phase content and photocatalytic activity. It could be seen that Ag dopant accelerated the TiO_2 anatase to rutile transformation and at 2mol%Ag, the largest surface area and the crystallite size increased when Ag addition above to 2%Ag.

Kwon et al. (2003) prepared and characterized TiO_2 nanocrystalline particles dispersed in SiO_2 prepared by the sol-gel method. They investigated different temperatures effect of SiO_2 content effect on anatase-rutile phase transformation and photocatalytic activity. Titanium solution prepared by titanium tetra-isopropoxide solution was diluting with isopropyl alcohol. The solution was subsequently peptized by stirring in the presence of water and nitric acid as a catalyst. Silicon solution prepared by silicon tetraethoxide in ethanol was hydrolyzed with water containing HNO_3 and mixing with titanium solution. The sol coated on the glass substrates by dip-coating technique. The crystal structure, particle size, and surface area of the TiO_2 photocatalyst were characterized using X-ray diffraction (XRD), transmission electron microscopy (TEM). Surface morphology was examined using an atomic force microscopy (AFM). Photocatalytic activity was evaluated by measurement of the decomposition of methylene blue. It was found that the size of the TiO_2 nanocrystalline particles in the TiO_2–SiO_2 ranged 5 to 8 nm. The crystalline structure of TiO_2 powders was identified as the anatase phase. As the content of SiO_2 increased, the anatase phase tended to be stabilized to higher temperature. Photocatalytic activity of the TiO_2–SiO_2 (1:1) thin films showed decomposition of about 95% of methylene blue solution in 2 h and a contact angle about 10^{o}. The photocatalytic activity of TiO_2–SiO_2 with the molar ratio of 1:1 showed the highest rate.

Harizanov et al. (2001) prepared titanium dioxide and mixed oxide systems TiO2–MnO by the sol–gel method using titanium ethylate and manganese nitrate as precursors. The xerogels of the solutions were dried at 80^{o}C and treated at 560^{o}C in air for 1 h and characterized by XRD, FT–IR spectroscopy and DTA analysis. Coatings with good optical

quality were obtained and investigated by UV–VIS spectroscopy. The result showed that the presence of MnO in titania xerogel is effective in decreasing the anatase–rutile transformation temperature. These coatings offered prospective applications in passive solar control glazing due to the relatively high refractive index.

Zhu et al. (2004) investigated Fe doped anatase titanium (IV) dioxide (TiO_2) samples were prepared by hydrothermal hydrolysis and crystallized in octanol-water solution. The samples were characterized by X-ray diffraction, BET-specific surface area determination, UV-Visible diffuse reflectance spectroscopy and electron paramagnetic resonance spectroscopy. UV-Visible diffuse reflectance spectra showed a slight shift to longer wavelengths and an extension of the absorption in the visible region for almost all the ion-doped samples, compared to the non-doped sample. The photocatalytic activity of those catalysts was investigated for the liquid phase photocatatlytic degradation of active yellow xerogel diluted in water under UV and visible light irradiation. It was found that the catalysts doped with $FeCl_3$ have better catalytic activity for photodegradation of xerogel than those doped with $FeCl_2$. The 0.09% $FeCl_3$–TiO_2 and 0.09% $FeCl_2$–TiO_2 have high specific surface area and small crystal sizes, which are of benefit to efficient photocatalytic reactions. Fe acting as both hole and electron traps can enhance photocatalytic activity of TiO_2.

Arana et al. (2004) studied the formic acid photocatalytic degradation by TiO_2 and Pd and Cu doped TiO_2. FT-IR spectroscopy has been used to characterize the different species formed on the catalyst surface and their evolution under irradiation. Cu/TiO_2 and Pd/TiO_2 improved photocatalytic efficiency and Cu/TiO_2 exhibited the highest rate of photocatalytic activity. The combination of catalyst doping with the addition of oxidising compounds notably improves the bare-TiO_2 photocatalytic efficiency.

Zhang et al. (2007) prepared TiO_2–SiO_2 metal oxide by a novel method in which hydrolysis and condensation of titanium tetraisopropoxide (TTIP) and tetraethoxysilane (TEOS) were controlled by pH changing of acidic solution. The Pt-modified TiO_2/SiO_2 catalysts were synthesized by the photo-reduction method. Photocatalytic activity was analyzed by degradation methyl orange in the visible-light range. The mechanism of dye degradation by Pt–TiO_2 or TiO_2–

SiO_2 catalysts under visible illumination explained by several researchers. Firstly, the dye (MO) is adsorbed on the SiO_2 sites but not on TiO_2 and only the metal oxide (MO) molecule is excited to produce the excited-state MO^* under visible illumination. The reactions could be expressed as

$$TiO_2–SiO_2 + MO \rightarrow TiO_2–SiO_2–MO_{(ads)} \quad (2.2)$$

$$TiO_2–SiO_2– MO_{(ads)} + h\nu \rightarrow TiO_2–SiO_2–MO^*_{(ads)} \quad (2.3)$$

Subsequently, the adsorbed MO* species injects an electron into the conduction band of TiO_2 with $MO_{(ads)}$ being converted to the radical cation $MO^{+\cdot}$ because the sites of SiO_2 are near the TiO_2 sites. That is,

$$TiO_2–SiO_2– MO^*_{(ads)} \rightarrow e^- – TiO_2–SiO_2–MO^{+\bullet}_{(ads)} \quad (2.4)$$

Then, the injected electrons are transferred to the Pt molecules that adsorbed on the surface of TiO_2–SiO_2 catalysts. This electron transfer leads to efficient electron-hole separation and prevents the recombination of electrons and holes.

$$e^- – TiO_2–SiO_2–MO^{+\cdot}_{(ads)} + Pt \rightarrow TiO_2–SiO_2–MO^{+\cdot}_{(ads)} + Pt – e^- \quad (2.5)$$

In turn, the electrons react with the adsorbed O_2 to produce superoxide $O_2^{-\cdot}$ radical anions. The surface-adsorbed water and hydroxyl groups can react with holes generated by illumination to produce active hydroxyl radicals ($^{\cdot}OH$). $O_2^{-\cdot}$ and $^{\cdot}OH$ radicals are generally assumed to be degrading oxidative agents promoting the photo-oxidation of methyl orange molecules on the surface of Pt-doping TiO_2–SiO_2 catalysts.

$$Pt – e^- + O_2 \rightarrow Pt + O_2^{-\cdot} \quad (2.6)$$

$$2\ O_2^{-\cdot} + 2H^+ \rightarrow O_2 + H_2O_2 \quad (2.7)$$

$$P^+ + H_2O \rightarrow {}^{\cdot}OH + H^+ \quad (2.8)$$

$$P^{+} + OH^{-} \longrightarrow {}^{\cdot}OH \quad (2.9)$$

$$H_2O_2 + e^{-} - TiO_2 - SiO_2 - MO^{+\cdot}{}_{(ads)} \longrightarrow OH^{-} + {}^{\cdot}OH + TiO_2 - SiO_2 - MO^{+\cdot}{}_{(ads)} \quad (2.10)$$

$$MO^{+\cdot} + O_2^{-\cdot} \text{ (and/or } {}^{\cdot}OH) \longrightarrow \text{Intermediates} \longrightarrow CO_2 + H_2O \quad (2.11)$$

The reaction could be expressed in the following scheme in Figure2.7

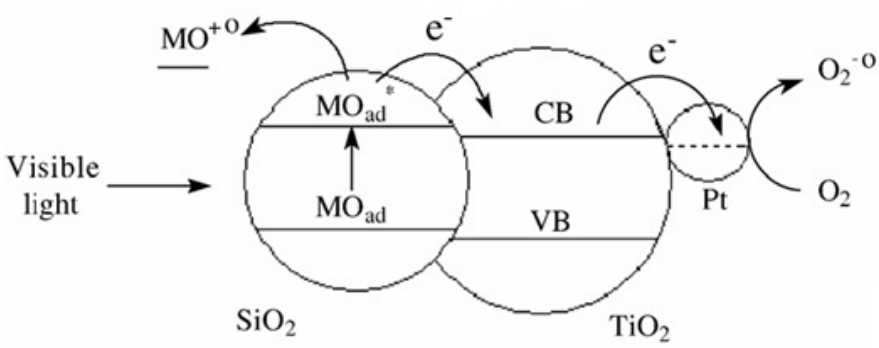

Figure2.7 Photocatalytic mechanism of Pt-modified TiO_2/SiO_2 catalysts (Zhang et al., 2007)

Metal doped titanium dioxide was prepared by two steps chemical solution decomposition (CSD) method (Ghorai et al., 2007). In the first step, the stock solutions of $Ni(NO_3)_2 \cdot 9H_2O$, $Cu(NO_3)_2 \cdot 6H_2O$, $Zn(NO_3)_2 \cdot 6H_2O$, $(NH_4)_2MoO_4$ and titanium tartarate solutions were prepared. In the second step, the equivalent amount of metal nitrate, $(NH_4)_2MoO_4$ and titanium tartarate solution were taken in a beaker. The complexing agent TEA (triethanolamine) (where molecular ratio of metal ion:TEA = 1:3) was added to the homogeneous solution of constituents maintaining pH at 6–7 by nitric acid and ammonia. This mixed solution after evaporation and decompositions at 473 K and calcination at temperatures of 823, 873 and 973K for 2 h. In summary, photocatalyst $NiMoO_4$ (5 mol%) doped TiO_2 synthesized by CSD method is more photoactive than P25 TiO_2 and other metal molybdate doped TiO_2 due to high surface area, lower energy band-gap and photo chemical generation of Ni^{3+}. The dye was sensitized by the catalyst in presence of UV light and the dye cation was formed. The dye cation was unstable and decomposes injecting an electron on the conduction band of TiO_2. Electron went to conduction

band and hole is captured by Ni^{2+} producing Ni^{3+}, which had been noticed by EPR spectrum and helped to degrade the dye molecule faster.

Jung and Park (2004) prepared silica/titania and zirconia/titania mixed oxides by the sol–gel technique. Titanium ethoxide (TEOT), tetraethylorthosilicate (TEOS), and zirconium (IV) propoxide were used as precursors of titania, silica, and zirconia, respectively. The calcinations were done at the temperatures between 400 and 800 ^{o}C. The result of photocatalytic activity for decomposition of trichloroethylene was found to have a linear relationship with the crystallite size of anatase phase. That is, larger crystallite size lead to higher photocatalytic activity of silica/titania and zirconia/titania mixed oxides. This result supported the contention that the crystallite size of photocatalyst was a critical factor to determine the photoactivity for the TCE decomposition and should be enlarged to get higher photoactivity regardless of the type of photocatalyst. Therefore, it was concluded that increasing the crystallite size was the best way to obtain high photoactive titania-based mixed oxides.

Muruganandham et al. (2007) attempted to develop a catalyst derived from sludge waste materials to enhance ozone decomposition. The catalyst was characterized by using X-ray fluorescence (XRF), transmission electron microscope (TEM), scanning electron microscope (SEM), and X-ray diffraction (XRD) techniques. The sludge mainly consisted of various metal and non-metal oxides. The effect of various experimental parameters such as catalyst loading, initial ozone concentrations, and various metal oxide catalysts on the decomposition of ozone was investigated. The decomposition of dissolved ozone was substantially enhanced by increasing the catalyst loading from 125 to 750 mg and by increasing the initial ozone concentration. The ozone decomposition efficiencies of Al_2O_3, SiO_2, TiO_2, Fe_2O_3, ZnO, and sludge had been studied and the efficiencies of these catalysts were found to be in the following order: ZnO $\approx$ sludge > TiO_2 > SiO_2 > Al_2O_3 $\approx$ Fe_2O_3. The catalytic stability was also investigated for up to four successive cycles and it was found that the catalyst was stable and ozone did not affect the catalyst morphology and its composition. However, the surface area of the catalyst increased after 1st cycle then it became stable. It was concluded that the sludge powder used in this study was a promising catalyst for aqueous ozone decomposition.

In general, TiO_2 has been applied under irradiation of UV light. Anatase phase have band gap energy about 3.2 eV., which corresponding to UV light (wavelength of 388 nm.), while band gap energy of rutile is 3.02 eV., corresponding to UV light (wavelength of 413 nm.). It is known that the UV part of the solar spectrum only accounts for about 5% of the incoming solar energy while the rest is visible light. So, this work focuses on the synthesis of the new photocatalysts to improve photocatalytic activity under the visible light. Several previous works have been attempted to development of photocatalytic activity in order visible region. For example, TiO_2 doped with transition metal, could slightly shifted in the band gap transition to longer wavelengths and an extension of the absorption in the visible region.

Ou et al. (2006) prepared multi-walled carbon nanotube, TiO_2 and Ni composite catalysts (MWNT–TiO_2: Ni) by a modified chemical vapor deposition. The nanoscaled composite materials were extensively characterized by TG, SEM, Raman and UV–vis spectra. The experimental results that MWNT-TiO_2:Ni composite catalysts could absorb at higher wavelength than TiO_2: Ni precursor. The photocatalytic activities of the TiO_2:Ni precursor and MWNT–TiO_2:Ni composite catalyst were evaluated by using H_2 evolution of water splitting under visible light irradiation. The mechanism of photocatalytic reaction on MWNT–TiO_2:Ni composite was shown in Figure2.8. The photocatalytic H_2 evolution increases steadily with increasing illumination time on the MWNT–TiO_2: Ni composite catalyst. The decrease in activity with higher MWNT/TiO_2 weight ratio is considered to be related to decreasing the absorption of visible light.

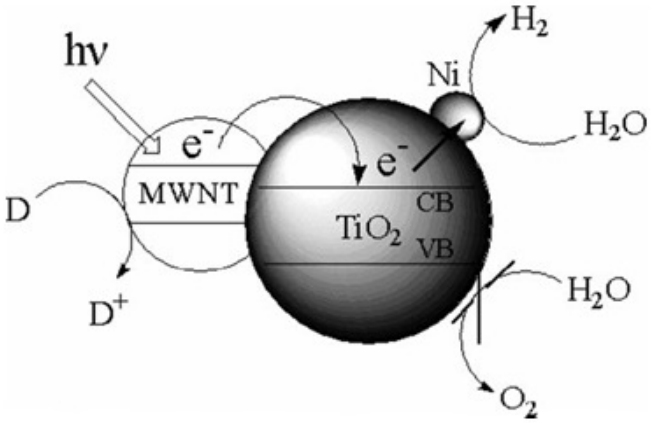

Figure2.8 Proposed process of H_2 evolution on MWNT–TiO_2:Ni composite catalyst under visible light irradiation.

Wang et al. (2005) prepared multi-walled carbon nanotubes (MWNT) and TiO_2 composite catalysts by sol–gel method. The nanoscaled composite materials were extensively characterized by TG, N_2 adsorption-desorption isotherm, XRD, SEM, EDX, TEM and UV–vis spectra. The photocatalytic degradation of phenol was performed under visible light irradiation on these catalysts. A more homogeneous MWNT dispersion in TiO_2 matrix and less agglomeration of TiO_2 particles on MWNT surface resulted in a strong interphase structure effect between MWNT and TiO_2, so as to increase the surface area of the composite catalysts. The photocatalytic activity was observed to increase the degradation rate of phenol when MWNT/TiO_2 ratio was increased from 5 to 20%.

CHAPTER 3

Experimental

The aim of this reserch is to prepare TiO_2 doped with Ag or MWNTs or both Ag and MWNTs in order to enhance the photocatalytic efficiency and hydrophilic property of TiO_2 photocatalyst. Pure TiO_2, Ag/TiO_2, $MWNTs/TiO_2$ and $Ag/MWNTs/TiO_2$ were synthesized in forms of powder and thin films coated on ceramic substrate by sol-gel and spin coating methods. The effect of dopant content, calcinations temperature and irradiation source of UV and visible light on crystallite size, TiO_2 phase, photocatalytic reaction hydrophilic property were investigated.

3.1 Preparation of pure TiO_2, Ag/TiO_2, MWNTs/ TiO_2 and Ag/MWNTs/ TiO_2 powders and thin films

3.1.1 Synthesis of pure TiO_2

Pure TiO_2 was prepared by adding the titanium (IV) isopropoxide (Fluka, United Kingdom) 10 ml into ethanol 95%(Merck, Germany) 150 ml and then slowly dropping nitric acid(J.T. Baker, Thailand) into solution mixed precursors under vigorously stirring at room temperature for 1h. The pH value of the solution was adjusted to be about 3. This solution was divided into 2 parts; (1) the sol was kept in a refrigerator for 24 h until the sol turned into a low viscosity clear gel. The gel was then coated on 7x7 cm ceramic tile substrate by spin coating method. The coated substrates were dried at the temperature of 100 ^{o}C for 24 h before calcining at the temperature range of 400-800 ^{o}C for 1 h, and (2) this sol was kept in a room temperature for several days to allow gel form and then dried for 24 h at the temperature of 100 ^{o}C followed by calcining at the temperature range of 400-800 ^{o}C for 1 h. The experimental procedure was schematically shown in Figure 3.1.

3.1.2 Synthesis of Ag/TiO_2

Ag/TiO_2 composites were prepared by sol-gel method shown in Figure 3.2 by adding the titanium (IV) isopropoxide (Fluka, United Kingdom) 10 ml into ethanol 95%(Merck, Germany) 100 ml and dropping a certain amount $AgNO_3$(VWR Prolabo, United Kingdom) in ethanol 50 ml solution together with nitric acid into the mixed precursors under vigorously stirring at room temperature for 1h. The pH value of the reaction system was adjusted to about 3. This solution was divided into 2 parts; (1) the sol was kept in a refrigerator of 5 ^{o}C for 24 h until the sol turned into a low viscosity clear gel. The gel was then coated on 7x7 cm ceramic tile substrate by spin coating method at 1500 rpm. The coated substrates were dried at the temperature of 100 ^{o}C for 24 h before calcining at the temperature range of 400-600 ^{o}C for 1 h., and (2) this sol was kept in a room temperature for several days to allow gel form and then dried for 24 h at the temperature of 100 ^{o}C followed by calcining at the temperature range of 400-600 ^{o}C for 1 h. The effect of Ag content varied as 0.5 mol%, 1 mol%, 2 mol% ,3 mol%, 4 mol% and 5 mol% on crystallize site, phase transformation, phase ratio and photocatalytic activity were studied.

3.1.3 Synthesis of $MWNTs/TiO_2$

The MWNTs used in the work were synthesized by the chemical vapor deposition (CVD) method. For purification, the raw MWNTs were boiled in concentrated nitric acid (65% HNO_3) for 30 min to get oxygenated functionalities on the nanotube surface (Yu et al.2005). Then the suspension was centrifuged and washed with distilled water to remove the residual nitric acid. After that, the purified MWNTs were dried at 80 ^{o}C for 24 h. The treated MWNTs of 0.1, 0.5 and 1 wt % were added into ethanol of 50 ml under ultrasonic bath in room temperature for 30 min.

$MWNT/TiO_2$ composite was prepared by sol-gel techniques, using titanium (IV) isopropoxide(Fluka, United Kingdom) as a precursor. This reagent of 10 ml was added into ethanol 95 %(Merck, Germany) 100 ml in which nitric acid (J.T. Baker, Thailand) was added controlling pH about 3. MWNTs (Chiang Mai University) were dispersed in ethanol, added into sol, for mixed and stirred under room temperature for 1h. This solution was divided into 2 parts; (1) the sol was kept in a refrigerator for 24 h until the sol become to be a low viscosity clear gel.

The gel was mixed in ultrasonic bath for 30 min and then coated on 7x7 cm^2 ceramic tile substrate by spin coating method. The coated substrates were dried at the temperature of 100 ^oC for 24 h before calcining at the temperature range of 400-600 ^oC for 1 h. (2) This sol was kept in a room temperature for several days to allow gel form and then dried for 24 h at the temperature of 100 ^oC followed by calcining at the temperature range of 400-600 ^oC for 1 h. The experimental procedure was schematically shown in Figure 3.3.

3.1.4 Synthesis of Ag/MWNTs/TiO_2

Ag/MWNT/TiO_2 composite was prepared by sol-gel method using titanium (IV)isopropoxide(Fluka, United Kingdom) of 10 ml added into ethanol 95%(Merck, Germany) 100 ml. A certain amount $AgNO_3$ (VWR Prolabo, United Kingdom) and MWNTs (Nanomaterials research unit CMU. Thailand) were mixed in the prepared solution at pH about 3. This sol was mixed by magnetic stirrer at room temperature for 1 h and divided into 2 parts; Part 1, sol was kept in a refrigerator for 24 h until the sol turned into a low viscosity clear gel. The gel was mixed in ultrasonic bath for 30 min and then coated on 7x7 cm^2 ceramic tile substrate by spin coating method. The coated substrates were dried at the temperature of 100 ^oC for 24 h before calcining at the temperature range of 400-600 ^oC for 1 h, part 2 sol was kept in a room temperature for several days to allow gel form and then dried for 24 h at the temperature of 100 ^oC followed by calcining at the temperature range of 400-600 ^oC for 1 h to get Ag/MWNTs/TiO_2 powders. The experimental procedure was schematically shown in Figure 3.4

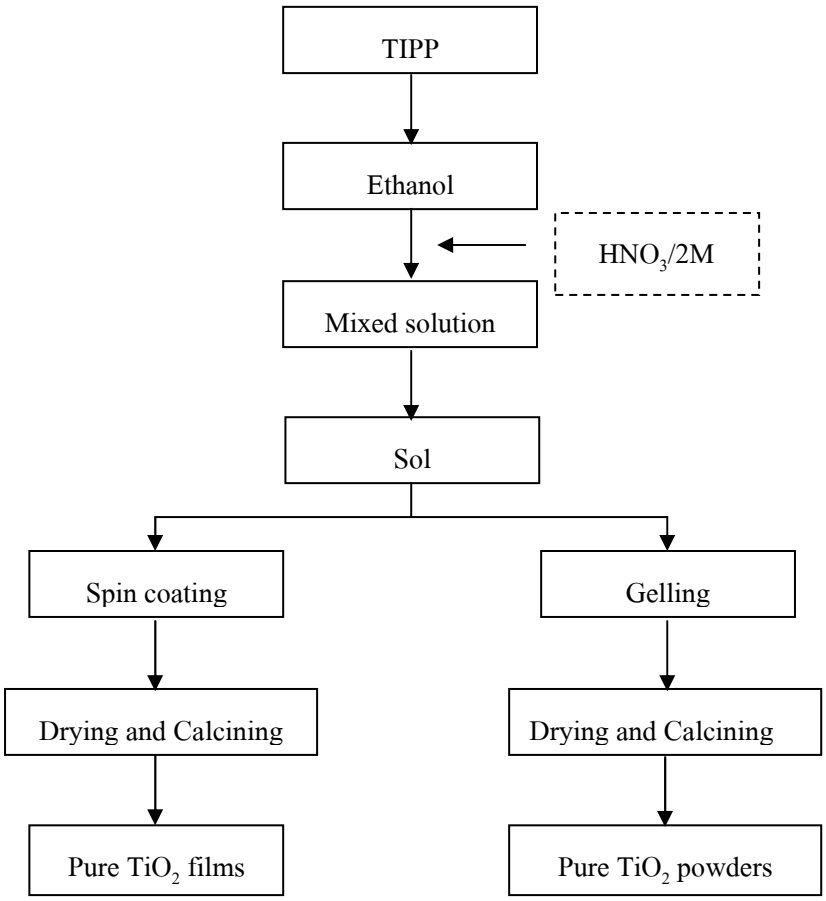

Figure 3.1 Flowchart of the synthesis of pure TiO_2 powders and thin films

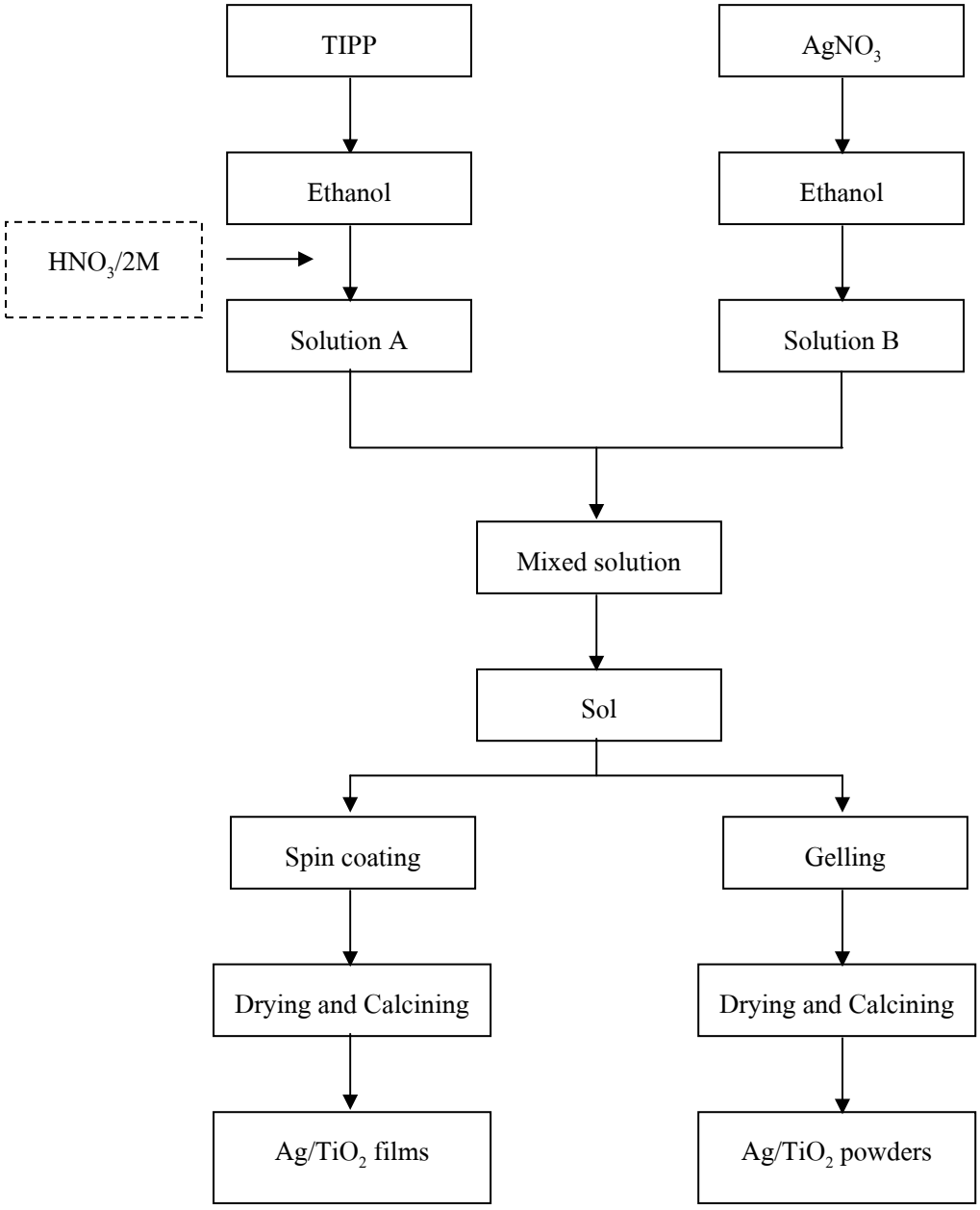

Figure 3.2 Flowchart of the synthesis of Ag/TiO_2 powders and thin films

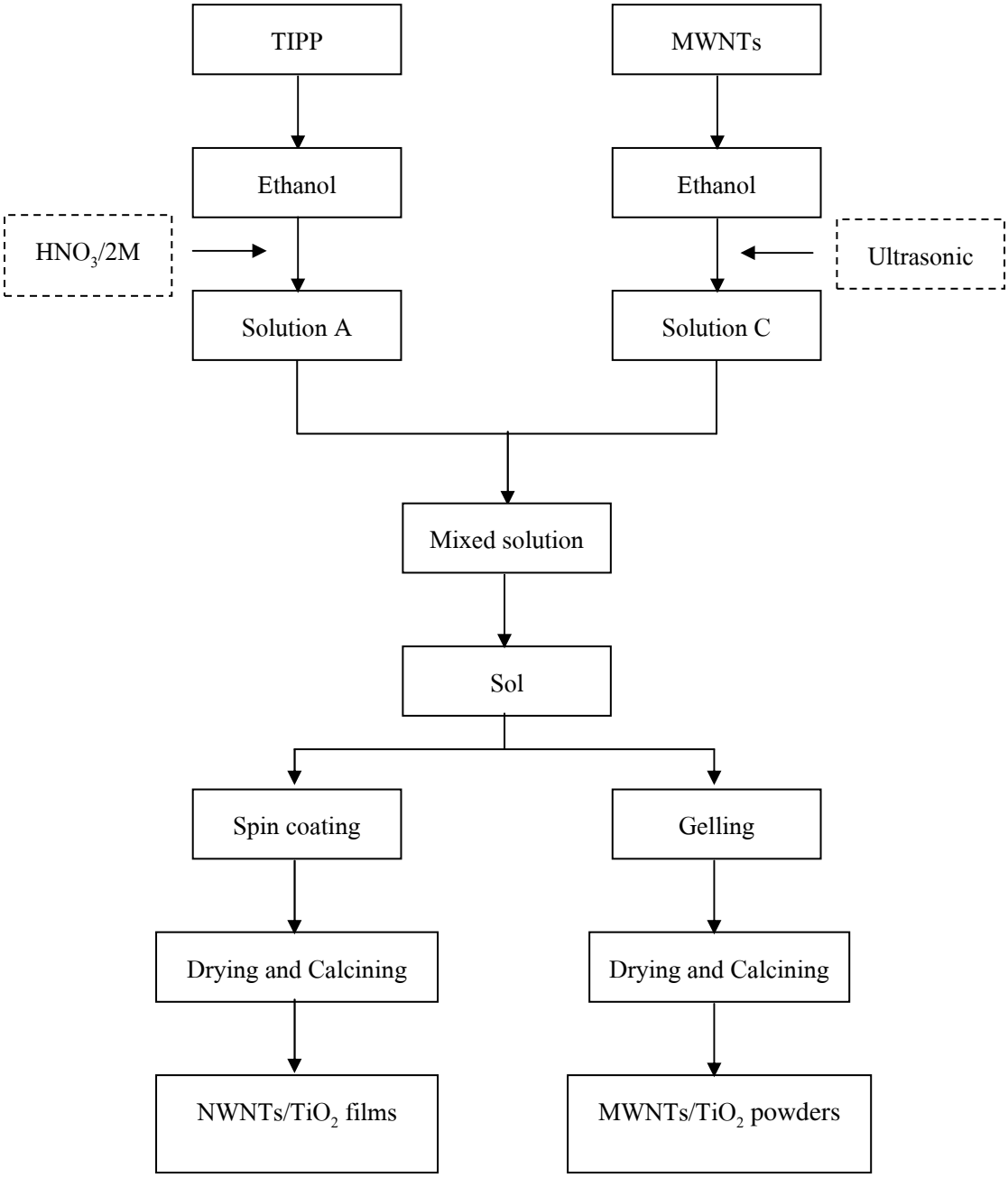

Figure 3.3 Flowchart of the synthesis of MWNTs/TiO_2 powders and thin films.

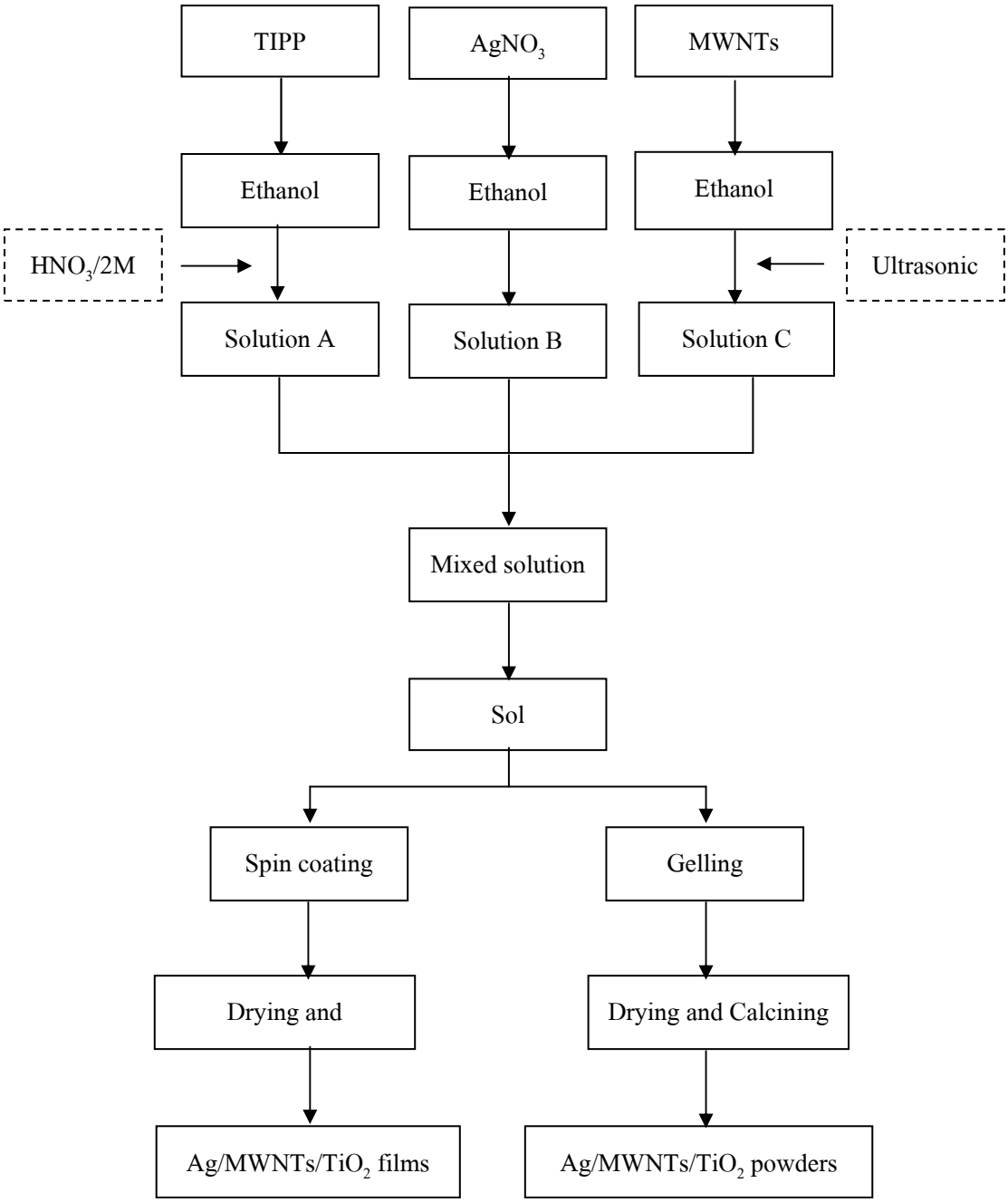

Figure 3.4 Flowchart of the synthesis of Ag/MWNTs/TiO_2 powders and thin films.

3.2 Characterization of pure TiO_2, Ag/TiO_2, $MWNTs/TiO_2$ and $Ag/MWNTs/TiO_2$ powders and thin films

3.2.1 Differential thermal analyzer (DTA)

The crystal phase and phase transformation of the synthesized pure TiO_2, Ag/TiO_2, $MWNTs/TiO_2$ and $Ag/MWNTs/TiO_2$ powders were characterized by DTA (Perkin-Elmer, DTA 7 with the temperature range of 50-1250 ^{o}C at the heating rate of 10 ^{o}C /min).

3.2.2 X-ray diffraction (XRD)

The crystalline phase, average crystallite size and phase content of the calcined pure TiO_2, Ag/TiO_2, MWNTs/ TiO_2 and Ag/MWNTs/ TiO_2 powders were determined from X-ray diffraction (Phillips, Cu-k_{∞} radiation of wave length 1.5418 Å). Pure TiO_2 and TiO_2 composite thin films were determine from X-ray diffraction (RIGAKU TTRAX III, 18 kW, Japan glancing angle X-ray diffraction = 0.4). The data were taken in the range of 10-90 (2θ). The phase content was determined from XRD pattern according to the following equations. (Zhu, et al.,2005)

$$W_a = \frac{0.884\ A_a}{0.884\ A_a + A_r} \tag{3.1}$$

$$W_r = \frac{Ar}{0.884\ A_a + A_r} \tag{3.2}$$

Where W_a is the weight fractions of anatase

W_r is the weight fractions of rutile

A_a is the individually integrated intensity for anatase at plane (1 0 1)

A_r is the individually integrated intensity for rutile at plane (1 1 0)

The average crystallite size (D) were determined from the XRD pattern by Scherer's equation,

$$D = \frac{k\lambda}{\beta \cdot \cos\theta} \tag{3.3}$$

Where D is the average crystallite size (nm)

k is a constant (shape factor, about 0.9)

λ is *the* x-ray wavelength (0.15418 nm)

β is the full width at half maximum (FWHM) of the diffraction line

θ is the diffraction angle.

The values of β and θ of anatase and rutile are taken from anatase (2 0 0) and rutile (1 1 0) diffraction line, respectively. It was assumed that the FWHM of anatase (2 0 0) peak is not affected by brookite (2 3 1) peak because the integrated intensity of anatase (2 0 0).

3.2.3 Ultraviolet-visible spectrophotometer (UV-VIS)

The UV–VIS spectroscopy (UV-2401, Shimadzu, Japan.) was used to measure the absorbance of the synthesized powder and to confirm the band gap of pure TiO_2, Ag/TiO_2, MWNTs/ TiO_2 and Ag/MWNTs/ TiO_2. The dry-pressed disk samples and absorption spectra of $BaSO_4$were used as the referent specimen. The band energy of TiO_2 is easily to measure. The onset absorbance were determined by the linear extra- polation of the steep part of the UV absorption toward the base line as shown in Figure 3.5 (Zhang et al. 2000). The corresponding band gap energy of sample can be calculated from the following Plank's equation:

$$E_g = \frac{hc}{\lambda} = \frac{1{,}240}{\lambda} \tag{3.4}$$

Where E_g is the band gap energy (eV)

h is Plank's constant (6.67×10^{-34} j.s.)

c is velocity of light (3×10^{8} m/s)

λ is the light wavelength at the onset of absorption

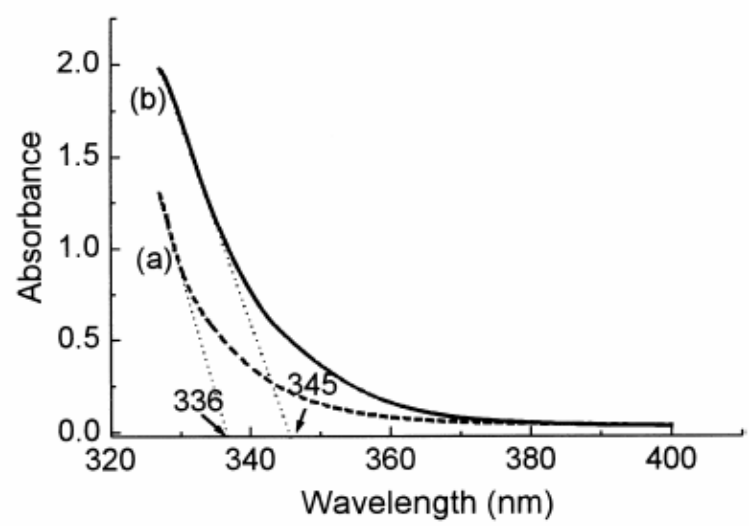

Figure 3.5 show the UV-VIS onset of absorption spectra

3.2.4 Fourier-transformed infrared spectrophotometer (FT-IR)

Fourier-transformed infrared spectrophotometer (FT-IR, Bruker Equinox 55) in KBr pellets and infrared spectra were recorded in the wave length between 4000-400 cm^{-1} was used to assess the presence of fucntional groups in different TiO_2.

3.2.5 Surface area/pore size measurement

The specific surface area and pore size were determined by the BET method (SA3100, Coulter, U.S.A.) by using nitrogen as adsorbed.

3.2.6 Scanning electron microscope (SEM)

The surface morphology and size of the pure TiO_2, Ag/TiO_2, $MWNTs/TiO_2$ and $Ag/MWNTs/TiO_2$ were observed with a SEM (JSM-5800 LV, JEOL).

3.2.7 Energy dispersive x-ray spectroscopy (EDS)

The dispersion of Ti in the film was characterized by EDS (EDS: Oxford ISIS 300) attached to the scanning electron microscope.

3.2.8 Surface roughness and film thickness measurements

The surface roughness and film thickness of pure TiO_2, Ag/TiO_2, $MWNTs/TiO_2$ and $Ag/MWNTs/TiO_2$ thin films were measured by atomic forced microscope (AFM) for an area of 1 x 1 μm^2.

3.3 Photocatalytic activity test of pure TiO_2, Ag/TiO_2, $MWNTs/TiO_2$ and $Ag/MWNTs/TiO_2$ thin films

The photocatalytic activity experiments on pure TiO_2, Ag/TiO_2, $MWNTs/TiO_2$ and $Ag/MWNTs/TiO_2$ thin film for the degradation of methylene blue with the concentrate of 2 mg/l under radiation of a UV light of 20x3 W power with the intensity of 4.77 mW/cm^2 in dark chamber. The area of thin film of photocatalyst used for this experiment was 49 cm^2. Sample of 5 ml was sampled every 1 h. and the concentrate of methylene blue was determined by UV-visible spectroscopy (8453, Hewlett Packard) at wave length of 665 nm. The effect of calcinations temperature and doping content of TiO_2 thin films were examined in terms of the decomposition of methylene blue solution. The photocatalytic decomposition rate was calculated from the graph plotted between the ratio of concentration of methylene blue solution at the treatment time (t) to the initial concentration (C/C_0) with UV and fluorescent irradiation time.

3.4 Contact angle measurement

Hydrophilic property of thin film was measured in terms of contact angle of water dropet on the film using a contact meter of CAM-PLUS Tantec company. The smaller contact angle shows the higher hydrophilic property of the film.

CHAPTER 4

Results and Discussion

The pure TiO_2, Ag/TiO_2, $MWNTs/TiO_2$ and $Ag/MWNTs/TiO_2$ composites were prepared by sol-gel method and spin coating process. In this work, the effect of Ag and MWNTs doping content and temperature calcinations on crystallite size, phase content, photocatalytic activity rate and hydrophilic property were investigated. The samples were characterized by DTA, XRD, FT-IR, BET, SEM, EDS, and AFM. Photocatalytic activity was determined by degradation methylene blue solution in dark box. The concentration of methylene blue solution under the irradiation of UV and visible light after degradation for a certain time was determined by UV-VIS spectrophotometer.

In this present work, the titanium dioxide composite were prepared by sol-gel process from titanium isopropoxide (Ti $[OCH(CH_3)_2]_4$) and ethanol were used as a precursor and a solvent, respectively. Dropping nitric acid into solution mixed for 1 h. The pH value of the solution was adjusted to be about 3. The sol was kept for 24 h for slow hydrolysis at room temperature to be a clear solution shown in Figure 4.1a. This sol was kept in a room temperature for several days to allow gel form as shown in Figure 4.1b. The gel was dried at 100^{o}C for 24 h and calcined at the temperature of 500^{o}C to form powder as illustrated in Figure 4.1c.

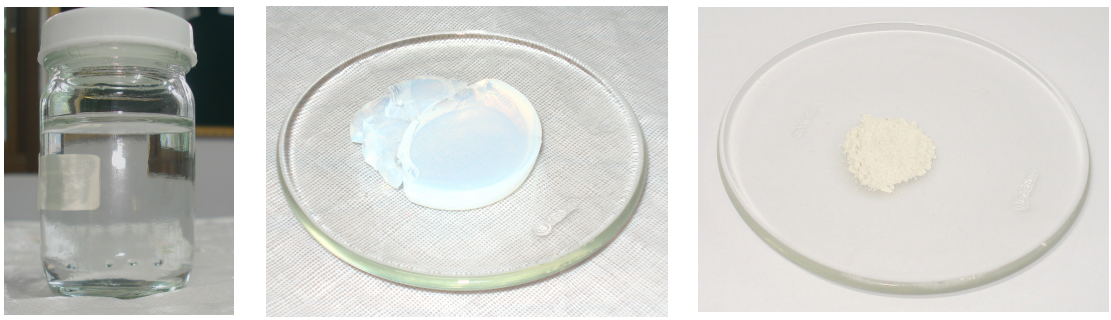

a b c

Figure 4.1 Illustrations of a) pure titanium dioxide sol, b) pure titanium dioxide gel and c) powder after calcinations at the temperature of 500^{o}C

For the case of Ag doped TiO_2 in this work, the calcined powder was changed from gray to black color. For thin films, they appear translucent on surface of ceramic tile.

In case of MWNTs doped TiO_2, the powders posses black to gray color (Figure 4.2). when it was calcined at the temperatures of 400 ^{o}C and 500-600 ^{o}C, respectively. Gasification took place as the calcinations temperature a at higher than 500 ^{o}C and the color of the sample turned to gray. (Wang et al. 2007)

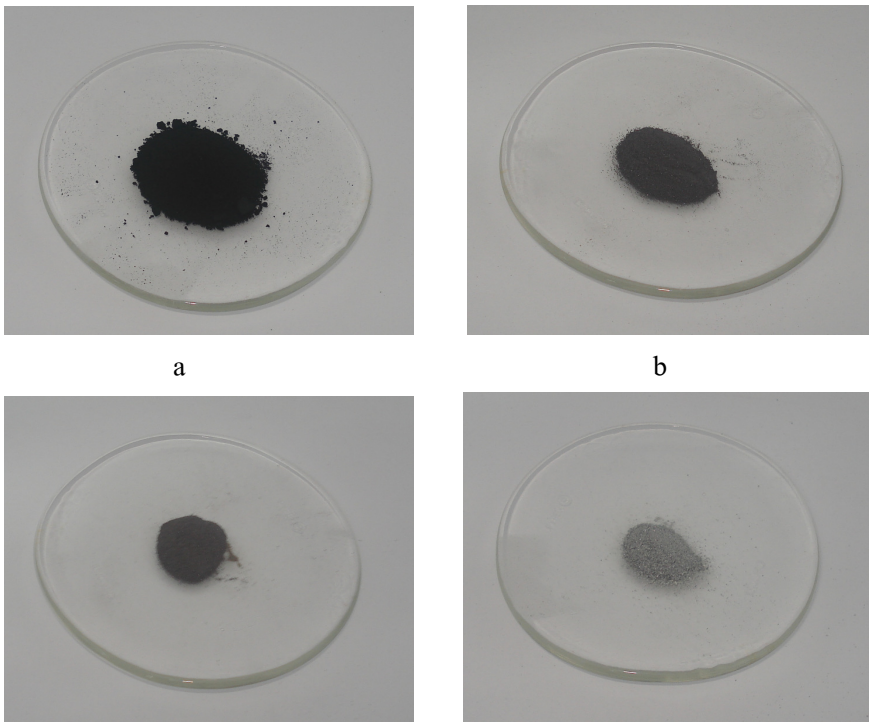

Figure 4.2 Illustration of MWNTs and 1MWNTs/TiO_2, a) MWNTs and 1MWNTs/TiO_2 calcined at the temperatures of b) 400 ^{o}C, c) 500 ^{o}C and d) 600 ^{o}C

4.1 Effect of dopant and calcinations temperature on phase transformation and crystallite size of TiO_2 powder and film

Powders from gel the solutions were dried at 100 ^{o}C in air for 24 h and analyzed by DTA at the temperature range of 50-1200 ^{o}C and heating rate of 10^{o}C /min. Figure 4.3a shows the thermal analysis curve of pure TiO_2 powder. The first endothermic peak at the temperature of 117^{o}C is attributed to the adsorptions of water and alcohol (Huang et al., 2006). The second exothermic peak at the temperature of 423^{o}C is attributed to the oxidation of the organic substances and the amorphous to anatase phase transformation. For 1Ag/TiO_2 composite, the first

peak is endothermic peak at the temperature of 127^{o}C attributed to the desorption of water and alcohol, the second peak at the temperature 161^{o}C is attributed to the reaction of hydroxyl containing organics and nitrate ions and the third peak at the temperature of 413 ^{o}C is exothermic peak attributed to the amorphous to anatase phase transformation and it exhibits good crystalline because Ag accelerates amorphous to be an anatase phase transformation as shown in Figure 4.3b. These results are in accordance with the values found in the literature of Harizano et al. 2001 and Sen et al. 2005. For 1MWNTs/TiO_2 powder shown in Figure4.3, first peak at the temperature of 108 ^{o}C is endothermic peak and the second peak at the temperature of 219 ^{o}C is exothermic peak attributed to the evaporation of water, alcohol solvent and the decomposition of TiO_2 precursor during TiO_2 crystallization process(Xia et al., 2007). For this sample, it could be seen that the peak area of this composite is larger than that of pure TiO_2. This means that these synthesized 1MWNTs/TiO_2 containing more amorphous phase than pure TiO_2. Endothermic peak at the temperature 127 ^{o}C shown in Figure4.3d is attributed to the adsorptions of water and alcohol and exothermic peak at the temperature of 417 ^{o}C is attributed to the amorphous phase transformed to anatase phase.

Result of Fourier transform infrared spectroscopy for TiO_2 degussa P25, pure TiO_2 before calcinations, pure TiO_2, 1Ag/TiO_2, 1MWNTs/TiO_2 and 1Ag/1MWNTs/TiO_2 calcined at the temperature of 500^{o}C in air for 1h are shown in Figure4.4. Figure 4.4a shows FT-IR spectra of TiO_2 degussa P25. The spectra are observed at the wavenumber around 3446, 2922, 2853, 1633 and 597. The band at 3446 cm^{-1} represents the stretching vibrations of the -OH bond (Wang et al., 2000). The spectra at 2922 and 2853 cm^{-1} are attributed to the C-H bond of the organic compounds (Yang et al. 2006 and Harizano et al., 2001). The spectrum at 1633 cm^{-1} is vibration line of the O-H bond of hydroxyl group. (Yang et al., 2006) and the spectrum at 597 cm^{-1} refers to the anatase phase of TiO_2 (Zhang et al., 2001). Figure 4.4b shows several spectra of pure TiO_2 before calcinations. The wavenumber of 3448 cm^{-1} band represents to-OH bond of water (Wang et al., 2000). The spectrum at 2923 is attributed to the C-H bond of organic compound (Harizano et al., 2001). The spectrum at 1625 cm^{-1} is O-H bond of hydroxyl group (Yang et al., 2006). The spectrum in the 1383 cm^{-1} exhibits the presence of nitrates, which were added as HNO_3 during the acidification in the sol–gel process. (Yoon et al., 2006) and the 614 cm^{-1} spectrum indicates the anatase phase of TiO_2 (Zhang et al., 2001). The spectra of pure TiO_2 calcinations at 500^{o}C are shown in Figure 4.4c. This Figure shows three peaks observed such as 3413, 1626 and 535 cm^{-1}.

The spectra of at 3413 and 1626 cm^{-1} are -OH bond of water and O-H bond of hydroxyl group, respectively. (Wang et al., 2000 and Yang et al., 2006). The 535 cm^{-1} spectrum is Ti-O bond of anatase phase (Yang et al. 2006). For spectra of $1Ag/TiO_2$ calcined at the temperature of 500^{o}C shown in Figure 4.4d the 3419, 2924 and 1628 cm^{-1} spectra are -OH bond of water, C-H bond of organic compound and O-H bond of hydroxyl group, respectively (Wang et al., 2000 and Yang, et al. 2006) The 1410 spectrum is vibrations of C-H in CH_2 and CH_3 organic material and the spectrum at 579 cm^{-1} is the anatase phase (Zhang et al., 2001).

a) Pure TiO_2

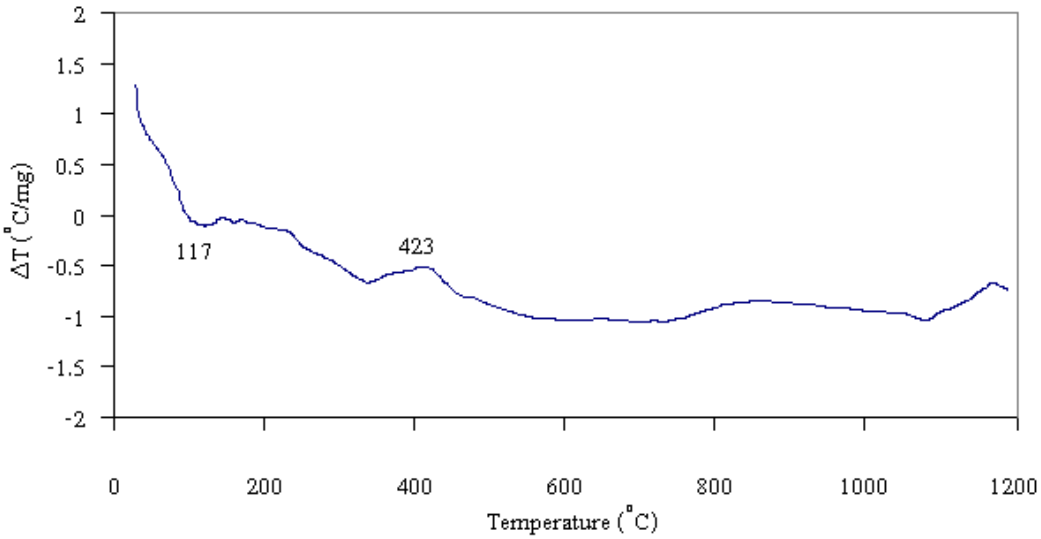

b) $1Ag/TiO_2$

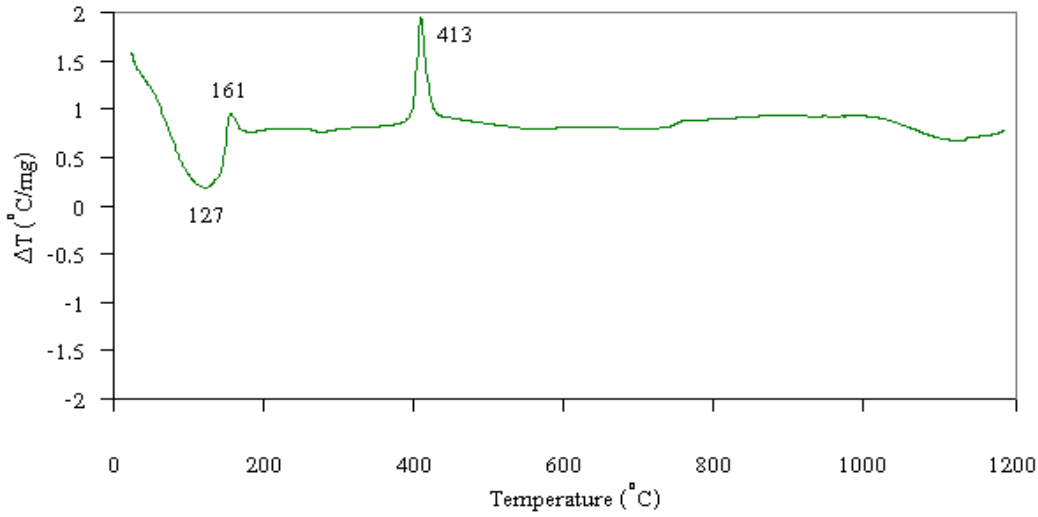

c) 1MWNTs/TiO_2

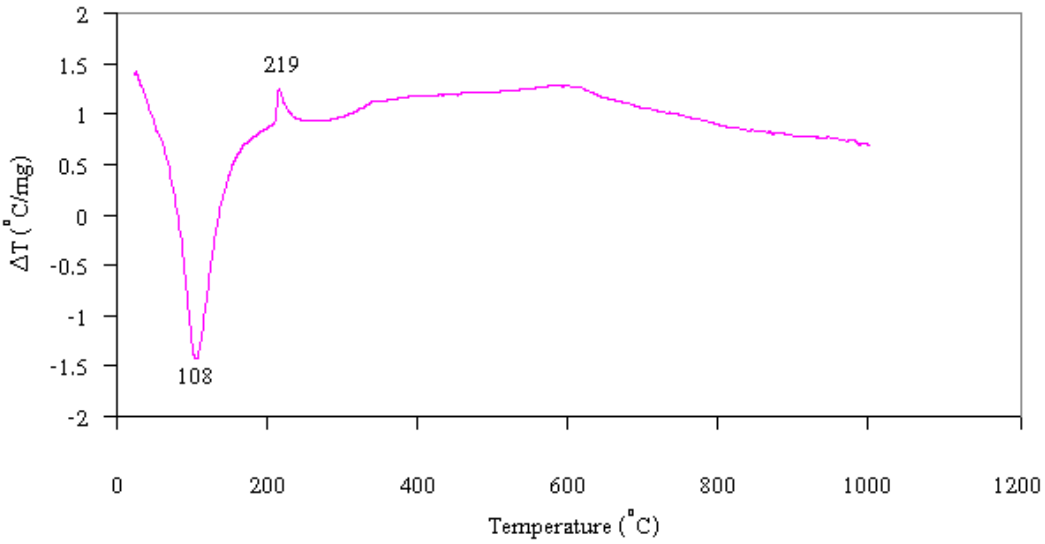

d) 1Ag/1MWNTs/TiO_2

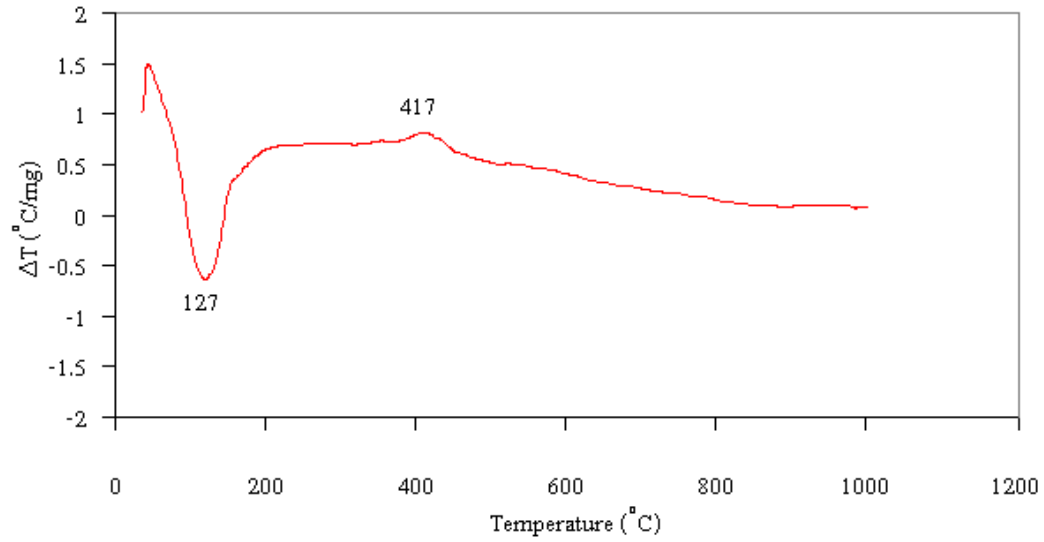

Figure 4.3 DTA curve of a) Pure TiO_2, b) 1Ag/TiO_2, c) 1MWNTs/TiO_2 and d) 1Ag/1 MWNTs /TiO_2

Figure 4.4e shows the spectra of 1MWNTs/TiO_2 calcined at the temperature of 500°C. The 3426cm^{-1} spectrum is attributed to -OH bond of water and the 2921 and 2853cm^{-1} spectra are C-H bond of the organic compounds (Yang et al., 2006 and Harizano et al., 2001). The 1629 and 521cm^{-1} spectra are attributed to O-H bond of hydroxyl group and Ti-O bond of anatase phase, respectively (Yang et al., 2006). Figure 4.4f shows the spectra of 1Ag/1MWNTs/TiO_2 calcined at the temperature of 500°C. The spectra at 3417, 2921, 1632 and 490 cm^{-1} are -OH bond

of water, the C-H bond of the organic compounds, O-H bond of hydroxyl group and the anatase phase. (Wang et al., 2000 Yang et al., 2006 and Harizano et al., 2001). Table 4.1 summarizes the FT-IR analysis of TiO_2 and TiO_2 doped with additives.

a) TiO_2 degussa P25

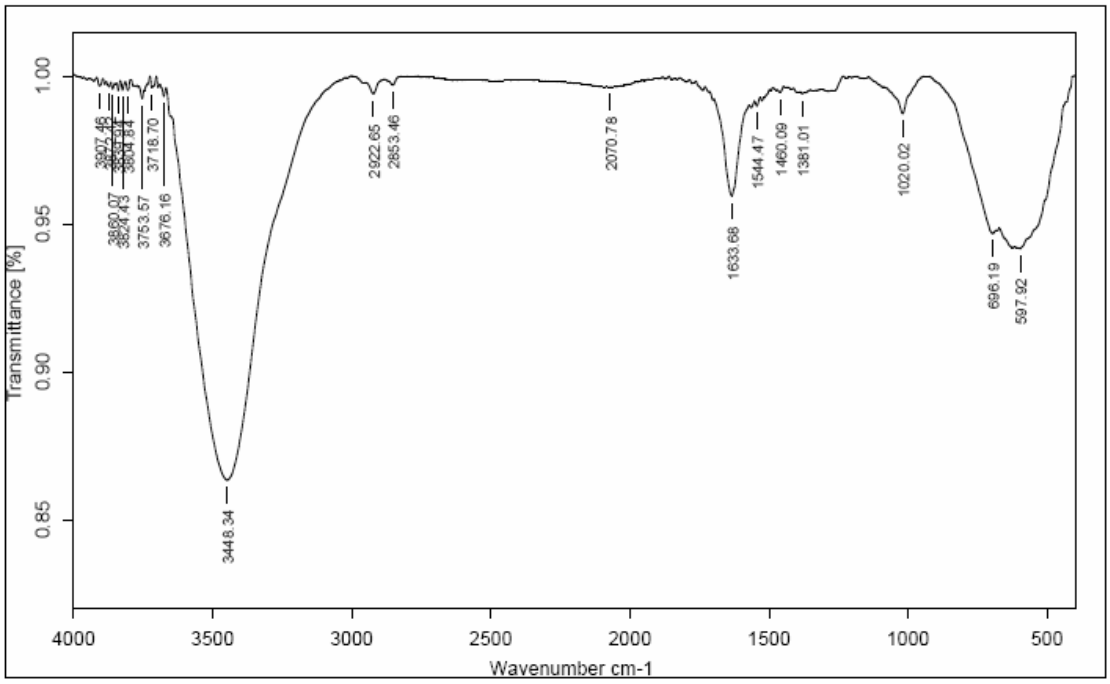

b) Pure TiO_2 before calcinations

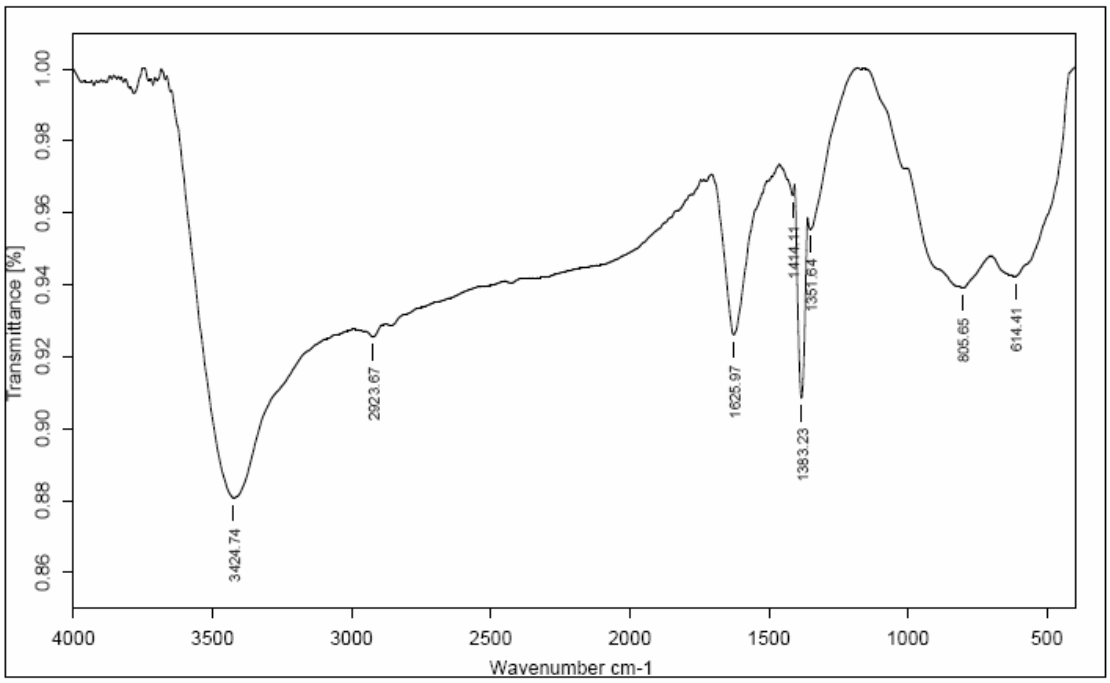

c) Pure TiO_2 _ 500°C

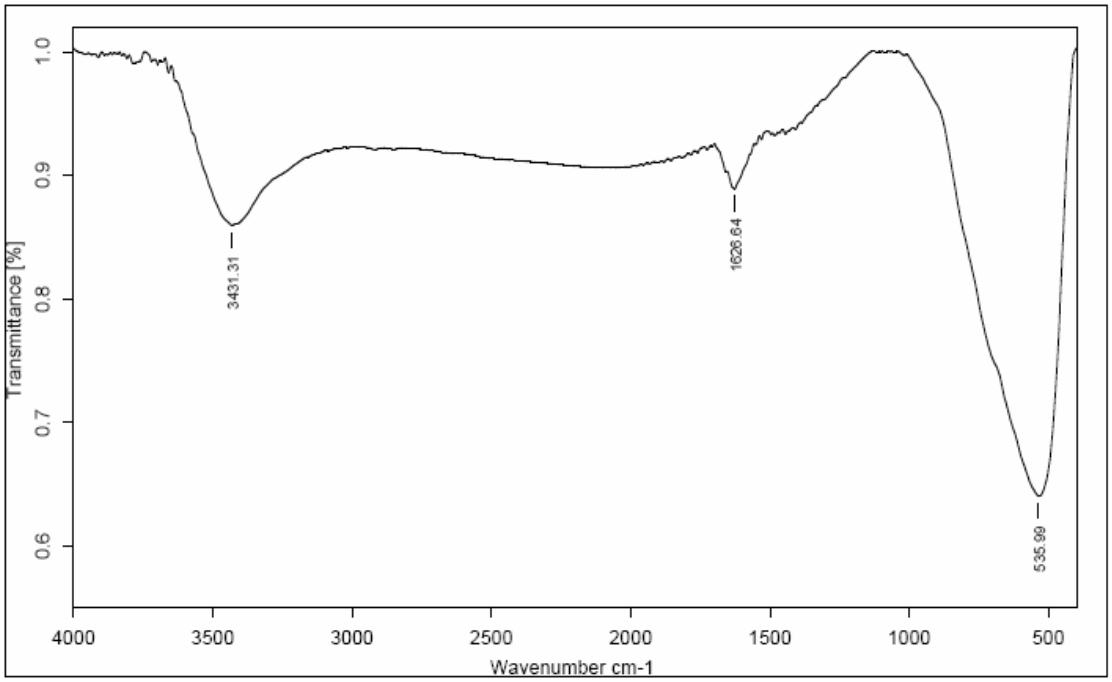

d) 1Ag/TiO_2_ 500°C

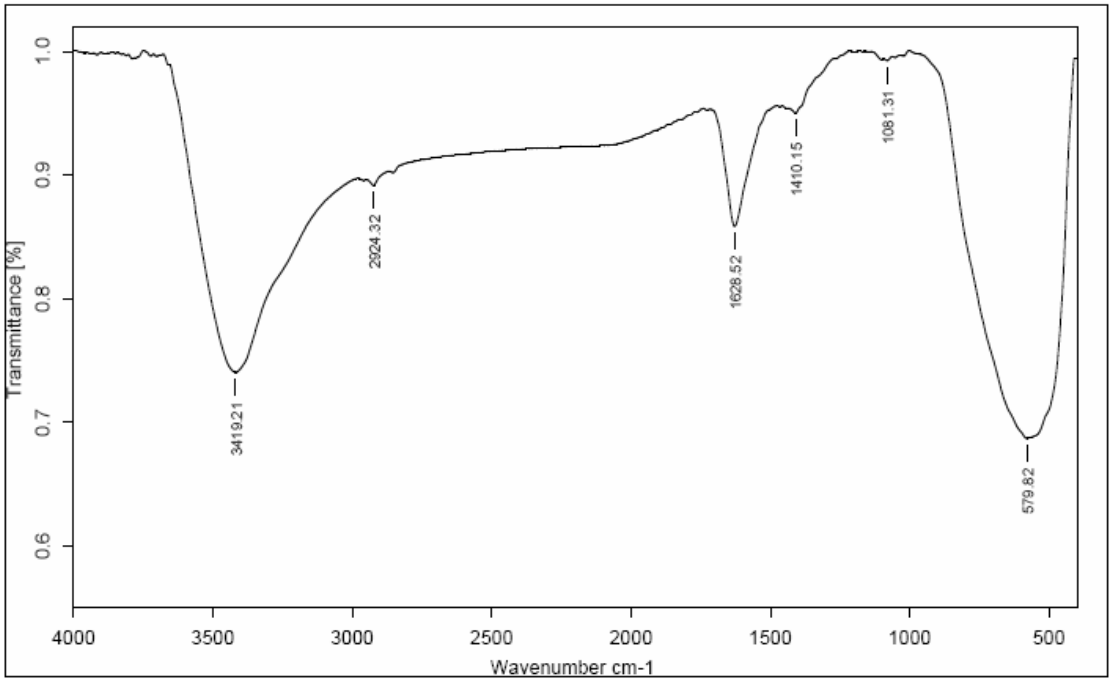

e) 1MWNTs/TiO_2_ 500^oC

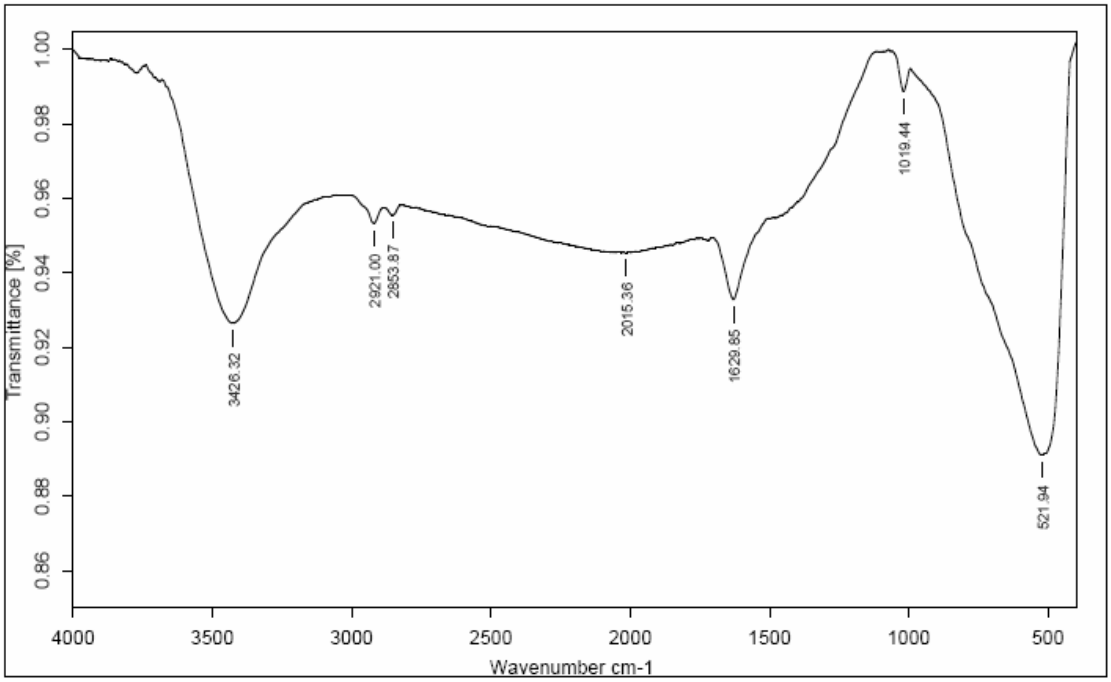

f) 1Ag/1MWNTs/TiO_2 _ 500^oC

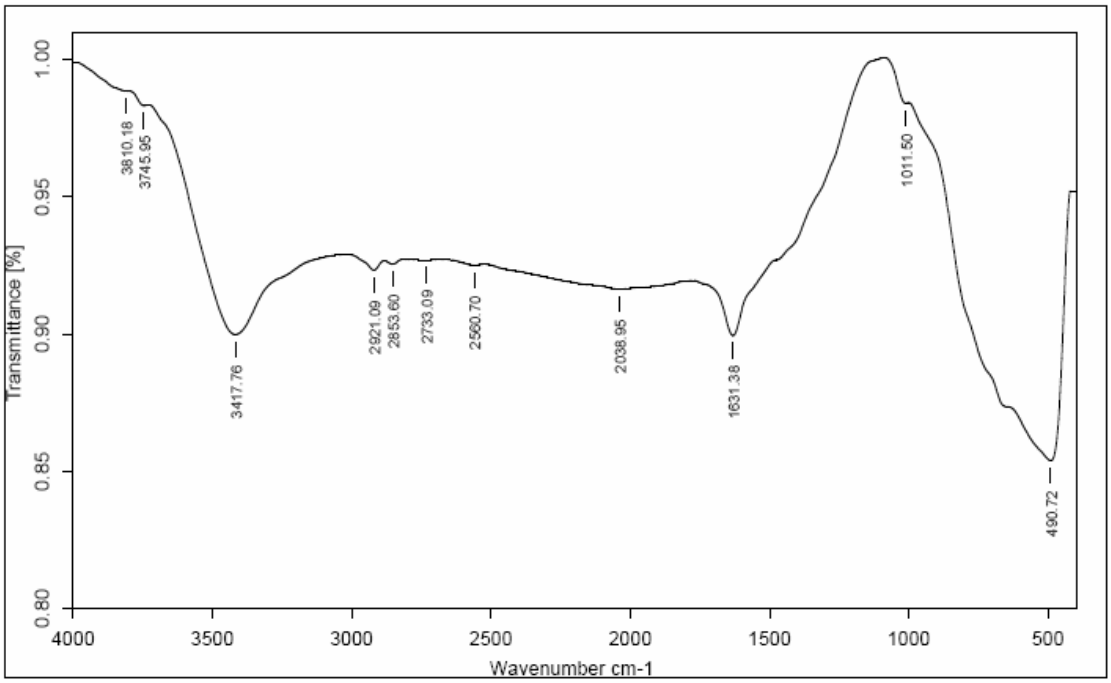

Figure 4.4 FT-IR spectra of a) TiO_2 degussa P25, b) pure TiO_2 before calcinations, c) pure TiO_2, d) 1Ag/TiO_2, e) 1MWNTs/TiO_2 and f) 1Ag/1MWNTs/TiO_2 calcined at the temperature of 500^oC in air for 1h.

Table4.1 FT-IR analysis of TiO_2 and TiO_2 doped with additives

Sample	Wavenumber (cm^{-1})	Assignment	Functional group/molecule	Reference
TiO_2 degussa P25	3446	-OH stretching	H_2O,Ti-OH and NH^{4+}	Wang et al. 2000
	2922	C-H bond	organic compounds	Yang et al. 2006
	2853	C-H bond	organic compounds	Harizano et al. 2001
	1633	O-H bond	hydroxyl group	Yang et al. 2006
	597	Ti-O stretching	TiO_2(anatase)	Zhang et al. 2001
pure TiO_2	3448	-OH stretching	H_2O,Ti-OH and NH^{4+}	Wang et al. 2000
	2923	C-H bond	organic compounds	Yang et al. 2006
	1625	O-H bond	hydroxyl group	Yang et al. 2006
	1383	NO_3	HNO_3	Arana et al. 2004
	614	Ti-O stretching	TiO_2(anatase)	Zhang et al. 2001
pure TiO_2_500^oC	3413	-OH stretching	H_2O,Ti-OH and NH^{4+}	Wang et al. 2000
	1626	O-H bond	hydroxyl group	Yang et al. 2006
	535	Ti-O bond	TiO_2(anatase)	Yang et al. 2006
1Ag/ TiO_2_500^oC	3419	-OH stretching	H_2O,Ti-OH and NH^{4+}	Wang et al. 2000
	2924	C-H bond	organic compounds	Yang et al. 2006
	1628	O-H bond	hydroxyl group	Yang et al. 2006
	1410	C-H bond	CH_2 and CH_3	Arana et al. 2004
	579	Ti-O stretching	TiO_2(anatase)	Zhang et al. 2001
1MWNTs/ TiO_2_500^oC	3426	-OH stretching	H_2O,Ti-OH and NH^{4+}	Wang, et al. 2000
	2921	C-H bond	organic compounds	Yang et al. 2006
	2853	C-H bond	organic compounds	Harizano et al. 2001
	1629	O-H bond	hydroxyl group	Yang et al. 2006
	521	Ti-O stretching	hydroxyl group	Zhang et al. 2001
1Ag/1MWNTs/ TiO_2_500^oC	3417	-OH stretching	H_2O,Ti-OH and NH^{4+}	Wang, et al. 2000
	2921	C-H bond	organic compounds	Yang et al. 2006
	1632	O-H bond	hydroxyl group	Yang et al. 2006
	490	Ti-O stretchin	hydroxyl group	Harizano et al. 2001

The XRD peak for pure TiO_2, Ag/TiO_2, $MWNTs/TiO_2$ and $Ag/MWNTs/TiO_2$ powders and flms exhibit anatase phase reflection plane (101) at $2\theta \approx 25.5$ and rutile reflection plane(110) at $2\theta \approx 27.5$. The crystallite size estimated from the line broadening of anatase reflection plane (200) at $2\theta \approx 48.0$ and rutile reflection plane (110) at $2\theta \approx 27.5$ by Sherrer's equation.

4.1.1 Pure TiO_2 powder

Figure 4.5 shows the XRD patterns of pure TiO_2 powder calcined at different temperatures from 400 to 800 ^{o}C. Peaks marked "A" and "R" correspond to anatase and rutile phases, respectively. It can be seen that the anatase single phase starts to appear when the pureTiO_2 calcined at the temperature range of 400 ^{o}C -500 ^{o}C and anatase phase will transform to rutile at above 500 ^{o}C. At the same time, the intensity of anatase phase increase with an increase temperature from 400 ^{o}C-500 ^{o}C and decreases at the temperature of 600 ^{o}C while the and intensity of rutile increases. Therefore, these samples cacined at the temperature of 600 ^{o}C-700 ^{o}C are the mixture of anatase and rutile phases. At these conditions, the mixed phase contain anatase about 64 and 23%, respectively (Table 4.4.). Furthermore, a completed transformation can be achieved at 800 ^{o}C. Data of crystalline phases at various conditions are shown in Table 4.2.

The crystallite size of anatase and rutile of pure TiO_2 are summarized in Table 4.3. The crystallite size of pure TiO_2 seems to increase with an increase in calcinations temperature. The single phase anatase has the crystallite size of about 14~15 nm when the calcinations temperature is 400~500 ^{o}C. The average crystallite size increases to about 42.9 nm at the calcinations temperature of 600^{o}C. The crystallite size of rutile phase increases from 41.6 nm to 55.4 nm when temperature increases from 600 ^{o}C to 800 ^{o}C, respectively. It is due to the grain growth of TiO_2 induced by higher calcinations temperature.

4.1.2 Ag/ TiO_2 powder

Figure 4.6 shows the XRD patterns of Ag/TiO_2 powders calcined at different temperature. It can be seen that the anatase phase starts to appear while the Ag/TiO_2 powders are calcined at 400 ^{o}C. It could also be seen that the peak area of anatse calcined at 400 ^{o}C larger than that of 500 ^{o}C. This means that at 400 ^{o}C, these samples contain more amorphous phase than other phases. The calcinations temperature seems to control phase transformation of TiO_2, anatase phase can be obtained as the calcinations temperature range of 400-500 ^{o}C (Figure 4.6a-b) while mixed phase of anatase and rutile can be obtained at 600 ^{o}C (Figure4.6c). Ag seems to promote anatase phase at low calcinations temperature of 400 ^{o}C and 500 ^{o}C due to its good thermal conductivity. More amount of Ag content in TiO_2 leads to more energy acceleration of anatase phase. However, at higher calcinations temperature of 600 ^{o}C, anatase seems to decrease and rutile phase seems to increase with an increase in Ag content.

Since Ag/TiO_2 powders calcined at 400 °C can be seen as an amorphous phase therefore the size of this condition can not be determined. For anatase phase of Ag/TiO_2 powders calcined at 500 °C, it can be seen that the crystallite size of 0.5–3 mol%Ag about 29.5 nm. and it decreases to about 17.7 nm when Ag content increases to 4-5%.

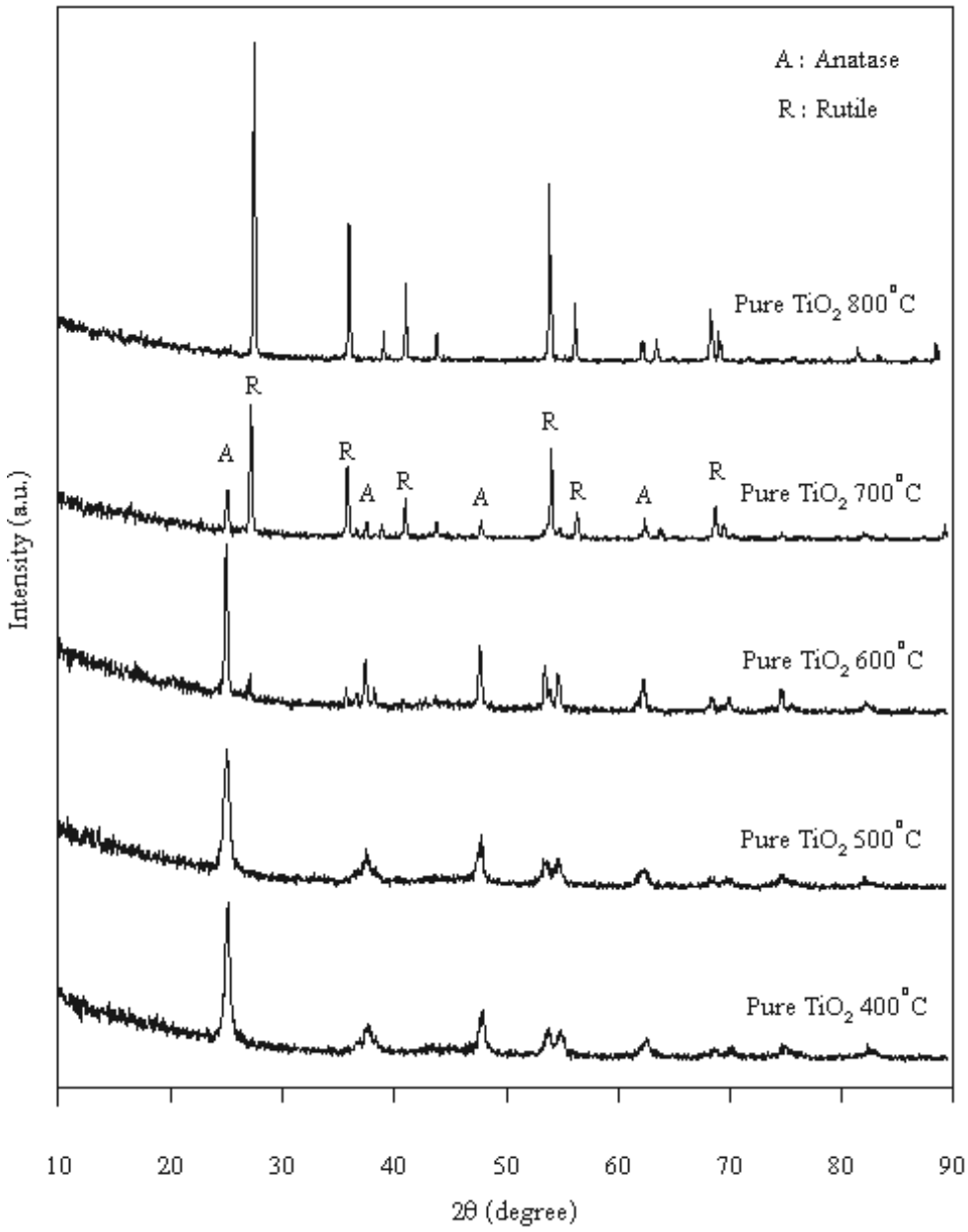

Figure 4.5 XRD patterns of pure TiO_2 calcinations at the temperatures of 400 °C, 500 °C, 600 °C, 700 °C and 800 °C

For calcining at 600°C (Figure 4.6c), it was found that, the phase content of anatase seems to increase with an increase in Ag addition from 0~2% and its crystallite size

decreases with an increase in Ag content. For the TiO_2 powder with 1%Ag doped, the smallest crystallite size was found to be about 25.3 nm. However, the intensity of rutile phase, the crystallite size and crystal phase increase when Ag is doped into TiO_2 more than 3%. Moreover, it was seen that the higher the Ag concentration, the lower the temperature at which the anatase to rutile transformation occurs. The TiO_2 phase transformation can be attributed to the following three facts. Firstly, the anatase grain size decreasing, the total boundary energy for TiO_2 powder increases. The driving force for rutile grain growth then increases and the anatase to rutile phase transformation is promoted. Secondly, because the radius of Ag^+ ion (ca. 126 pm) is much larger than that of Ti^{4+} ion (ca. 68 pm), the Ag^+ ions introduced by the sol-gel process could not enter into the lattice of anatase phase to form a stable solid solution. During the drying and calcination process with the elimination of liquids and organic substance and the crystallization of anatase phase, the uniformly dispersed Ag^+ ions would gradually migrate from the volume of anatase grains to the surface and further to the surface of the TiO_2 powder. The density of surfaces defects at the surface of anatase grains then increases, which favors the rutile nucleation. And thirdly, during drying and calcining process Ag^+ ions spreading on the surface anatase grains would gradually be reduced to Ag^0 were effect to start oxygen vacancies occur. The concentration of oxygen vacancies at the surface of the TiO_2 powder then increases, which facilitates the bond rupture and ionic movement necessary for the formation of the rutile phase. The anatase to rutile phase transformation is then accelerated (Chao et al., 2003).

4.1.3 MWNTs/TiO_2 powder

The XRD patterns of MWNTs/TiO_2 composite with different MWNTs content and calcinations temperature are compared in Figure 4.7. Generally, the main intensity peak of MWNTs shows at (200) plane (Jitianu et al., 2004). It no peak of MWNTs in MWNTs/TiO_2 composite because the main peak of MWNTs at (200) plane is overlapped with the main peak of anatase TiO_2 at (101) plane and their positions are so close. The crystalline extent of MWNTs is much lower than that of TiO_2, leading to the shielding of the peaks of MWNTs by those of TiO_2. Moreover, the surface of MWNTs was covered with anatase (Lee et al. 2007). The results of MWNTs/TiO_2 calcined at 400-500 ^oC, show a single anatase phase. The rutile and brookite phases of TiO_2 are not observed. When MWNTs/TiO_2 calcined at the temperature of 600 ^oC, it was found that 0.1MWNTs/TiO_2 has rutile phase about 5.59%. MWNTs/TiO_2 with 0.5 and 1wt% MWNTs

have a single anatase phase. It can be concluded that MWNTs of 0.1-1 wt% doped seem to have slight effect on phase transformation of TiO_2 calcinations at the temperature range of 400 ^{o}C-600 ^{o}C. At the calcinations temperature of 600 ^{o}C, MWNTs/TiO_2 exhibits anatase single phase compared with pure TiO_2 which exhibits the mixture of anatase and rutile phases.

a) Ag/ TiO_2_400 ^{o}C

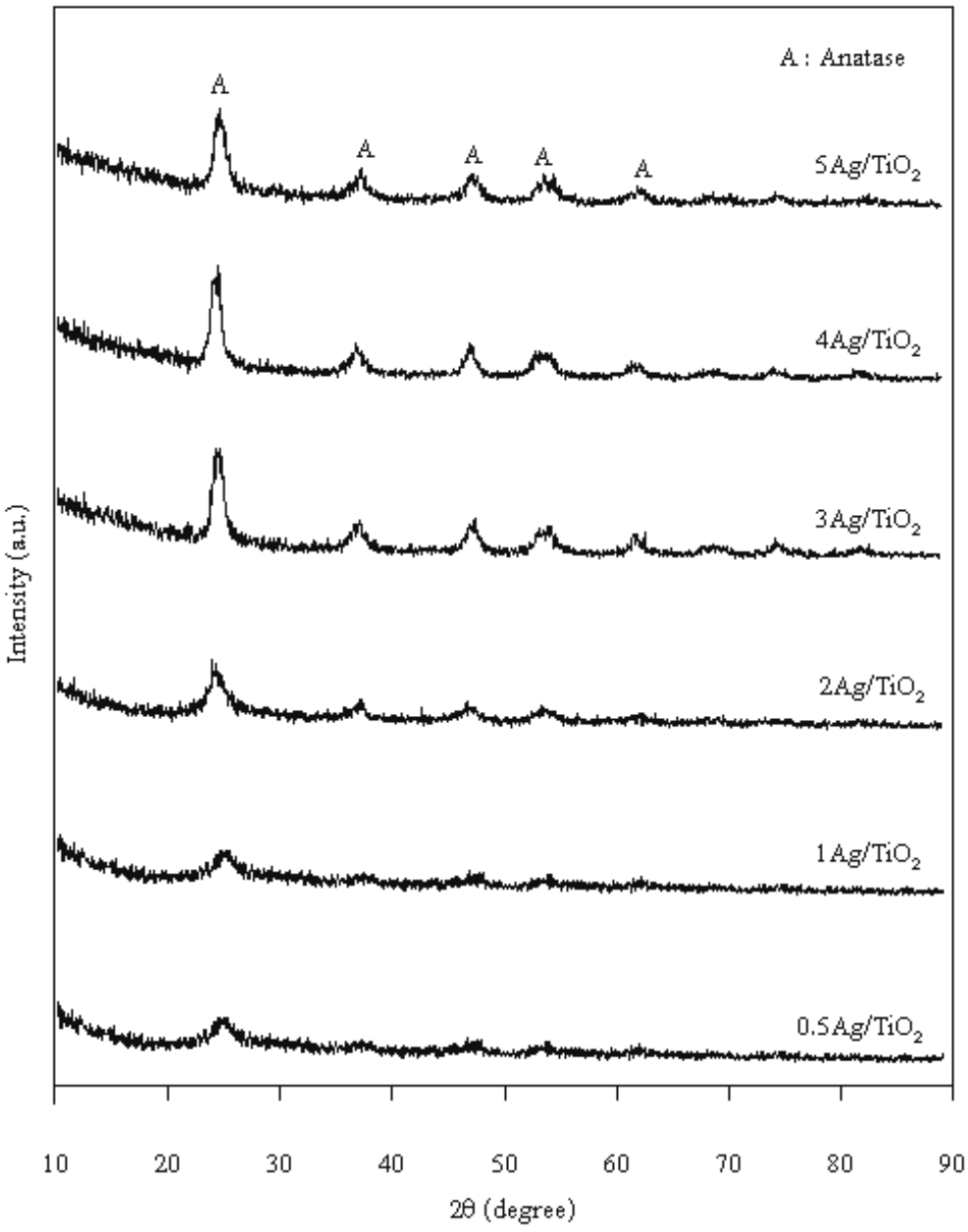

b) Ag/ TiO_2_500 ^{o}C

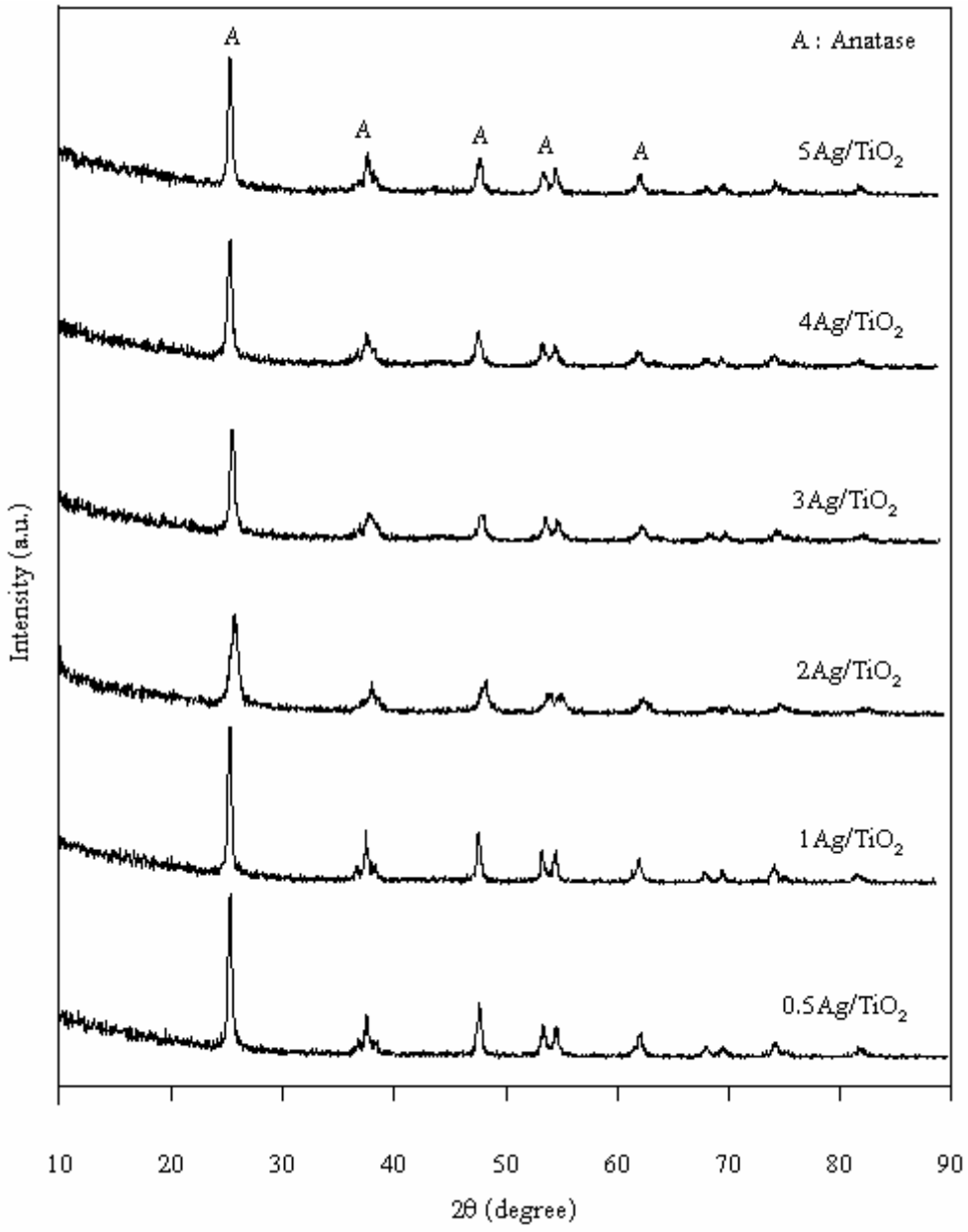

c) Ag/TiO_2_600 °C

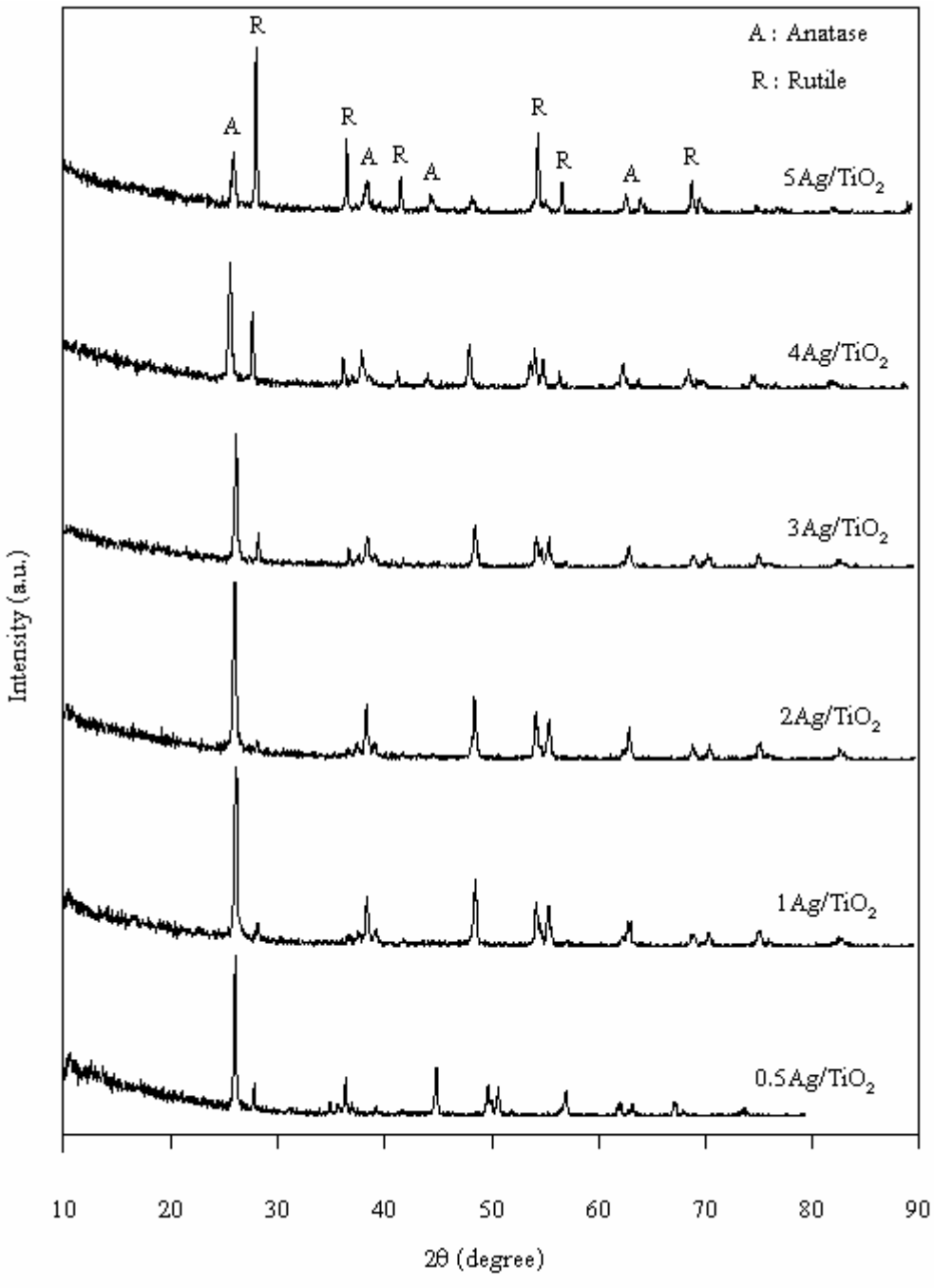

Figure4.6 XRD patterns of Ag/TiO_2 powder calcined at the temperature of a) 400 °C, b) 500 °C and c) 600 °C

The crystallite sizes estimated from the line broadening of the anatase TiO_2 of (200) reflection plane of 0.1 MWNTs/ TiO_2 calcined at the emperature of 400^{o}C was found to be about 14.7 nm and crystallite sizes decrease to 12.6 nm when MWNTs content increases to 1 wt%. For calcinations temperature at 600 ^{o}C, it was found that crystallite sizes of 0.1 MWNTs/ TiO_2 decreases from 32.45 nm to 29.5 nm when MWNTs content increases to 1 wt%. The addition of MWNTs in TiO_2 system favors the decrease of the crystallized TiO_2 on the surfaces of the MWNTs and thus prevents the TiO_2 particles from agglomeration (Xia et al. 2007)

4.1.4 1Ag/1MWNTs/TiO_2 powder

The XRD patterns of 1Ag/1MWNTs/TiO_2 with different calcinations temperature are compared and shown in Figure 4.8. In this case, it is prepared by mixing three materials in order to enhance the photocatalytic activity. It was found that all samples exhibit single anatase phase and no peak of MWNTs in Ag/MWNTs/TiO_2 composite. For the calcinations temperature of 400 ^{o}C, it was found that the peak area of anatase calcinations at the temperature of 400 ^{o}C is larger than that of calcined at 500 ^{o}C and 600 ^{o}C. These mean that the phase transformation depends on the calcinations tamperature , At the calcinations temperature of 600 ^{o}C, 1Ag/1MWNTs/TiO_2 exhibits anatase single phase compared with pureTiO_2 and 1Ag/ TiO_2, both exhibits the mixture of anatase and rutile phases. Therefore, the MWNTs in 1Ag/1MWNTs/TiO_2 has an effects to the transformation of anatase to rutile phase

The average crystallite size of 1Ag/1MWNTs/TiO_2 powders for calcining at different temperatures of 400, 500 and 600 ^{o}C were 11.0, 20.3 and 29.5 nm, respectively. They seem to be smaller than pure TiO_2. Moreover, at the calcinations temperature of 500 ^{o}C, it was found that the crystallite size in order as pure TiO_2 > 1Ag/TiO_2 > 1MWNTs/TiO_2 > 1Ag/1MWNTs/TiO_2, respectively (Table 4.3.)

a) MWNTs/ TiO_2_400 °C

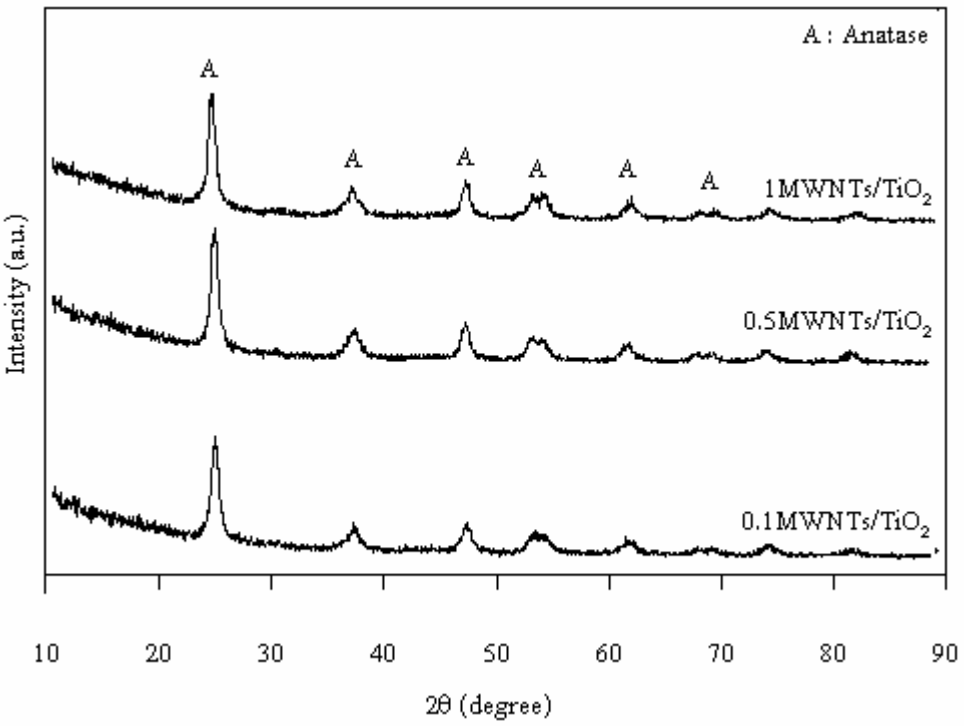

b) MWNTs/ TiO_2_500 °C

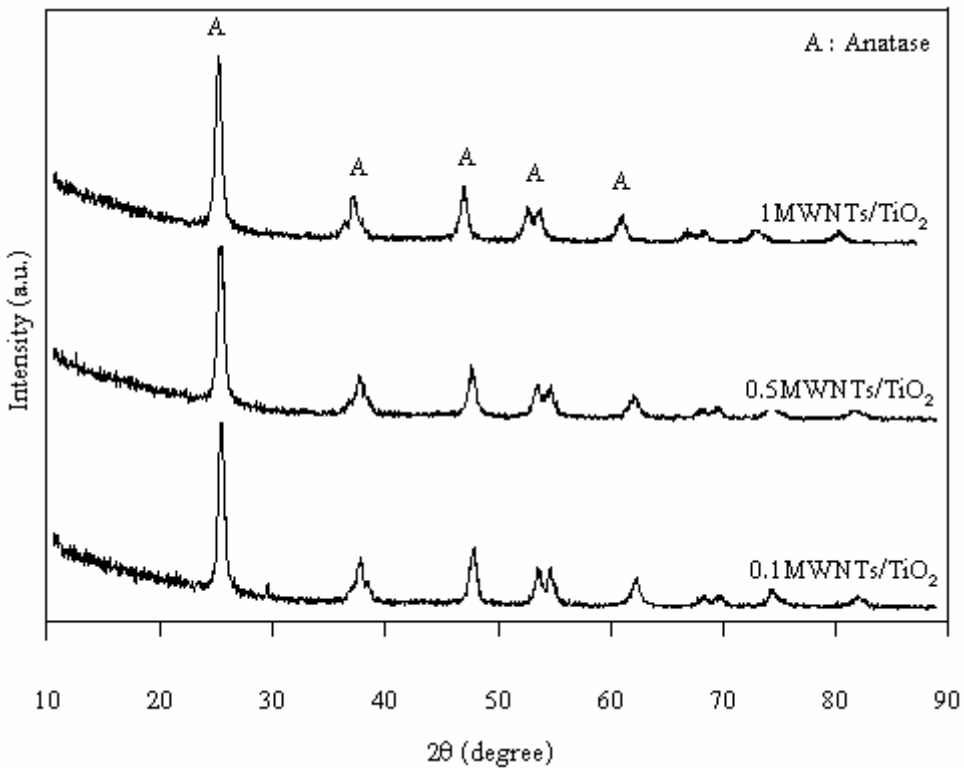

c) MWNTs/ TiO_2_600 °C

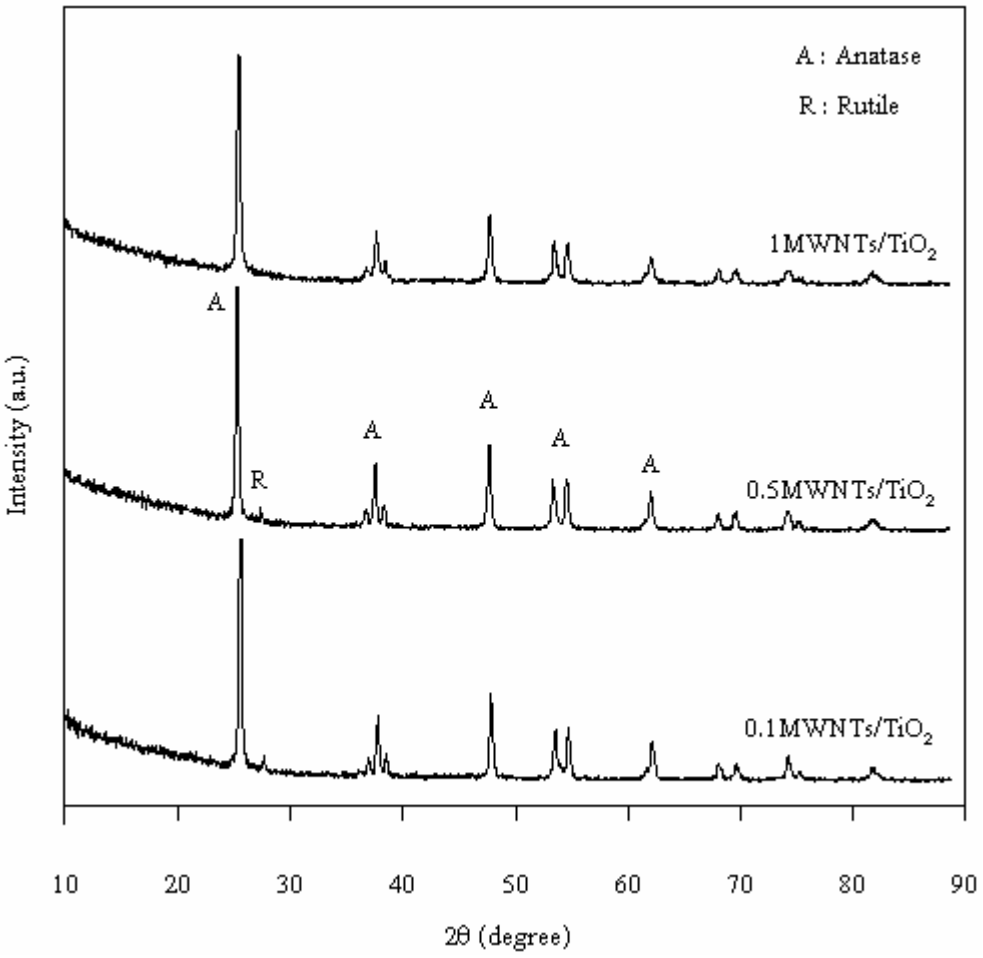

Figure4.7 XRD patterns of MWNTs/ TiO_2 powder calcined at the temperatures of a) 400 °C, b) 500 °C and c) 600 °C

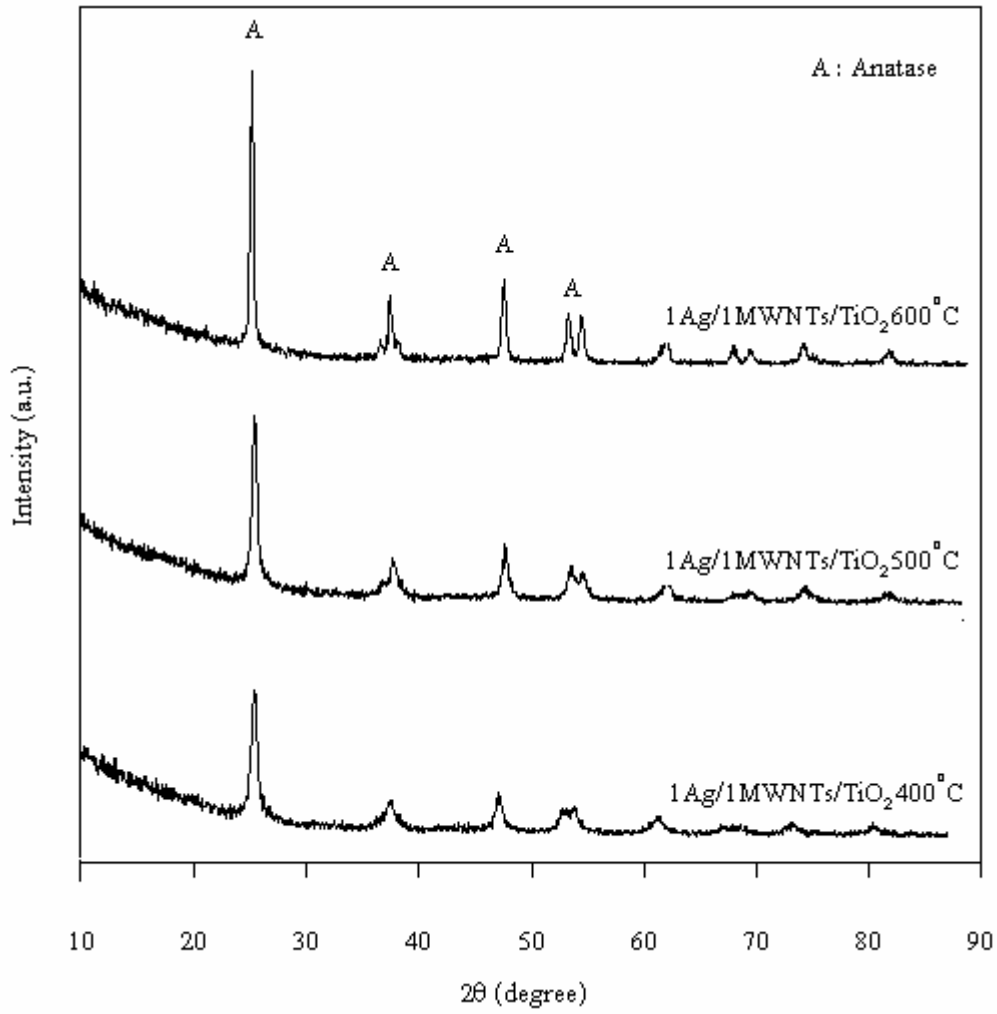

Figure4.8 XRD patterns of 1Ag/1MWNTs/ TiO_2 powders calcined at the temperatures of 400 °C, 500 °C and 600 °C

Table4.2 The crystalline phase of pure TiO_2 and TiO_2 composite powders

Samples	crystalline phase				
	Calcination Temperature (^oC)				
	400	500	600	700	800
Pure TiO_2	A	A	A+R	A+R	R
Ag/TiO_2					
$0.5Ag/ TiO_2$	Am	A	A+R	-	-
$1Ag/ TiO_2$	Am	A	A+R	-	-
$2Ag/TiO_2$	A	A	A+R	-	-
$3Ag/TiO_2$	A	A	A+R	-	-
$4Ag/ TiO_2$	Am	A	A+R	-	-
$5Ag/ TiO_2$	Am	A	A+R	-	-
$MWNTs/TiO_2$					
$0.1MWNTs/ TiO_2$	A	A	A+R	-	-
$0.5MWNTs/ TiO_2$	A	A	A	-	-
$1MWNTs/ TiO_2$	A	A	A	-	-
$1Ag/1MWNTs/TiO_2$	A	A	A	-	-

A = Anatase phase, R = Rutile phase and Am = Amorphous phase

Table4.3. The crystallite size of pure TiO_2 and TiO_2 composite powders

Samples	Crystallite size (nm)		
	Anatase	Rutile	Average
Pure TiO_2			
Pure TiO_2_400°C	13.90	-	13.90
Pure TiO_2_500°C	14.70	-	14.70
Pure TiO_2_600°C	44.20	41.60	42.90
Pure TiO_2_700°C	44.20	55.40	49.80
Pure TiO_2_800°C	-	55.40	55.40
Ag /TiO_2_400 °C			
0.5Ag/TiO_2	Am	-	Am
1Ag/TiO_2	Am	-	Am
2Ag/TiO_2	9.1	-	9.1
3Ag/TiO_2	10.3	-	10.3
4Ag/TiO_2	Am	-	Am
5Ag/TiO_2	Am	-	Am
Ag /TiO_2_500 °C			
0.5Ag/ TiO_2	29.5	-	29.5
1Ag/TiO_2	25.3	-	25.3
2Ag/TiO_2	29.5	-	29.5
3Ag/TiO_2	29.5	-	29.5
4Ag/TiO_2	17.7	-	17.7
5Ag/TiO_2	17.7	-	17.7
Ag/TiO_2_600 °C			
0.5Ag/TiO_2	29.50	41.61	35.50
1Ag/TiO_2	25.30	27.70	26.50
2Ag/TiO_2	29.50	-	29.50
3Ag/TiO_2	29.50	55.40	42.45
4Ag/TiO_2	35.40	55.40	45.40
5Ag/TiO_2	42.10	55.60	48.85
MWNTs/TiO_2_400 °C			
0.1MWNTs/TiO_2	14.70	-	14.70
0.5MWNTs/TiO_2	12.60	-	12.60
1MWNTs/TiO_2	12.60	-	12.60
MWNTs/TiO_2_500 °C			
0.1MWNTs/TiO_2	14.70	-	14.70
0.5MWNTs/TiO_2	17.70	-	17.70
1MWNTs/TiO_2	14.70	-	14.70
MWNTs /TiO_2_600 °C			
0.1MWNTs/TiO_2	29.50	55.40	42.54
0.5MWNTs/TiO_2	29.50	-	29.50
1MWNTs/ TiO_2	29.50	-	29.50
1Ag/MWNTs /TiO_2			
1Ag/MWNTs /TiO_2_400 °C	11.00	-	11.00
1Ag/MWNTs /TiO_2_500 °C	20.30	-	20.30
1Ag/MWNTs /TiO_2_600 °C	29.5	-	29.5

Am = Amorphous phase

Table4.4 The phase content of pure TiO_2 and TiO_2 composite powders

Sample	Phase content (%)	
	Anatase	Rutile
Pure TiO_2		
Pure TiO_2_400°C	100	-
Pure TiO_2_500°C	100	-
Pure TiO_2_600°C	64	36
Pure TiO_2_700°C	23	71
Pure TiO_2_800°C	-	100
Ag /TiO_2_400 °C		
0.5Ag/ TiO_2	100	-
1Ag/ TiO_2	100	-
2Ag/ TiO_2	100	-
3Ag/ TiO_2	100	-
4Ag/ TiO_2	100	-
5Ag/ TiO_2	100	-
Ag /TiO_2_500 °C		
0.5Ag/ TiO_2	100	-
1Ag/ TiO_2	100	-
2Ag/ TiO_2	100	-
3Ag/ TiO_2	100	-
4Ag/ TiO_2	100	-
5Ag/ TiO_2	100	-
Ag /TiO_2_600 °C		
0.5Ag/ TiO_2	85	12
1Ag/ TiO_2	90	10
2Ag/ TiO_2	94	6
3Ag/ TiO_2	87	13
4Ag/ TiO_2	71	29
5Ag/ TiO_2	21	79
MWNTs /TiO_2_400 °C		
0.1MWNTs/ TiO_2	100	-
0.5MWNTs/ TiO_2	100	-
1MWNTs/ TiO_2	100	-
MWNTs /TiO_2_500 °C		
0.1MWNTs/ TiO_2	100	-
0.5MWNTs/ TiO_2	100	-
1MWNTs/ TiO_2	100	-
MWNTs /TiO_2_600 °C		
0.1MWNTs/ TiO_2	94.41	5.59
0.5MWNTs/ TiO_2	100	-
1MWNTs/ TiO_2	100	-
1Ag/MWNTs /TiO_2		
1Ag/MWNTs /TiO_2_400 °C	100	-
1Ag/MWNTs /TiO_2_500 °C	100	-
1Ag/MWNTs /TiO_2_600 °C	100	-

4.1.5 Pure TiO_2 and TiO_2 composite films

Pure TiO_2 and TiO_2 composites thin films were prepared by sol-gel and spin coating methods. The gel was then coated on 7x7 cm ceramic tile substrate. The coated substrates were dried at the temperature of 100 ^{o}C for 24 h before calcining at several temperatures. In this research, the effect of dopant and calcinations temperature on phase content characterized by XRD patterns of pure TiO_2 powder calcined at different temperatures from 400 to 600 ^{o}C are shown in Figure 4.9. Peaks marked "A", "R" and "Z" corresponds to anatase, rutile and zircon phases, respectively, it was found that pure TiO_2 films calcined at 400 ^{o}C was amorphous phase and anatase phase increased with the increase in calcinations temperature from 400 ^{o}C to 500 ^{o}C. For calcinations temperature of 600 ^{o}C, anatase phase decreases because of the transformation of anatase to rutile phase. However, the ruitle peak overlaps with zircon at reflection plane of 2θ about 27^{o} (Figure4.9). The effect of dopant and calcined temperature of Ag/TiO_2 thin films were show in Figure 4.10. The anatase phase can be observed for all samples calcined at the temperatures of 400 ^{o}C-600 ^{o}C. It was also found anatase phase of Ag/TiO_2 thin film has well crystallinity than that of pure TiO_2. For $MWNTs/TiO_2$ thin films, anatase phase was found with high degree of crystallinity. It was also apparent that the peak intensity of anatase phase increases as shown Figure 4.11. For $1Ag/1MWNTs/TiO_2$ calcined at the temperaturesof 400 ^{o}C -600 ^{o}C, it was found that amorphous phase transforms to anatase phase as the temperature increases from 400 ^{o}C to 500 ^{o}C while at calcinations temperature of 600 ^{o}C, the anatase phase decreases because of the transformations of anatase to rutile phase overlaping with zircon phase as shown in figure 4.12.

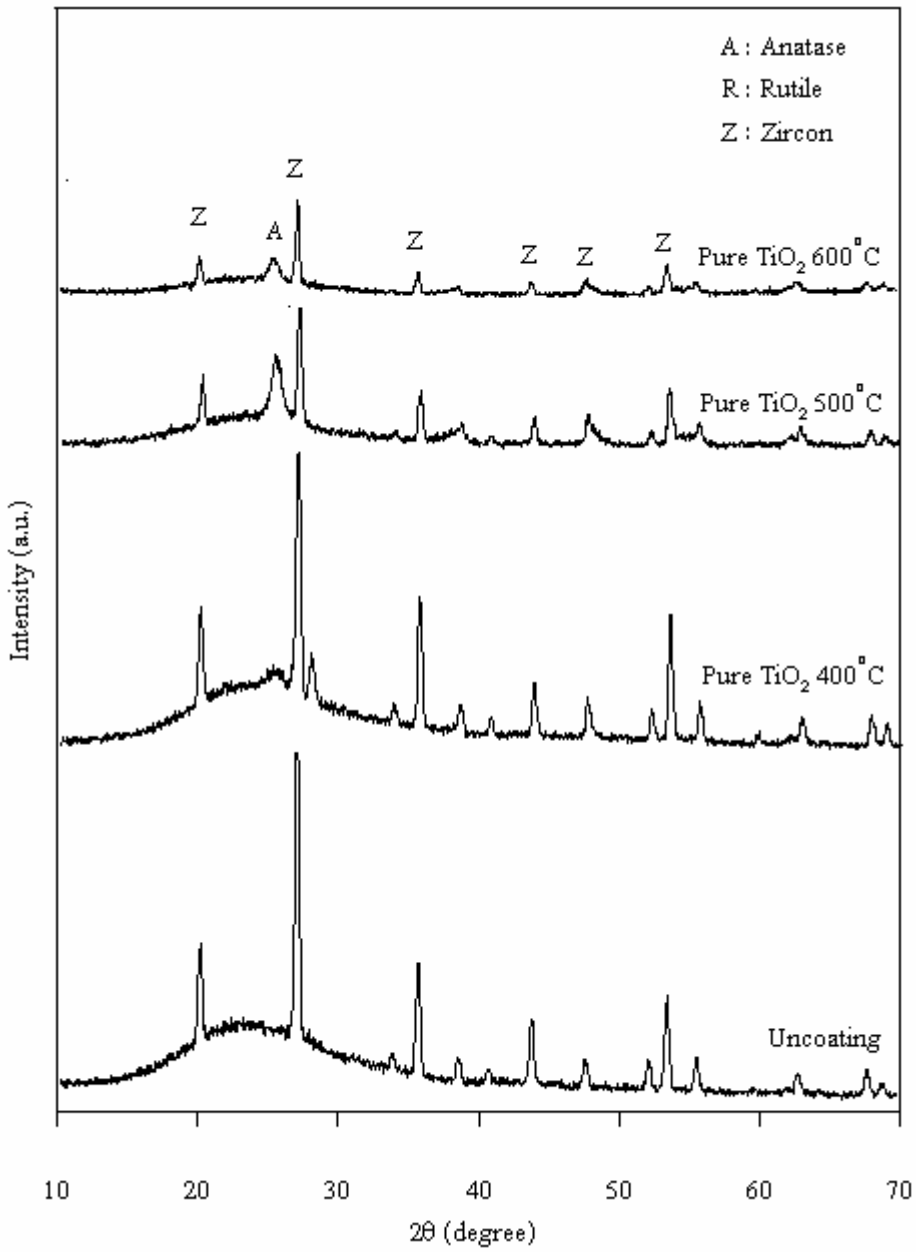

Figure 4.9. XRD patterns of uncoated and pure TiO_2 thin film calcined at the temperatures of 400 °C, 500 °C and 600 °C

a) Ag/TiO_2_400 °C

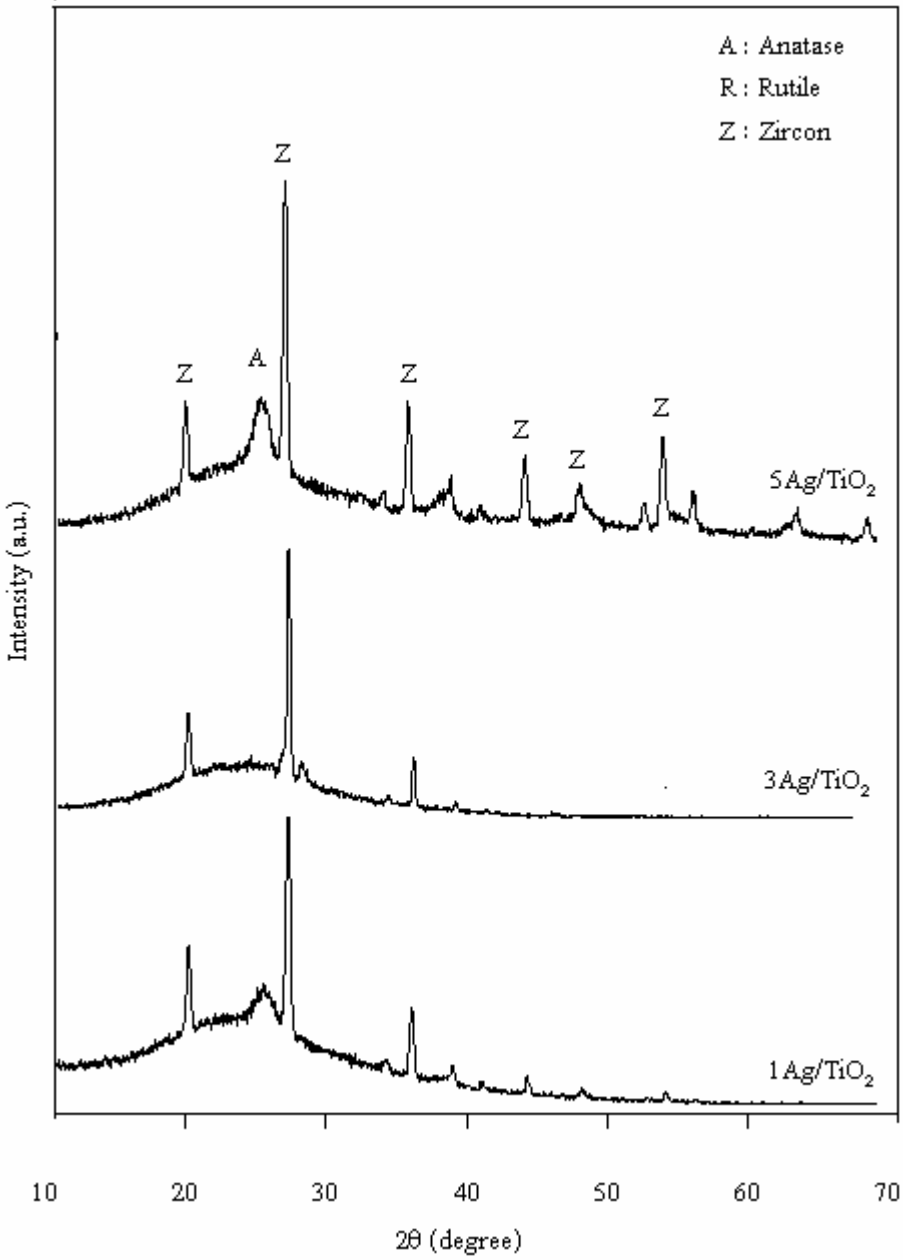

b) Ag/TiO_2_500 ^oC

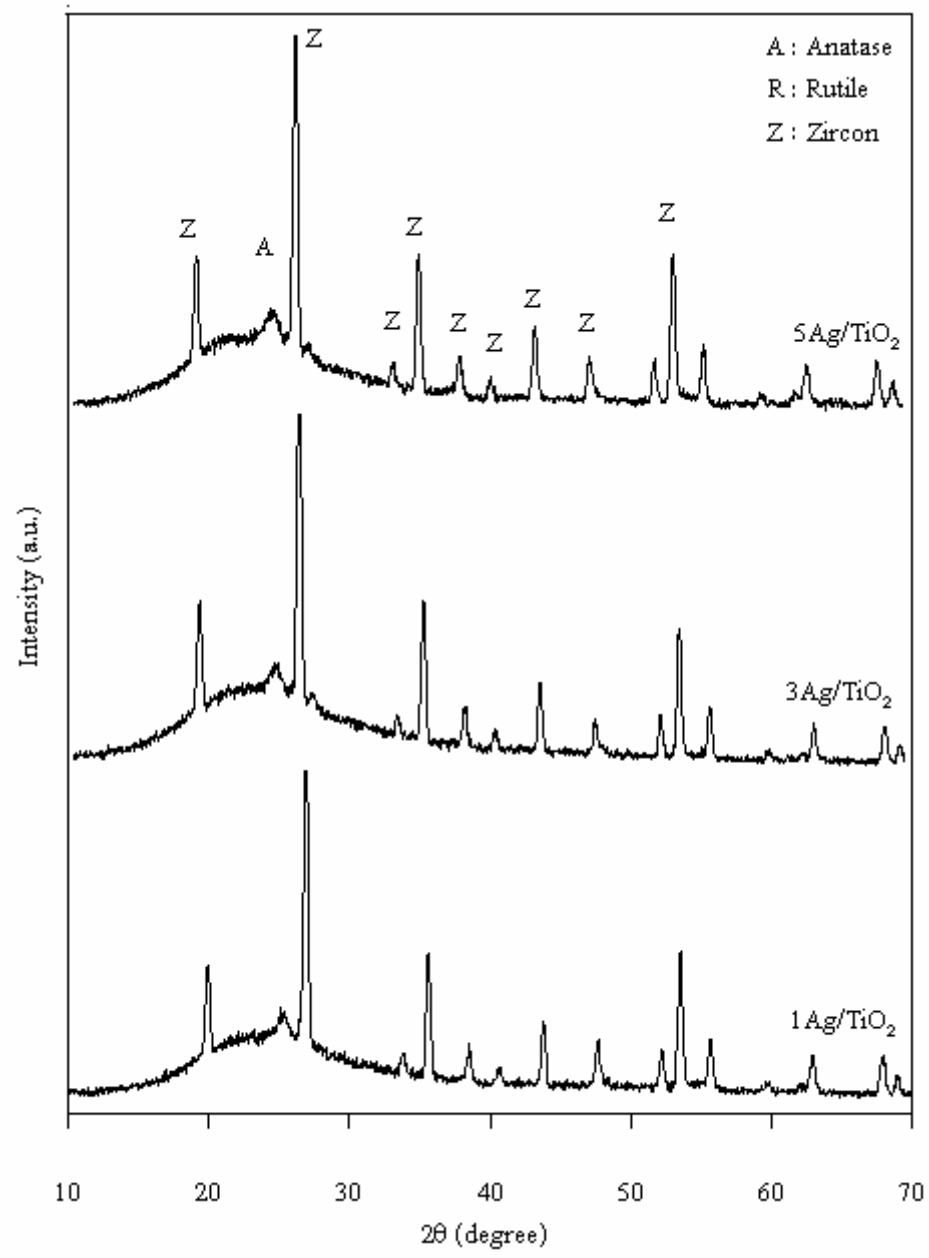

c) Ag/TiO_2_600 °C

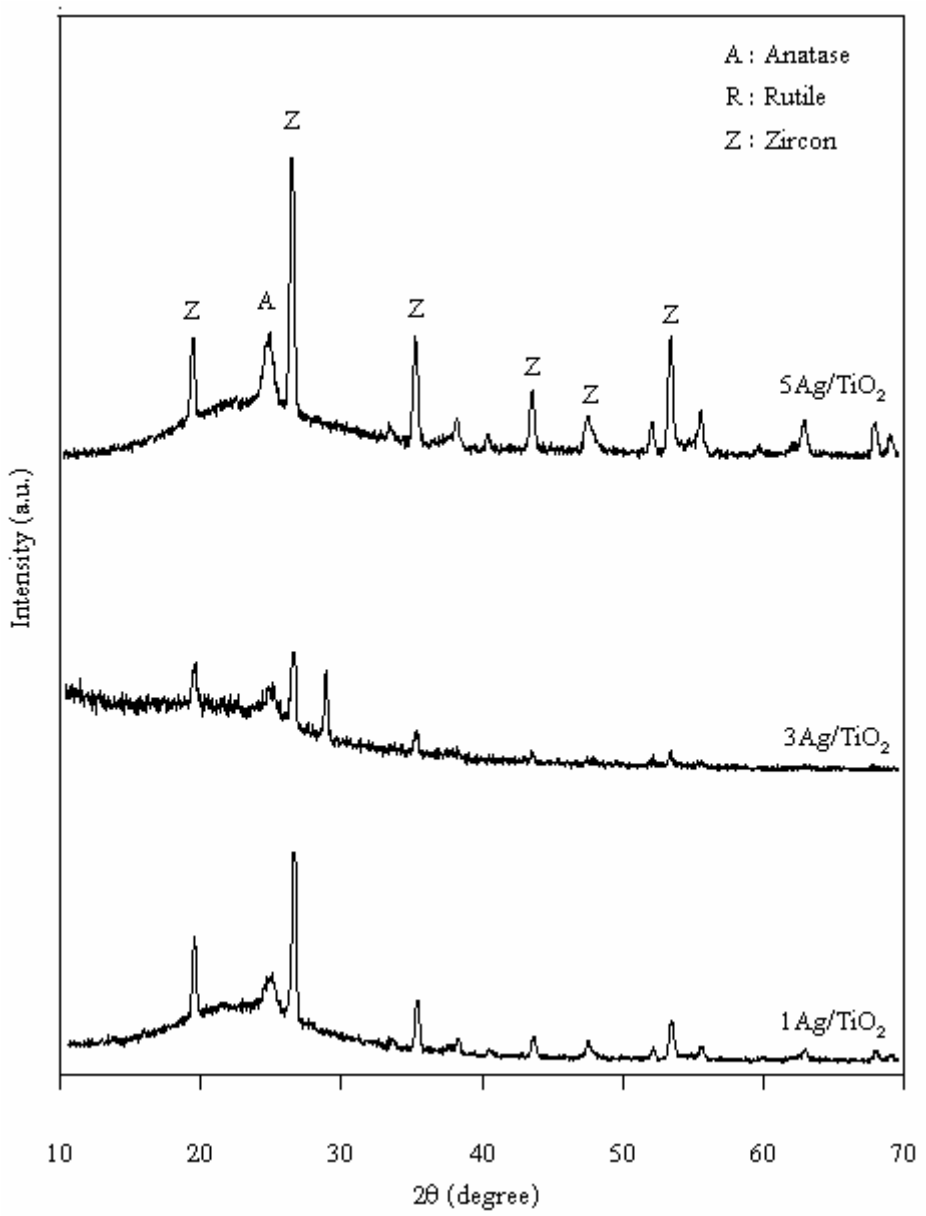

Figure 4.10 XRD patterns of Ag/TiO_2 thin films calcined at the temperatures of a) 400 °C, b) 500 °C and c) 600 °C

a) MWNTs/TiO_2_400^{o}C

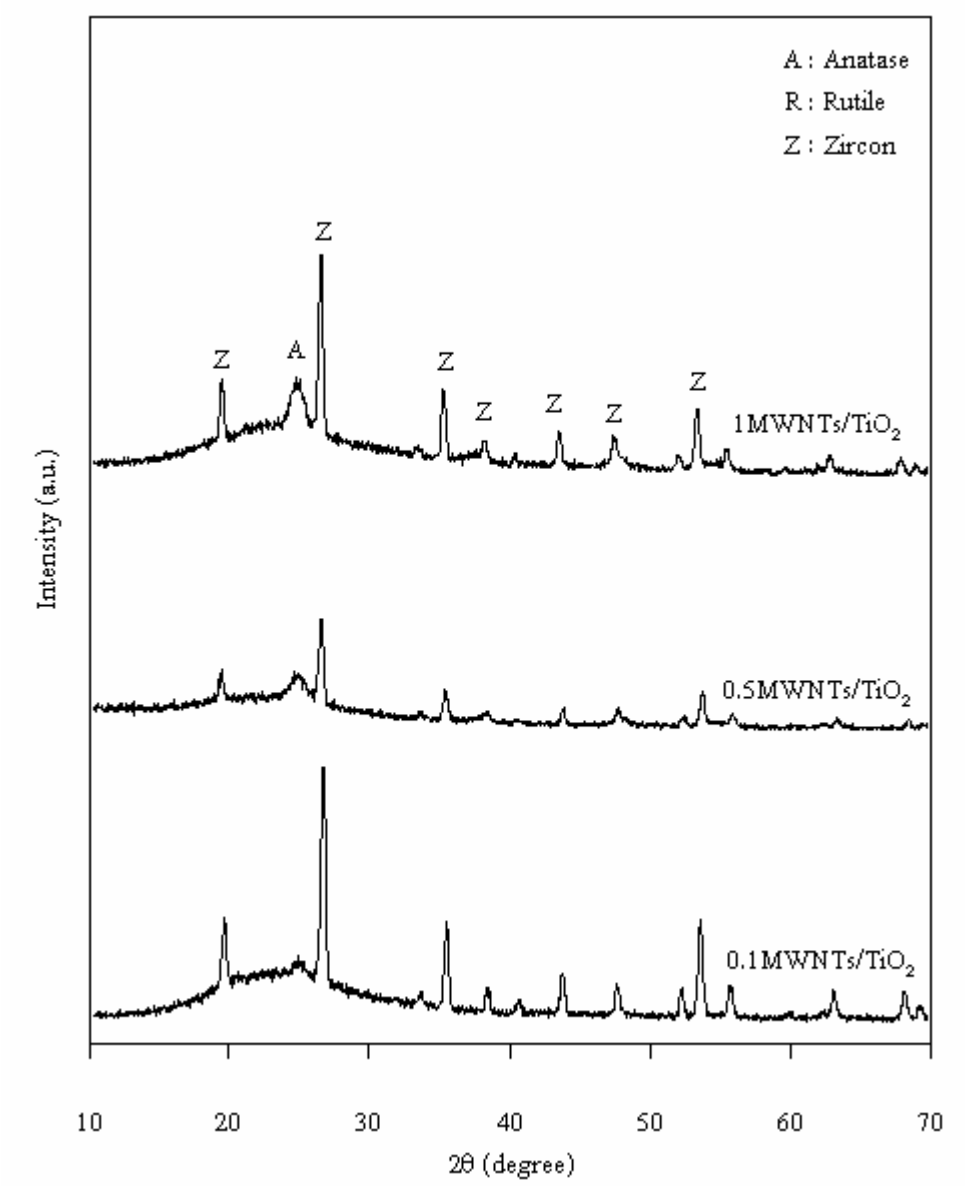

b) MWNTs/TiO_2_500^oC

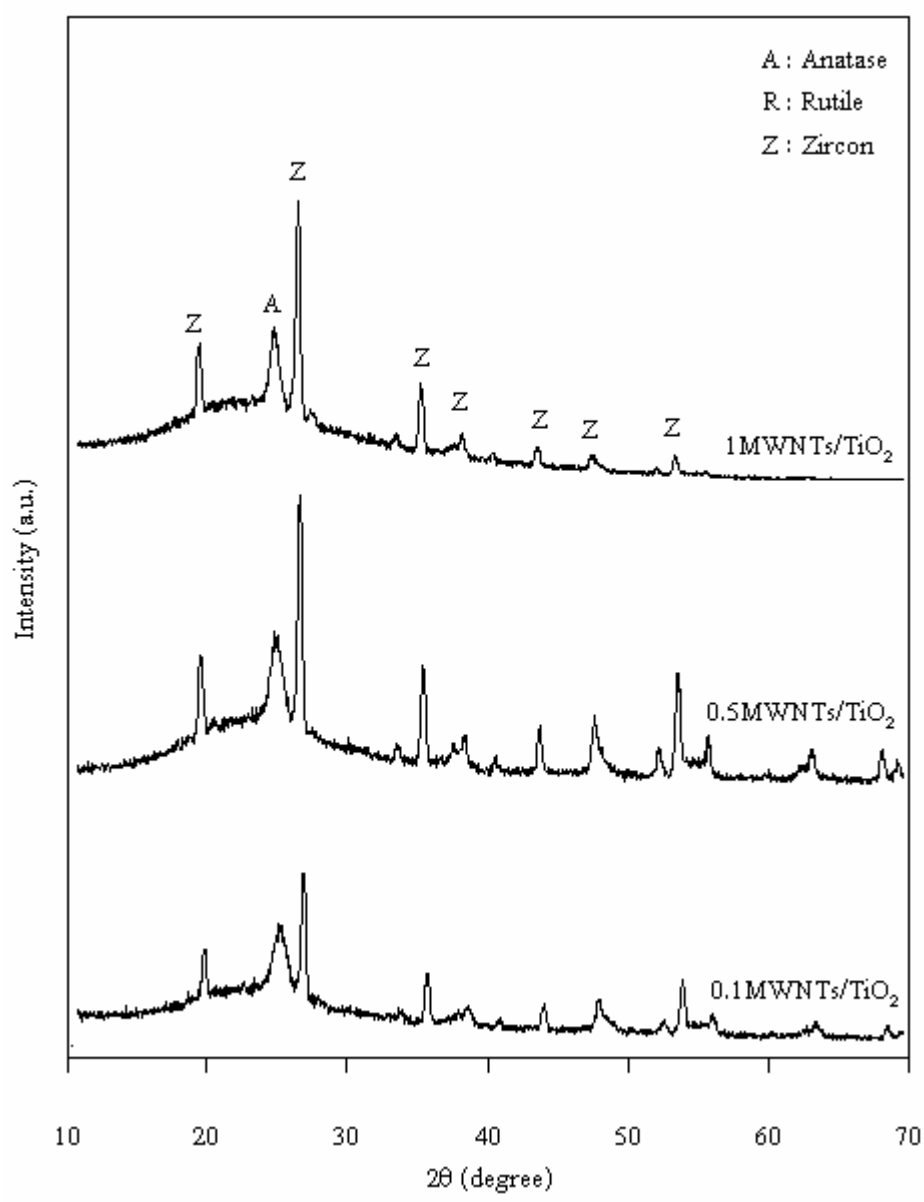

c) MWNTs/TiO_2_600^oC

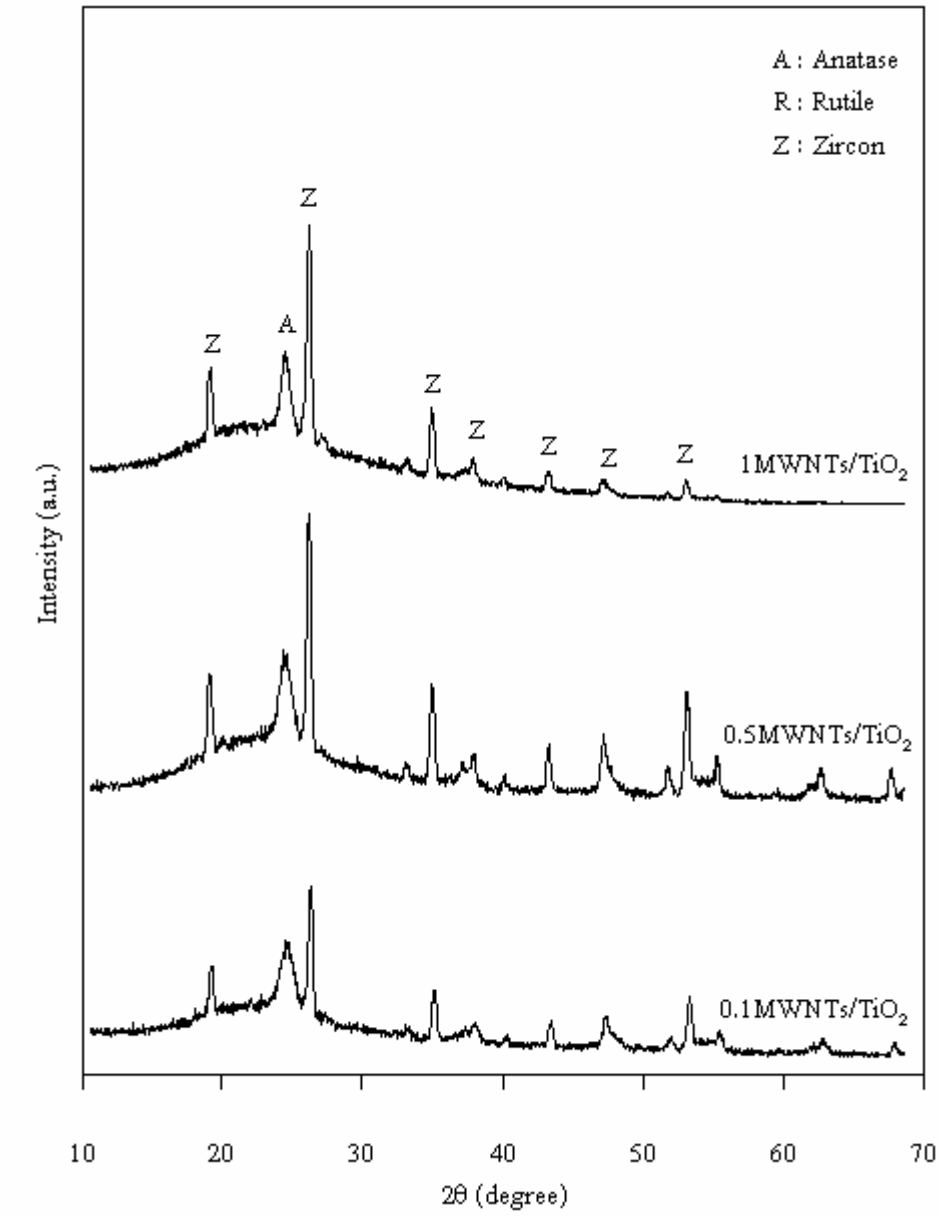

Figure 4.11 XRD patterns of MWNTs/TiO_2 thin films calcined at the temperatures of a) 400 ^oC, b) 500 ^oC and c) 600 ^oC

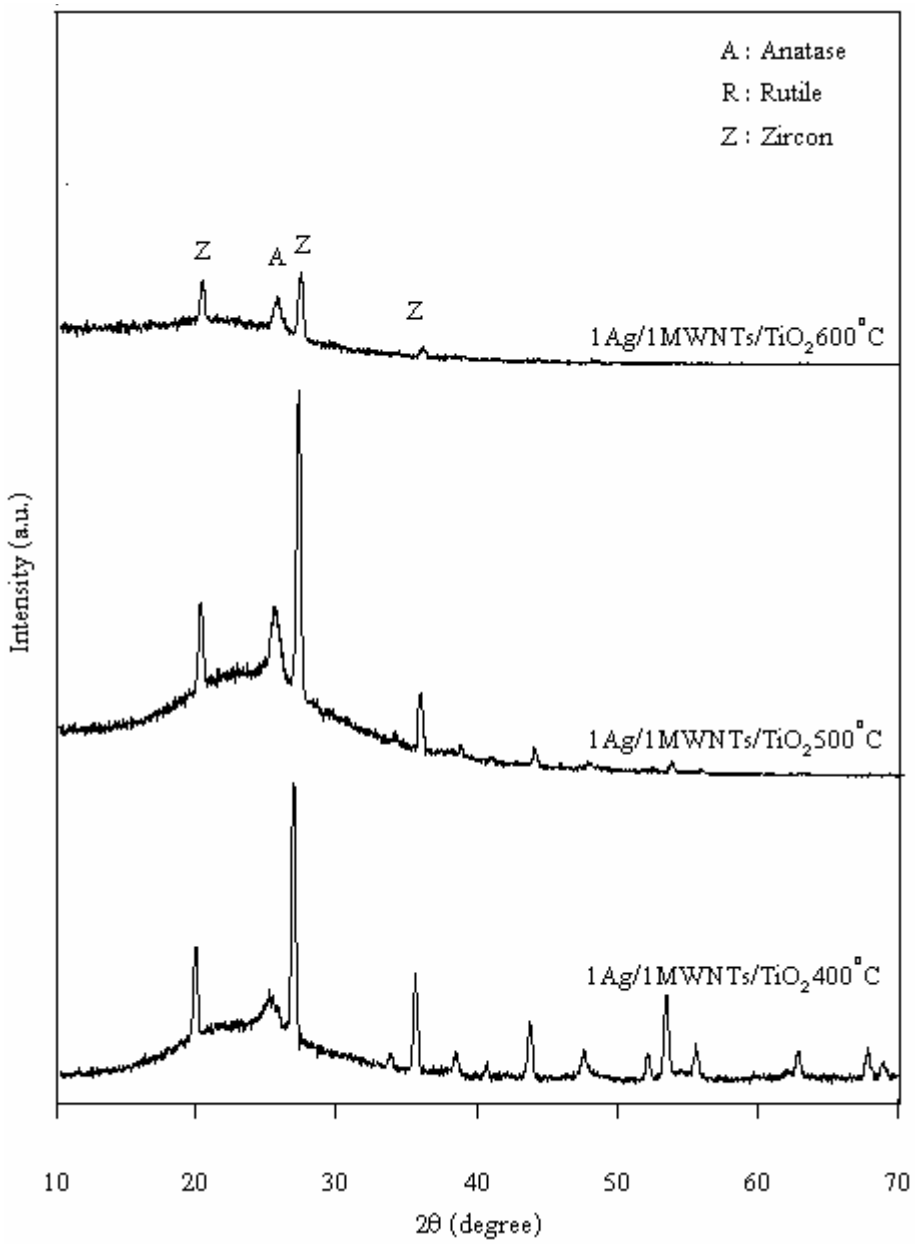

Figure 4.12XRD patterns of 1Ag/1MWNTs/TiO_2 thin films calcined at the temperatures of a) 400 ^{o}C, b) 500 ^{o}C and c) 600 ^{o}C

4.2 Effect of dopant and calcinations temperature on specific surface area and morphology of TiO_2 films and powders

4.2.1 Specific surface area of TiO_2 powder

The specific surface area was determined by the BET method by using nitrogen as adsorbed gas. The specific surface areas of pure TiO_2 and TiO_2 composites are listed in Table4.5. It can be seen that pure TiO_2 has smaller surface area than TiO_2 composites. When adding a small amount of Ag into TiO_2 enhance the specific surface area of TiO_2 composite. $0.5Ag/TiO_2$,$1Ag/TiO_2$ and $2Ag/TiO_2$ powders have the specific surface areas about 111.53, 110.50 and 102.24 nm, respectively. TiO_2 doped with MWNTs has surface area smaller than that of TiO_2 doped with Ag, however, it has larger surface area than pure TiO_2 because the MWNTs prevent TiO_2 particles from agglomeration, thus increasing the specific surface area of the composites (Xia et al., 2007).

Table4.5 Specific surface area of pure TiO_2 and TiO_2 composite powders calcined at the temperature of 500^oC

Sample	Surface area (m^2/g)
Pure TiO_2	43.07
$0.5Ag/TiO_2$	111.53
$1Ag/TiO_2$	110.50
$2Ag/TiO_2$	102.24
$0.1MWNTs/TiO_2$	59.89
$0.5MWNTs/TiO_2$	74.32
$1MWNTs/TiO_2$	73.00
$1Ag/1MWNTs/TiO_2$	106.42

4.2.2 Morphology of films and powders of TiO_2

The surface morphology and size of the pure TiO_2, Ag/TiO_2, $MWNTs/TiO_2$ and $Ag/MWNTs/TiO_2$ were observed with a scanning electron microscope (SEM).

Figure 4.13 shows morphology of the pure TiO_2 calcined at the temperatures of 400 ^oC, 500 ^oC and 600 ^oC. It was observed that the particle sizes increase with an increase in temperature. Pure TiO_2 has a lower aggregation and spherical shape with a uniform size.

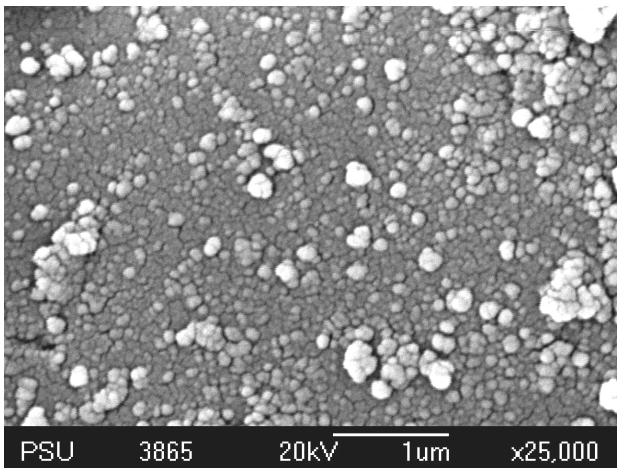

a) Pure TiO_2_400^oC

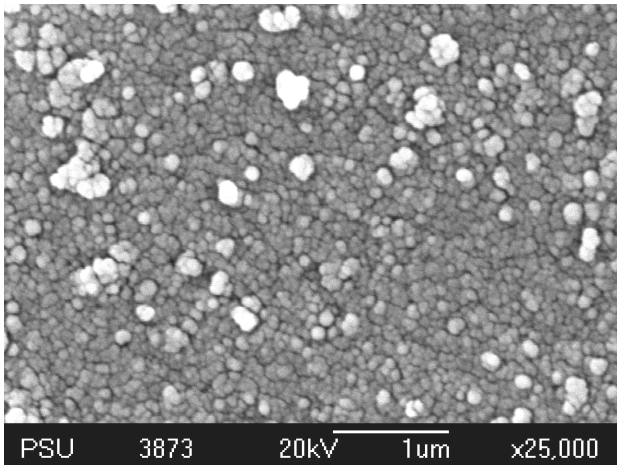

b) Pure TiO_2_500^oC

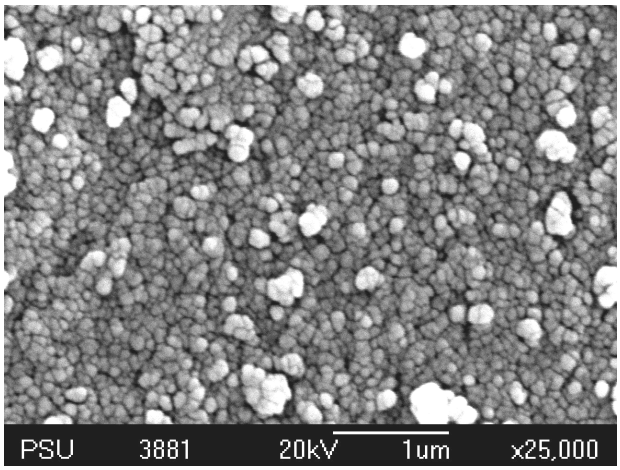

c) Pure TiO_2_600^oC

Figure 4.13 SEM images of pure TiO_2 calcined at the temperatures of a) 400 ^oC, b) 500 ^oC and d) 600 ^oC

Figure 4.14 shows SEM micrographs of the Ag/TiO_2 powders calcined at 500 ˚C. The Ag/TiO_2 composite, has a dense and smaller particle size than that of pure TiO_2. Further observation indicates that the morphology of TiO_2 powders is very rough and may be beneficial to enhancing the adsorption of reactants due to its great surface roughness and large speccific surface area.

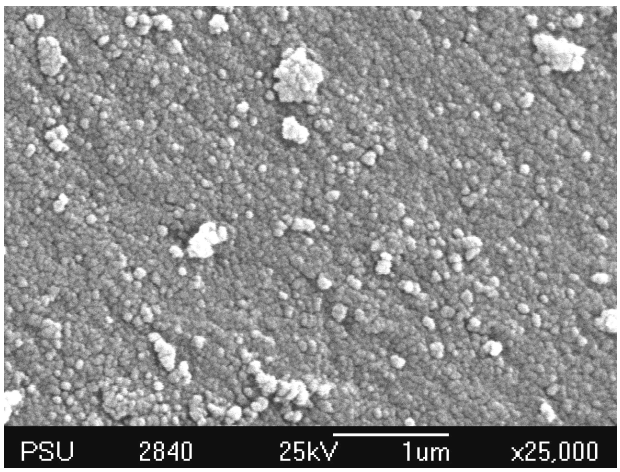

a) $0.5Ag/TiO_2$

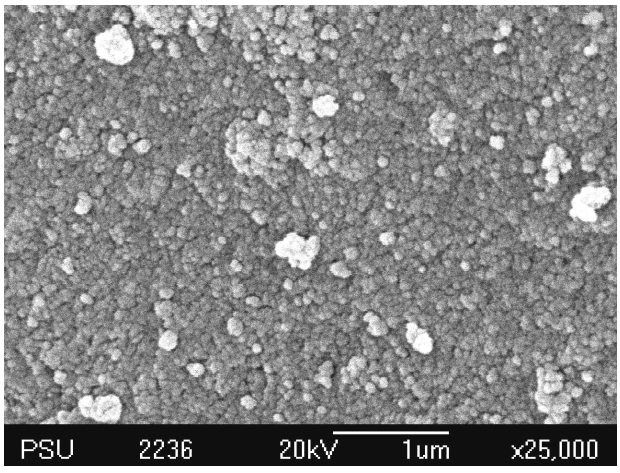

b) 1 Ag/TiO_2

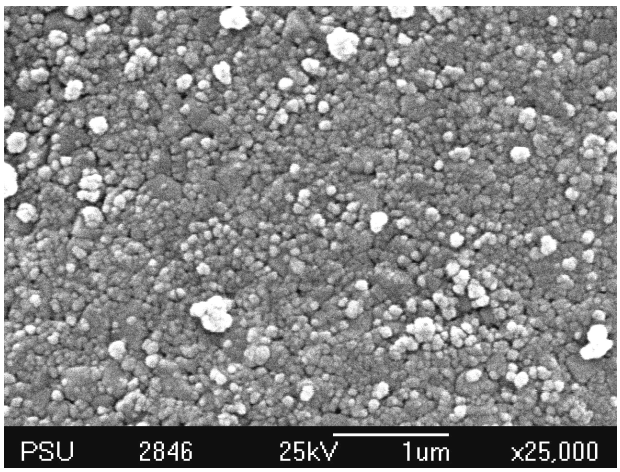

c) 2Ag/TiO_2

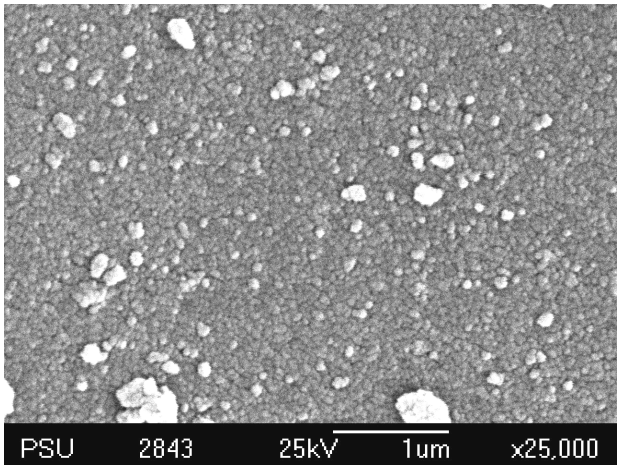

d) 3Ag/TiO_2

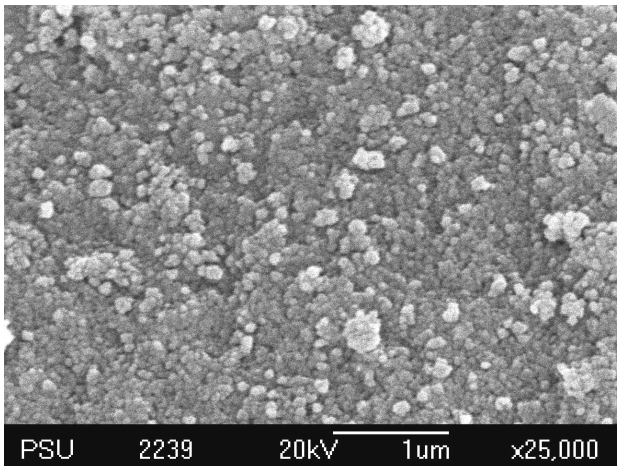

e) 4Ag/TiO_2

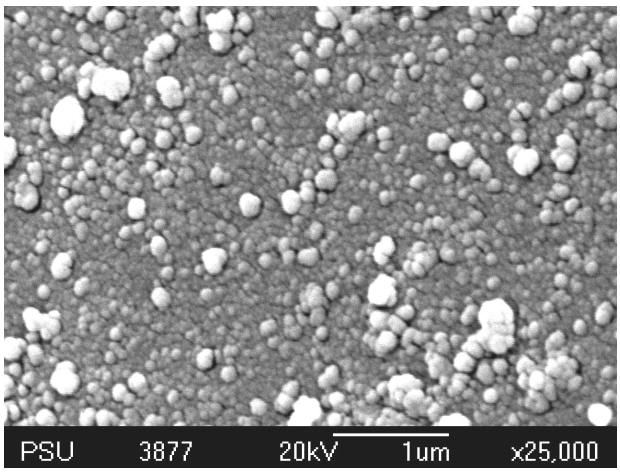

f) 5Ag/TiO_2

Figure 4.14 SEM images of Ag/TiO_2 powders calcined at the temperature of 500 ^{o}C a) 0.5 Ag/TiO_2, b) 1 Ag/TiO_2, c) 2 Ag/TiO_2, d) 3Ag/TiO_2, e) 4 Ag/TiO_2 and f) 5 Ag/TiO_2

The morphologies of MWNTs treated with nitric acid and MWNTs/TiO_2 composite are shown in Figure 4.15. MWNTs have amorphous carbon more than MWNTs treated with nitric acid. For MWNTs/TiO_2 composite, as shown in Figure 4.15c-e, MWNTs seem to be coated by TiO_2 and the agglomerated TiO_2 was found.

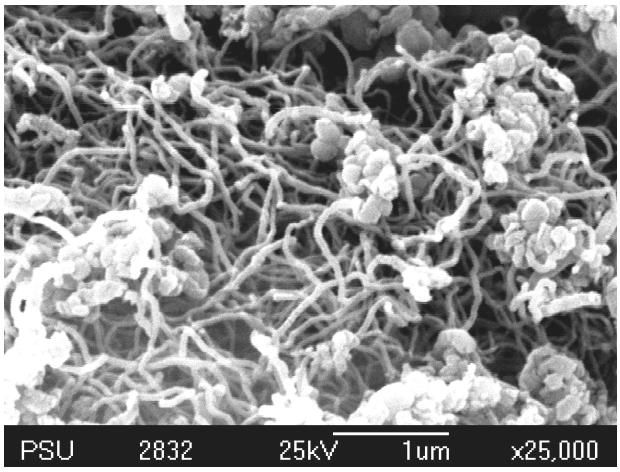

a) MWNTs untreated with nitric acid

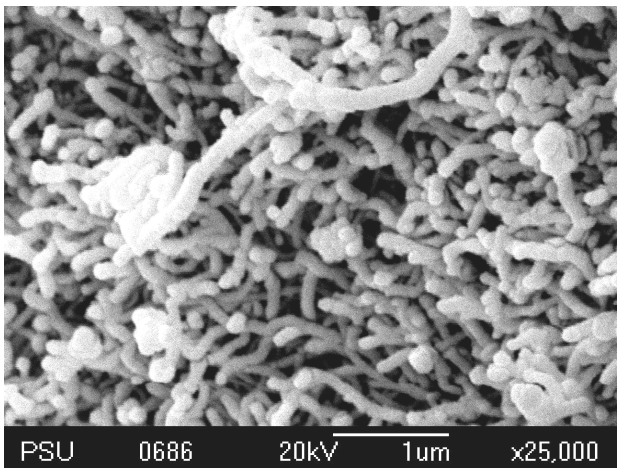

b) MWNTs treated with nitric acid

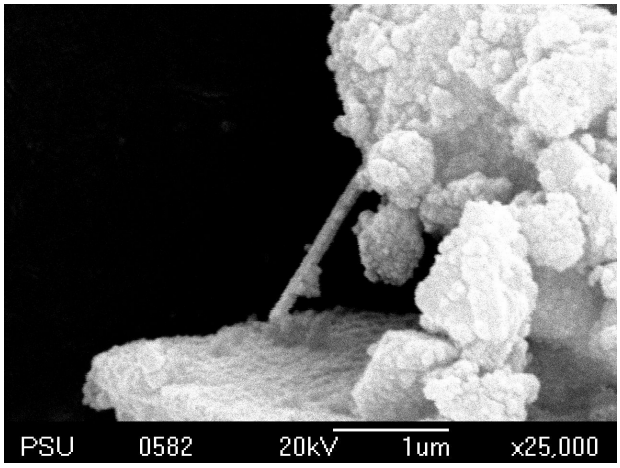

c) 0.1MWNTs/TiO_2

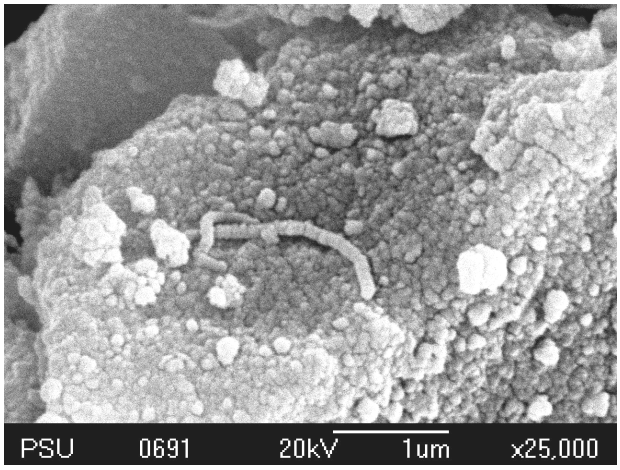

d) 0.5MWNTs/TiO_2

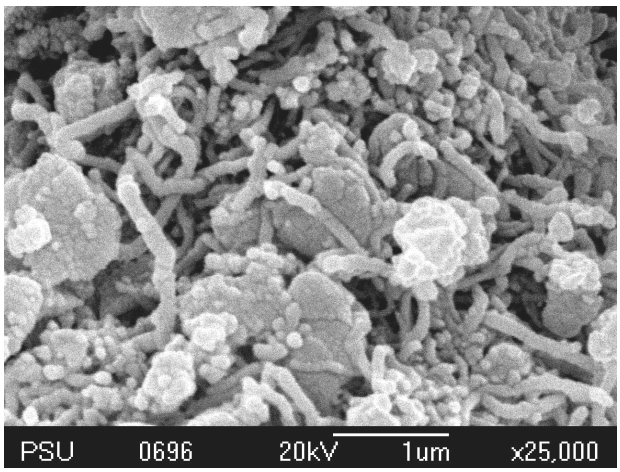

e) 1MWNTs/TiO_2

Figure 4.15 SEM images of a) MWNTs, b) MWNTs treated with nitric acid and c) 0.1MWNTs/TiO_2, d) 0.5MWNTs/TiO_2 and e) 1MWNTs/TiO_2 powders calcined at the temperature of 500^{o}C

Figure4.16 shows the morphology of 1Ag/1MWNTs/TiO_2 calcined at the temperature of 400, 500 and 600^{o}C. It was observed that at 400 and 500 ^{o}C, the powders have dense and smaller particle size than those calcined at 600 ^{o}C. This means calcinations temperature has an effect on crystallite size and surface area of the composite. From Table4.3, the crystallite sizes are about 11.0, 20.0 and 29.5 nm for calcination at 400 ^{o}C, 500 ^{o}C and 600 ^{o}C, respectively. Therefore, the crystallite size of the composite was increases with an increase in calcination temperature.

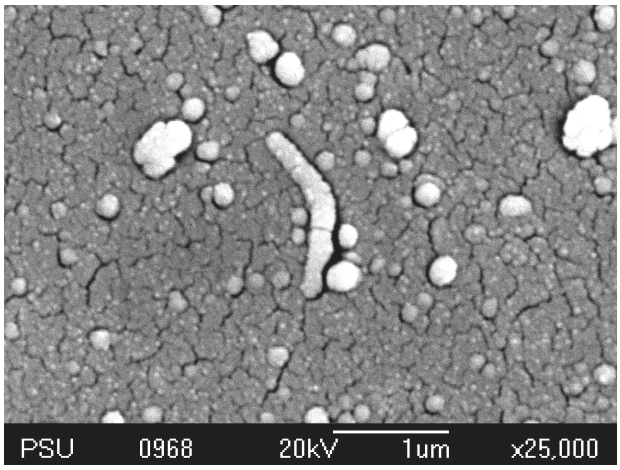

a) 1Ag/1MWNTs/TiO_2_400^{o}C

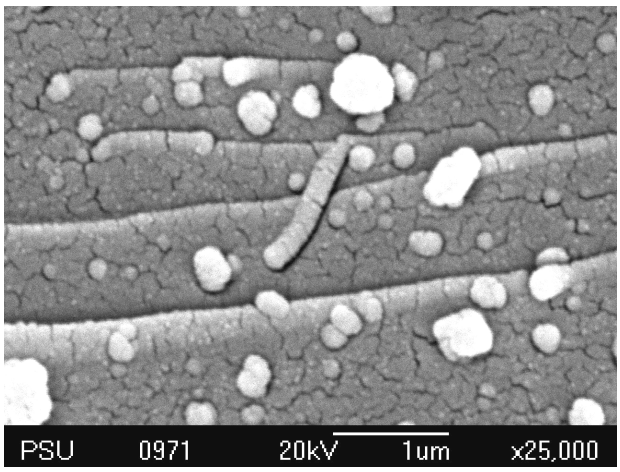

b) 1Ag/1MWNTs/TiO_2_500^oC

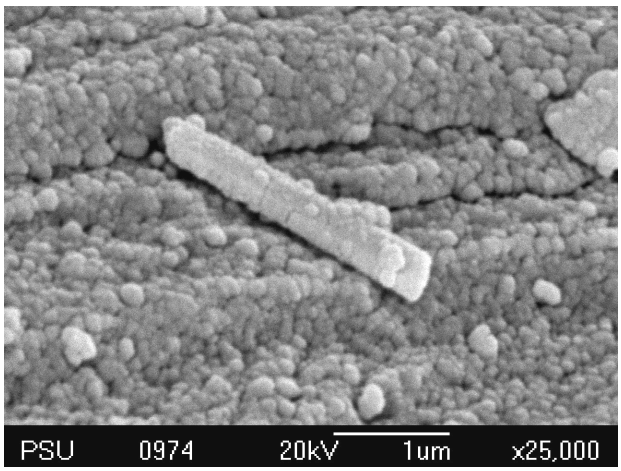

c) 1Ag/1MWNTs/TiO_2_600^oC

Figure4.16 SEM images of 1Ag/1MWNTs/TiO_2 powders calcined at the temperatures of a) 400 ^oC, b) 500 ^oC and c) 600 ^oC

Figure4.17 exhibits the cross section and surface of thin films of pure TiO_2 and TiO_2 composites prepared by sol-gel and spin coating processes and calcined at the temperature of 500^oC. Figure 4.17a shows uncoating ceramic tile surface of substrate and Figure4.16b shows the surface of substrates coated with pure TiO_2, 1Ag/ TiO_2, 1MWNTs/ TiO_2 and 1Ag/1MWNTs/ TiO_2 films, respectively. All samples of TiO_2 composite thin films have the thickness in range of 100-200 nm. Their surfaces are dense and very smooth. For TiO_2 doped with MWNTs, it can not be seen MWNTs on the coated surface because MWNTs content is present in small amount compared to TiO_2 content.

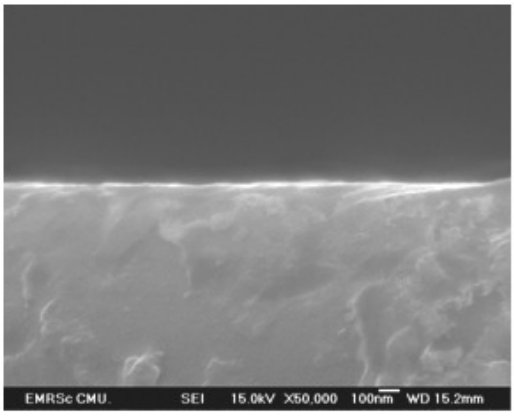

a) uncoating surface

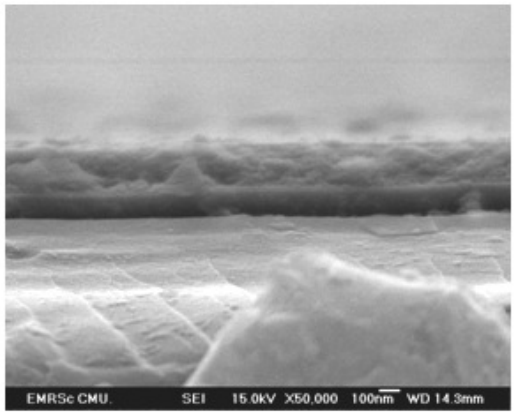

b) pure TiO_2 film

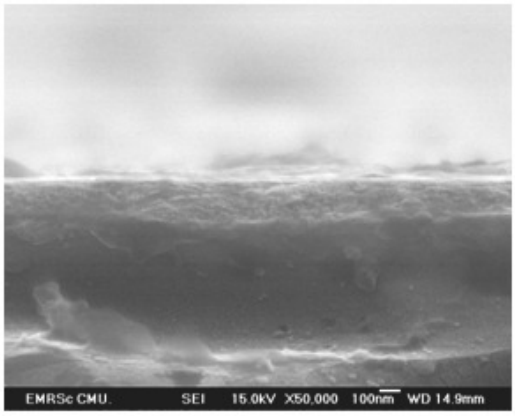

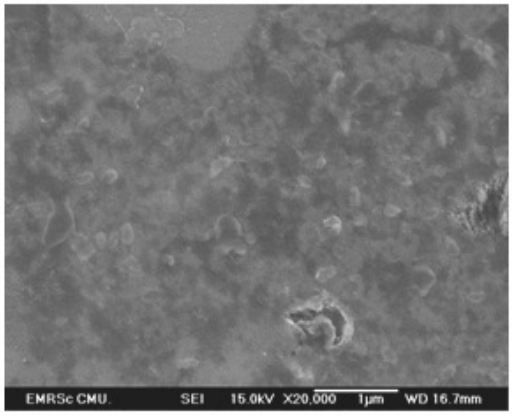

c) 1Ag/TiO_2 film

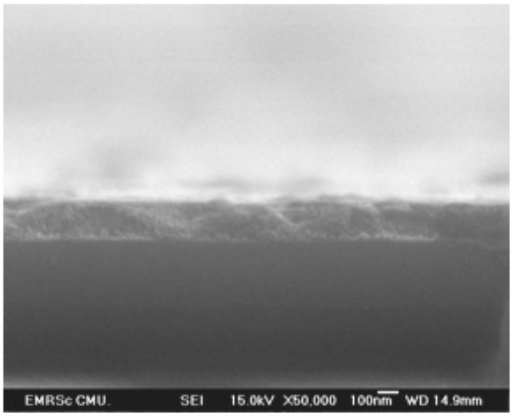

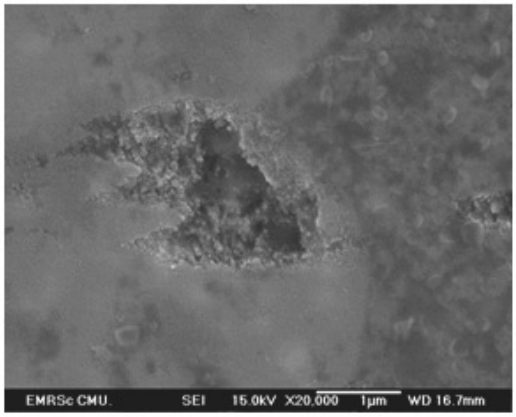

d)1MWNTs/TiO_2 film

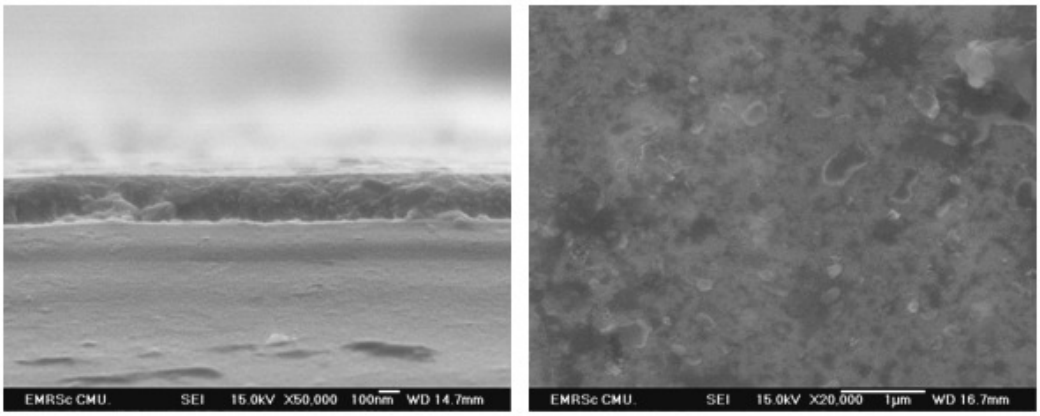

e) 1Ag/1MWNTs/TiO_2 film

Figure4.17 SEM images of ceramic tile surface a) uncoated surface, and thin films of b) pure TiO_2, c) 1Ag/TiO_2 film, d) 1MWNTs/TiO_2 film and e) 1Ag/1MWNTs/TiO_2film calcined at the temperature of 500 ^{o}C

4.2.3 The distribution of TiO_2 in the films coated

The presence of Ti in pure TiO_2 and TiO_2 composite and dopant in the coated films were determined by EDS spectra shown in Figure4.18. The result indicates the presence of Ti, Ag and C in the films. The spectra of Ag/ TiO_2 and 1Ag/1MWNTs/TiO_2 composite are shown in Figure 4.18c and 4.18e. showing very low intensity of Ag and a very high intensity of Ti. It is due to a small amount of Ag doped in TiO_2. For uncoated surface, Ti spectrum cannot be observed (Figure 4.18a)

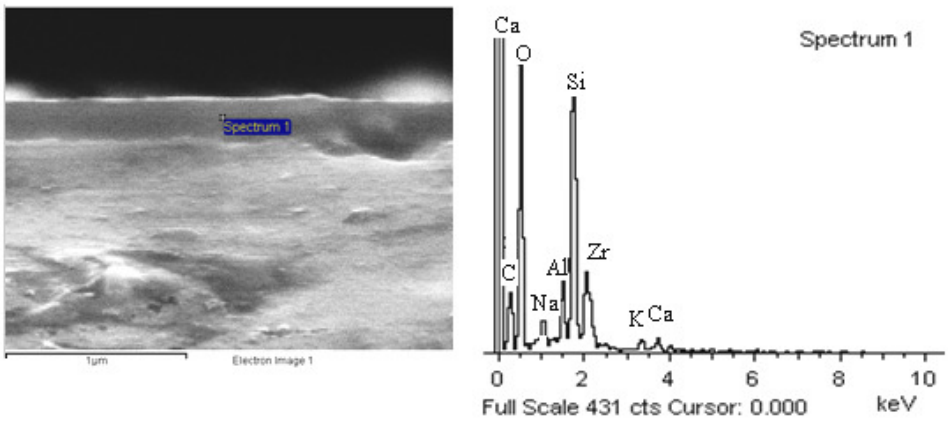

a) uncoated surface

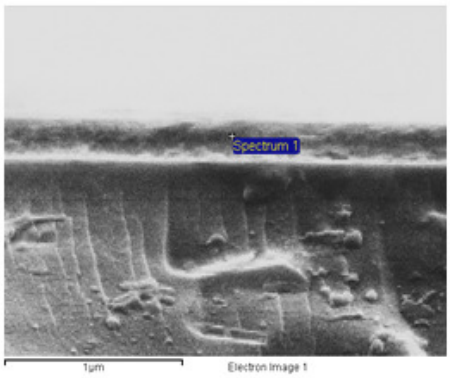

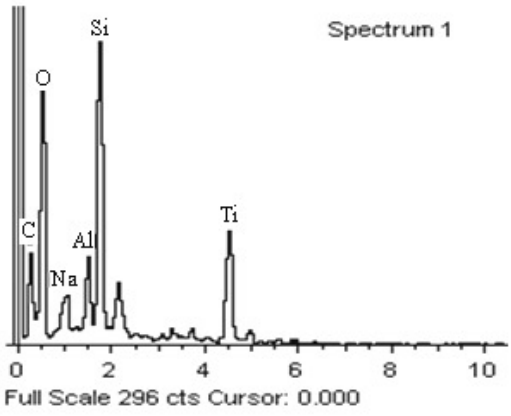

b) pure TiO_2 film

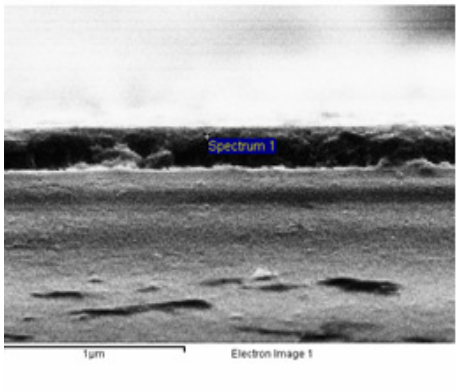

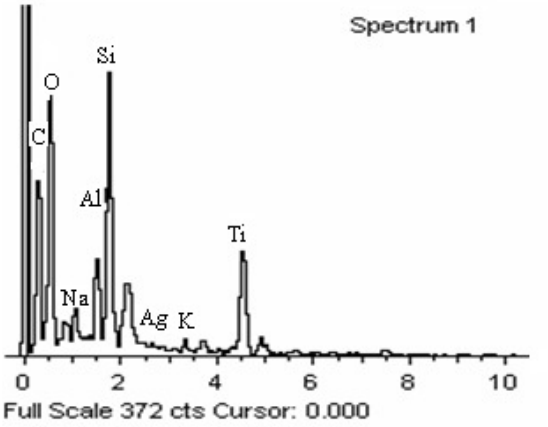

c) 1Ag/TiO_2 film

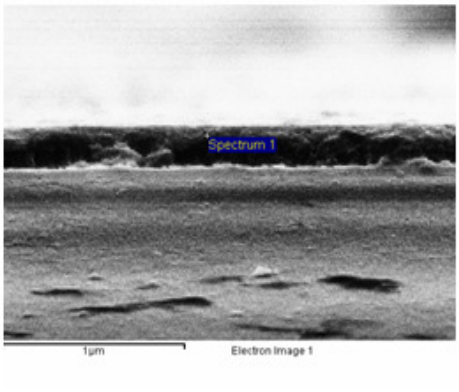

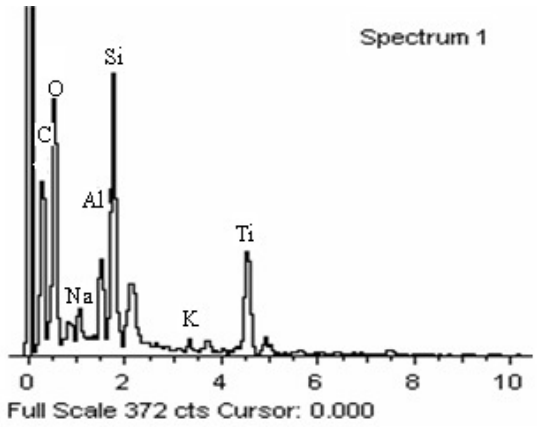

d) 1MWNTs/TiO_2 film

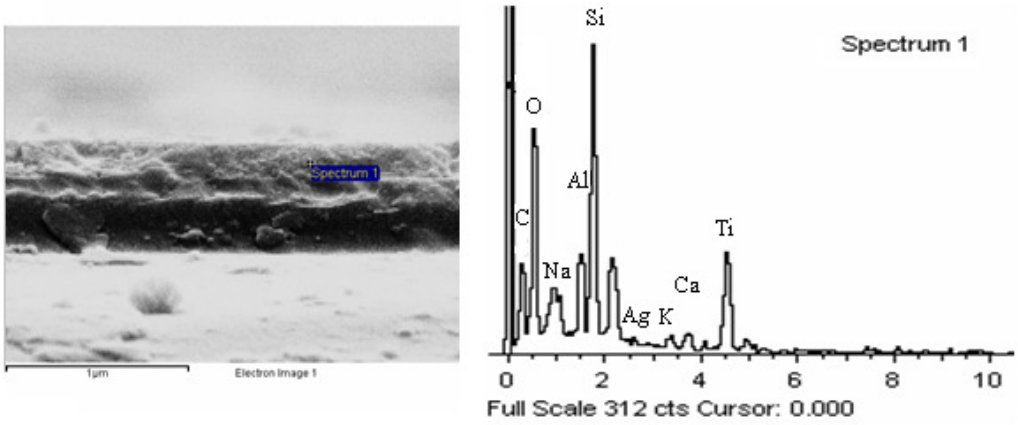

e) 1Ag/1MWNTs/TiO_2 film

Figure 4.18 EDX spectra of a) uncoated surface, b) pure TiO_2 film, c) 1Ag/TiO_2 film, d) 1MWNTs/TiO_2 film and e) 1Ag/1MWNTs/TiO_2 film calcined at the temperature of 500 ^{o}C

4.2.4 The roughness of TiO_2 and dopant in the films coated

Figure 4.19 show a typical surface morphology of pure TiO_2 and TiO_2 composite thin films for an area of 1 x1 μm determined by AFM. The image shows a smooth surface with a roof mean square (rms) roughness about 1.609, 1.383, 1.775 and 2.191 nm for the samples of pure TiO_2, 1Ag/TiO_2, 1MWNTs/TiO_2 and 1Ag/1MWNTs/TiO_2, respectively. Pure TiO_2 thin film calcined at the temperature of 400 ^{o}C has smoother surface and smaller crystallite size small than that pure TiO_2 calcined at temperature of 500 and 600 ^{o}C, respectively. For Ag doped TiO_2 thin films, 1Ag/TiO_2 surface roughness is lower than 3Ag/TiO_2 and 5Ag/TiO_2, respectively. For 0.1MWNTs/TiO_2 and 1MWNTs/TiO_2 film has the surface roughness are about 1.7 nm. whereas 1Ag/MWNTs/TiO_2 the surface roughness about 2.19 nm

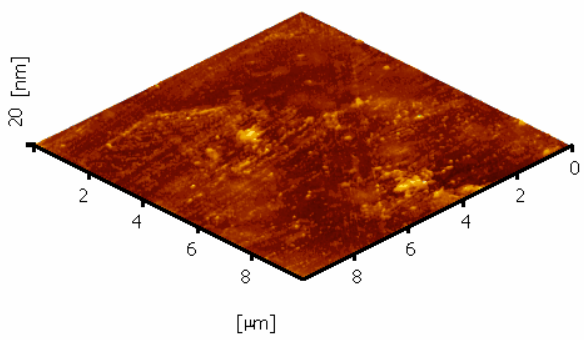

a) Uncoating

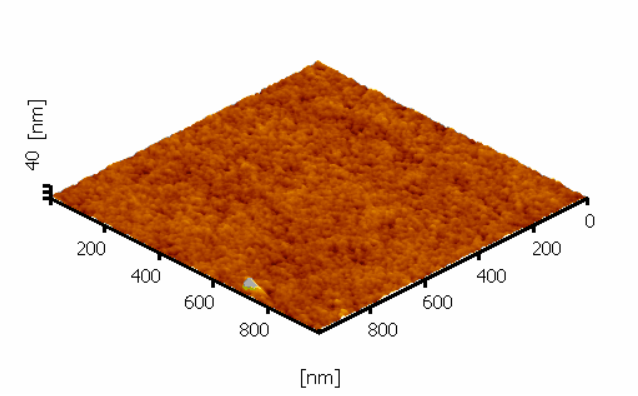

b) Pure TiO_2 calcined at the temperature of 400^{o}C

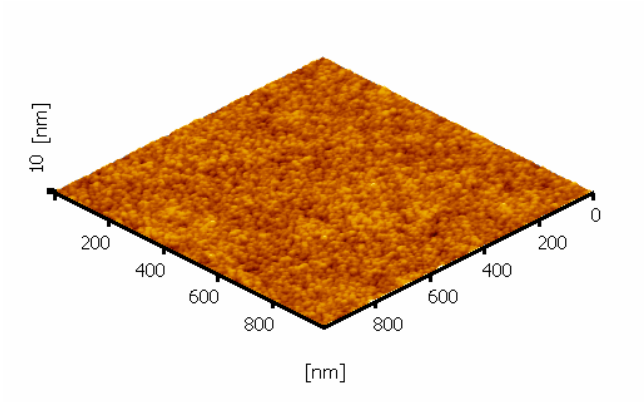

c) Pure TiO_2 calcined at the temperature of 500^{o}C

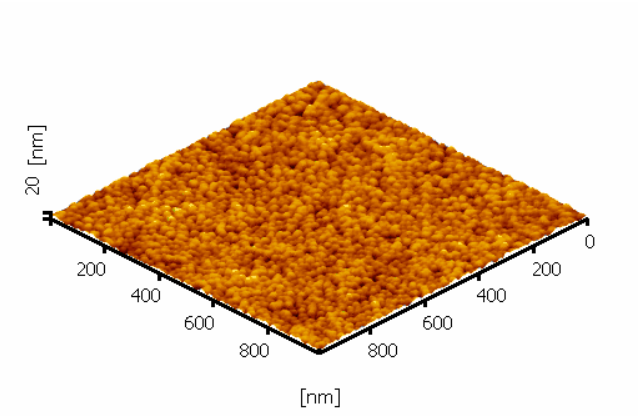

d) Pure TiO_2 calcined at the temperature of 600^{o}C

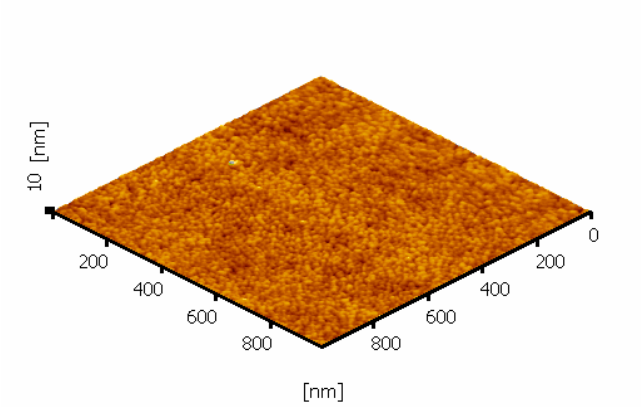

e) 1Ag/TiO_2 calcined at the temperature of 500^{o}C

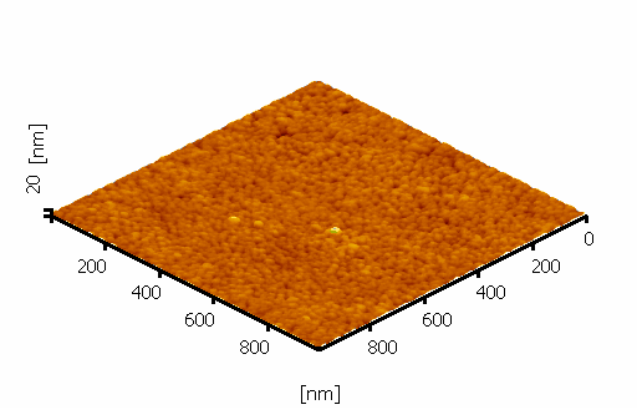

f) 3Ag/TiO_2 calcined at the temperature of 500^{o}C

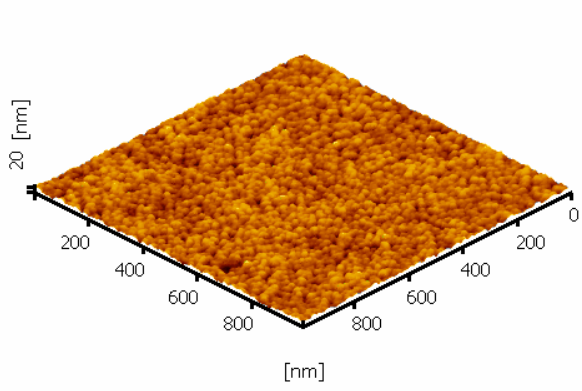

g) 5Ag/TiO_2 calcined at the temperature of 500^{o}C

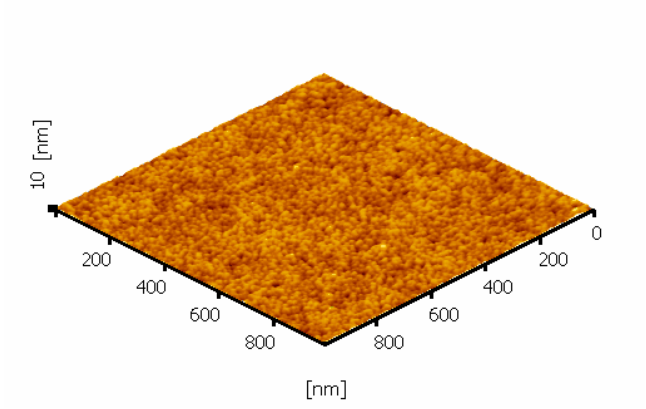

h) 0.1MWNTs/TiO_2 calcined at the temperature of 500^{o}C

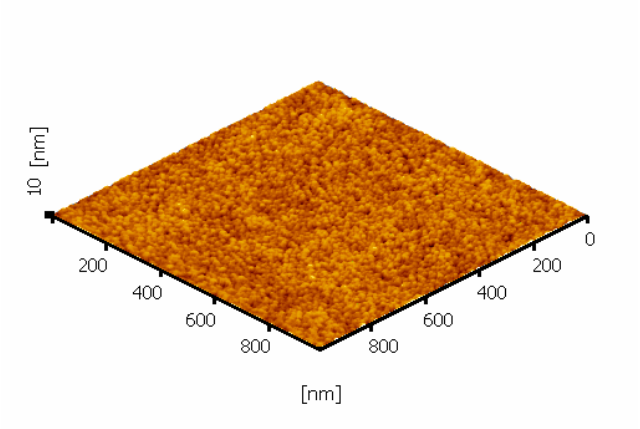

i) 1MWNTs/TiO_2 calcined at the temperature of 500^{o}C

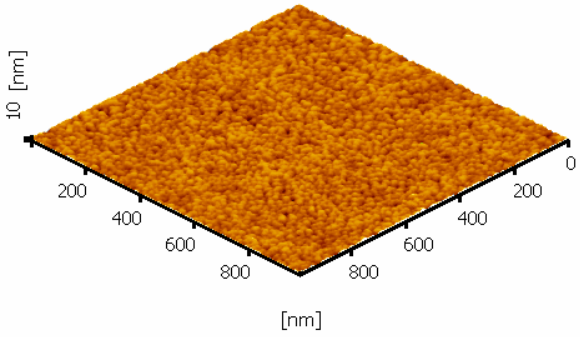

j) 1Ag/1MWNTs/TiO_2 calcined at the temperature of 500^{o}C

Figure 4.19 Surface morphology of pure TiO_2 and TiO_2 composite thin films

Table4.6 The roughness and crystallite size of TiO_2 composite thin films

Sample	Roughness	Crystallite size (nm)
Uncoating	2.649	15.10
Pure_ 400 °C	2.322	10.76
Pure _500 °C	1.609	6.98
Pure_ 600 °C	2.964	16.88
1Ag/TiO_2_500 °C	1.383	7.67
3Ag/TiO_2_500 °C	1.773	11.71
5Ag/TiO_2_500 °C	3.173	19.95
0.1MWNTs/TiO_2_500 °C	1.739	10.86
1MWNTs/TiO_2_500 °C	1.775	10.72
1Ag/MWNTs/TiO_2_500 °C	2.919	11.06

4.3 Effect of dopant and calcinations temperature on absorbed wavelength and band gap energy of the TiO_2 composites.

The UV–VIS spectroscopy was used to measure the absorbance of the synthesized powders and to confirm the band gap energy of pure TiO_2, Ag/TiO_2, MWNTs/TiO_2 and Ag/MWNTs/TiO_2. The measurements were obtained for the dry-pressed disk samples and absorption spectra were referenced to $BaSO_4$. The onset absorbance was determined by the linear extrapolation of the steep part of the UV absorption toward the base line and the corresponding band gap energy of sample can be calculated from the Plank's equation.

The optical absorbance spectra of the pure TiO_2 were measured by the UV–VIS spectroscopy as shown in Figure 4.20. The onset of the absorption spectrum of pure TiO_2 calcinaed at 500 °C and 600 °C appear at about 400 and 435 nm, which corresponds to bandgap energy of 3.1 and 2.85 eV, respectively. The pure TiO_2 calcined at the temperature of 600°C showed the mixed value of anatase and rutile phase. It notes that the spectrum shift to more visible light as the calcinations temperature increases.

The optical absorbance spectra of the Ag/TiO_2 powders were measured in the UV–VIS region as shown in Figure 4.21. At the calcinations temperature of 500°C, the wave length were shifted from 430 to 480 nm and the band gap energy decrease from 2.88 to 2.58 eV when increase Ag content from 0.5-5 mol% Ag. The calculated values of band gap energy and wave length are listed in Table 4.6. These show the absorption edge shifts towards a longer

wavelength, led to the decrease of the band gap with an increase in Ag doped. Because the electron–hole pair separation efficiency induced by enhancing the charge pair separation and inhibiting their recombination by the Ag dopant (Rengaraj and Li. 2006). As same as pure TiO_2, the spectrum of Ag/TiO_2 composite shift to more visible light as the calcinations temperature increase due to the effect of rutile phase occurred in higher temperature.

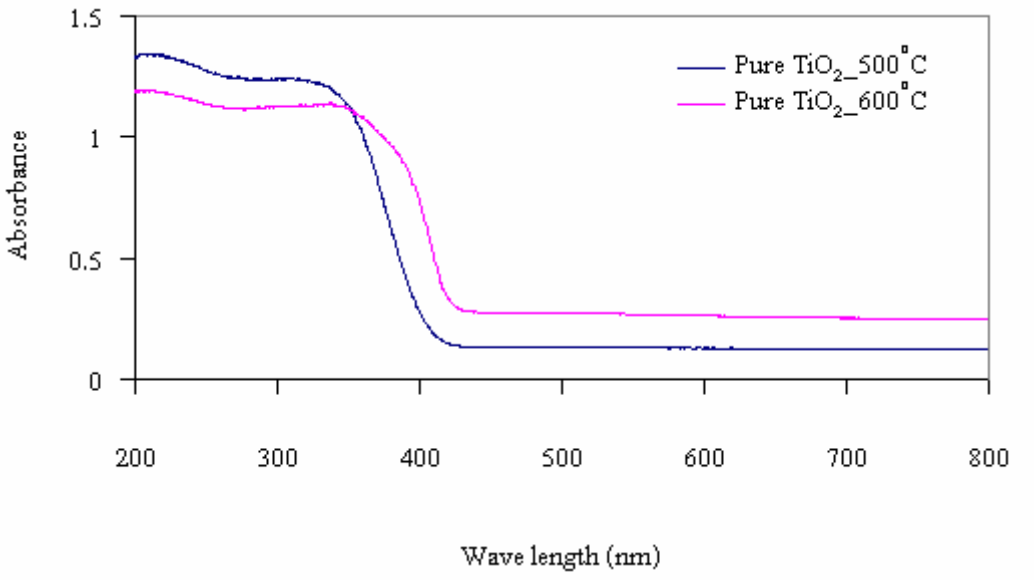

Figure 4.20 The UV-VIS absorbance spectra of pure TiO_2 powders calcined at the temperature of 500 °C and 600 °C

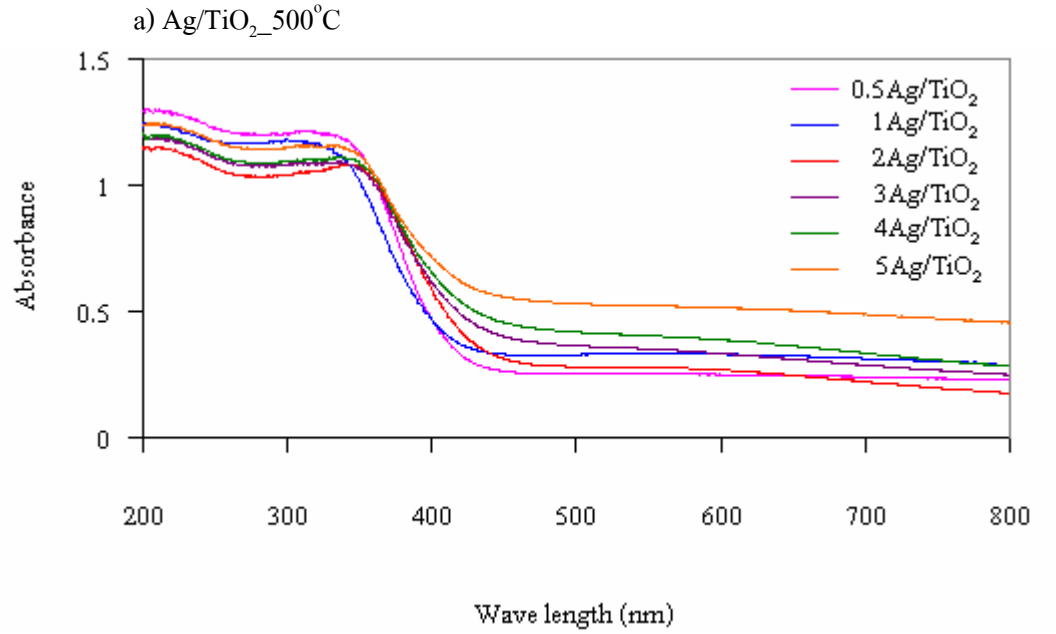

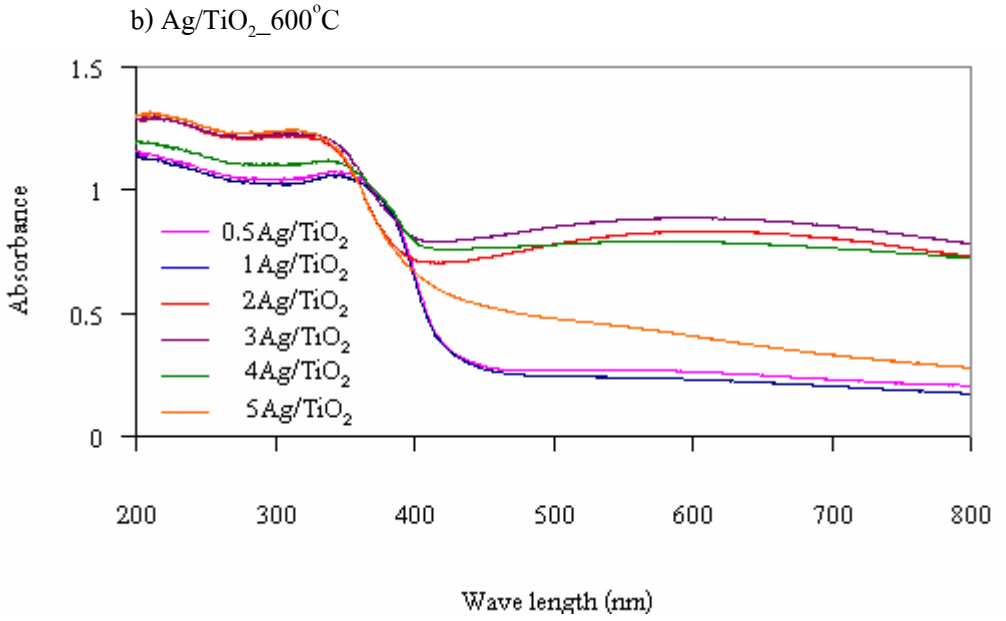

Figure 4.21 The UV-VIS absorbance spectra of Ag/TiO_2 powders calcined at the temperature of a) 500 °C and b) 600 °C

From Figure 4.22 the optical absorbance spectra of the $MWNTs/TiO_2$ powder calcined at the temperatures of 500 °C and 600 °C shift a bit into visible light region. It was apparent that the absorption spectra of $MWNTs/TiO_2$ have longer wavelength in the UV–VIS range than pure TiO_2 (Figure 4.20). It is attributed to the indubitable interaction of TiO_2 nanoparticles with the MWNTs, which may modify the process of the electron/hole pair formation under visible light irradiation. For comparison, the optical absorbance spectra of the $MWNTs/TiO_2$ calcined at the temperatures of 500 °C and 600 °C, are shown in Figure 4.22a and 4.22b, respectively. It was found that the wavelength of the sample calcined at the temperature of 600 °C shifts to visible light more than that of 500 °C. Furthermore, the band gap energy decreases with an increase in MWNTs content.

The absorbed wavelengths of the $1Ag/1MWCNTs/TiO_2$ powder calcined at temperatures of 500 °C and 600 °C are at 430 and 435 nm, respectively (Figure4.23). The data of onset of absorbance and band gap energy of all samples are summarized in Table4.7.

a) MWNTs/TiO_2_500 °C

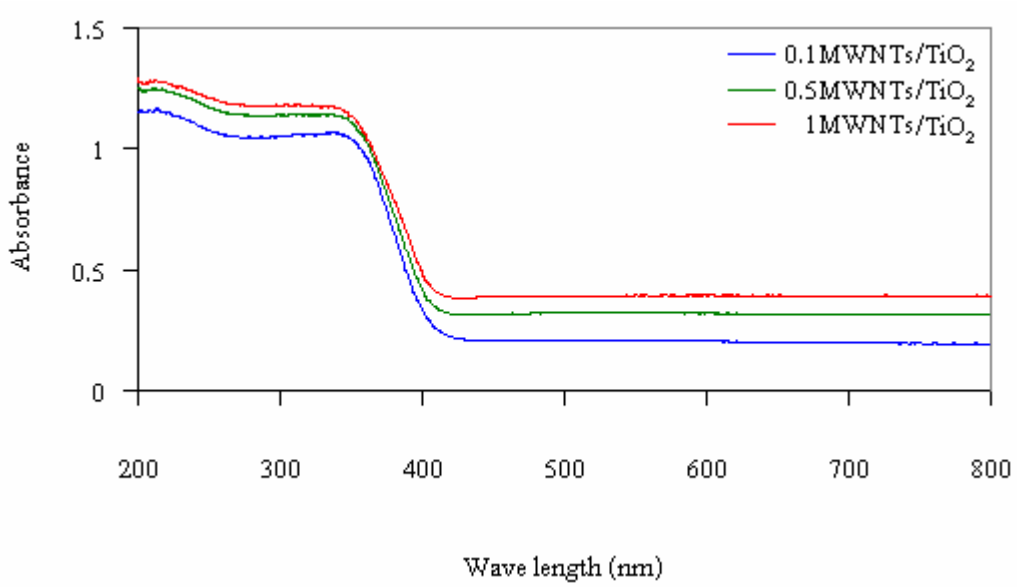

b) MWNTs/TiO_2_600 °C

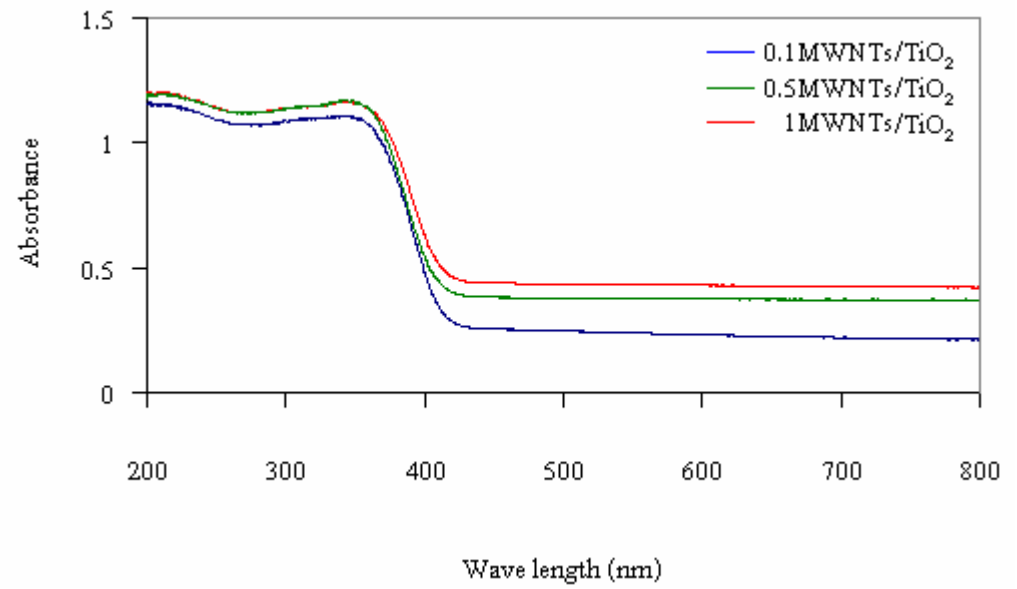

Figure 4.22 The UV-VIS absorbance spectra of MWNTs/TiO_2 powders calcined at the temperatures of a) 500 °C and b) 600 °C

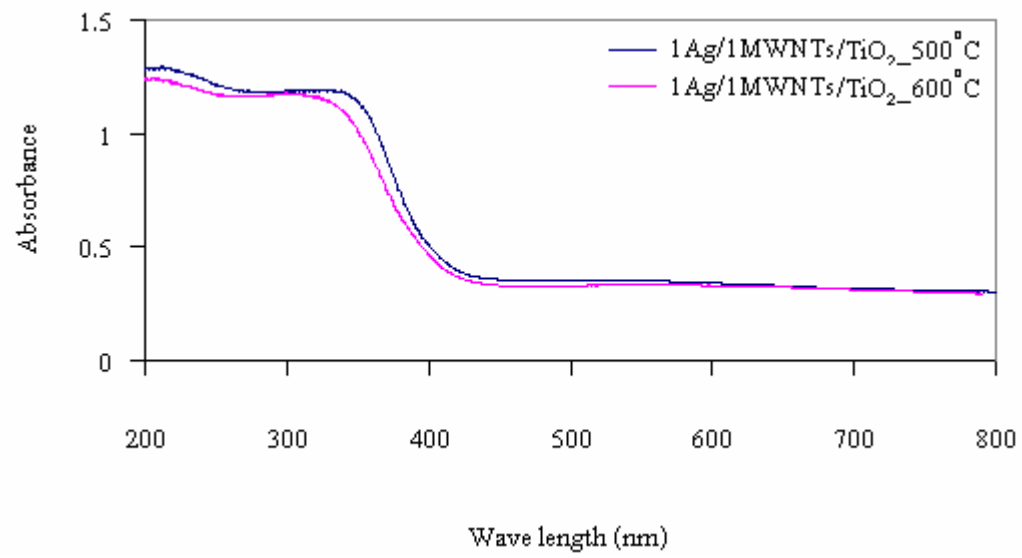

Figure 4.23 The UV-VIS absorbance spectra of 1Ag/1MWNTs/TiO_2 powders calcined at the temperatures of 500 °C and 600 °C

Table4.7 The onset of absorption and band gap energy of titanium dioxide composite

Sample	Onset of absorbance wavelength, λ (nm)	Band gap energy (eV)
Pure TiO_2		
Pure TiO_2_500°C	400	3.10
Pure TiO_2_600°C	435	2.85
Ag /TiO_2_500 °C		
0.5Ag/ TiO_2	430	2.88
1Ag/ TiO_2	435	2.85
2Ag/ TiO_2	457	2.71
3Ag/ TiO_2	462	2.68
4Ag/ TiO_2	478	2.62
5Ag/ TiO_2	480	2.58
Ag /TiO_2_600 °C		
0.5Ag/ TiO_2	438	2.83
1Ag/ TiO_2	440	2.82
2Ag/ TiO_2	458	2.70
3Ag/ TiO_2	500	2.48
4Ag/ TiO_2	510	2.43
5Ag/ TiO_2	502	2.47
MWNTs /TiO_2_500 °C		
0.1MWNTs/ TiO_2	418	2.97
0.5MWNTs/ TiO_2	422	2.98
1MWNTs/ TiO_2	430	2.88
MWNTs /TiO_2_600 °C		
0.1MWNTs/ TiO_2	430	2.88
0.5MWNTs/ TiO_2	435	2.85
1MWNTs/ TiO_2	440	2.82
1Ag/MWNTs /TiO_2		
1Ag/MWNTs /TiO_2_500 °C	430	2.80
1Ag/MWNTs /TiO_2_600 °C	435	2.85

4.4 Effect of dopant and calcinations temperature on photocatalytic activity

The photocatalytic activity of pure TiO_2 and Ag/TiO_2 and $MWNTs/TiO_2$thin films for the degradation of methylene blue under radiation of a UV light and fluorescent light were carried out in dark chamber by using methylene blue solution concentration of 2 mg/l. The area of thin film photocatalyst used for this experiment was 49 cm^2. Sample of 5 ml was taken at every 1 h and the concentration of methylene blue was determined by UV-visible spectroscopy at wave length 665 nm.

The degradation curves of all sample may express as the following rate equation,

$$R = 1.00\, e^{-kt} \quad \text{or} \quad \ln\left[\frac{C}{C_0}\right] = 1.00 - kt \qquad 4.1$$

Where R is Degradation rate or rate of disappearance of methylene blue solution

k is kinetics rate constant (h^{-1})

T is UV or fluorescent light irradiation time (h)

C_0 is Initial concentration of methylene blue

C is The concentration of methylene blue after treatment for t hours

The k value derived from the equation above indicates the degradation rate of methylene blue photocatalytic reaction. Higher k-value shows the higher kinetic rate.

Photocatalytic performance of the pure TiO_2 thin films calcined at the temperature of 400 ^oC, 500 ^oC and 600^oC are shown in Figure 4.24. It can be seen that the degradation increases with increasing UV irradiation time. For photocatalytic activity of the TiO_2 thin films after 6 h treatment the rate conststants (k) are 0.22, 0.31 and 0.26 for the sample calcined at the temperature of 400 ^oC, 500 ^oC and 600˚C, respectively. This observation coincides with XRD data shown in Figure4.5 that the film calcined at the temperature of 500˚C, exhibits the higher the photocatalytic reaction rate than those of 400^oC and 600 ^oC because the film of 500 ^oC has more anatase phase than the others. The film of 400 ^oC has more amorphous phase while

that of 600 °C has a rutile phase together with anatase phase and has a larger crystallite size (42.90nm) compared to that of 500 °C (14.70nm)

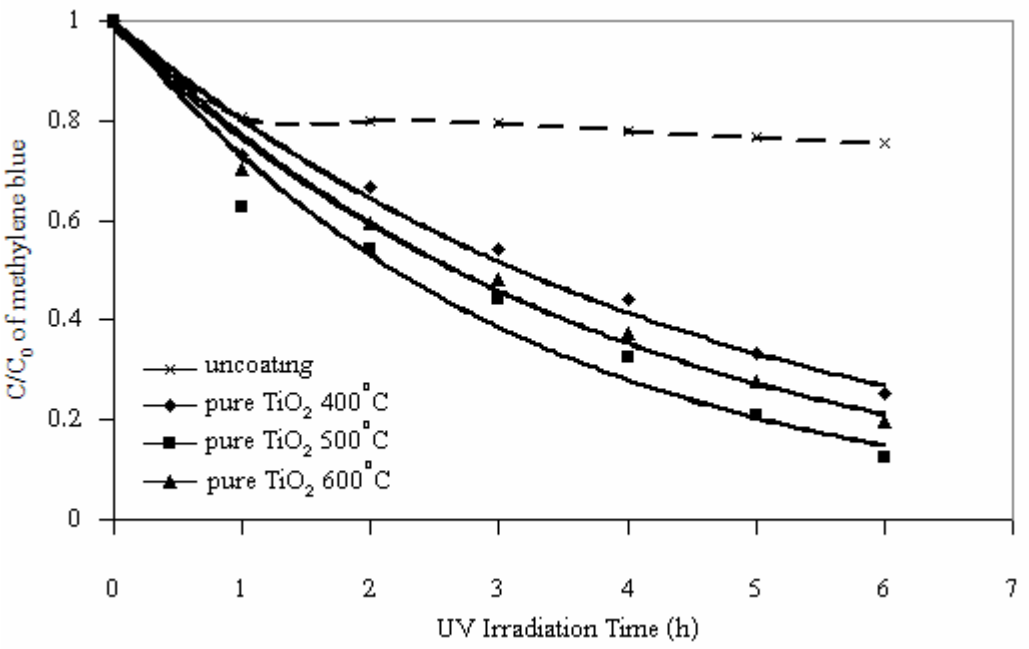

Figure 4.24 Photocatalytic degradation of methylene blue with pure TiO_2 catalysts calcined at the temperatures of 400 °C, 500 °C and 600 °C

Figure 4.25 shows the photocatalytic activity of Ag/TiO_2 composite films calcined at the temperatures of 400, 500 and 600 °C. It can be seen that photocatalytic activity at 500˚C was highest and decreased with increasing calcination temperature. At 500 ˚C, the results showed that the photocatalytic activity of pure TiO_2 is lower than that of Ag/TiO_2 with Ag content below 3 mol%. The degradation rate constant, k of methylene blue for 1mol%Ag doped TiO_2 film is 0.50. From these results, a small amount of Ag containing in TiO_2 film, it prevents the recombination of charges and oxidation by producing more $OH^{\cdot}$. The reduction potential of silver ion is suitable positioned for the effective photocatalytic reduction $Ag^+ + e^- \rightarrow Ag^0$ producing metallic silver on TiO_2 surface. Thus it was observed that the catalyst slightly darkens during the irradiation. However, a high concentration of Ag decreases the photocatalytic property of TiO_2 due the filter effect (Gupta et al., 2006). The thin film calcined at 500°C is observed to have the highest rate to photocatalytic activity and the film calcined at 400 °C has the lowest rate (Table 4.8). Because, from XRD pattern of film calcined at 400 °C show in Figure 4.11a, an amorphous phase appears where as at the 500 °C, an anatase single phase with small crystallite size is found.

It has been known that, anatase phase has better photocatalytic activity under UV light than other phase such as rutile or amorpous phase.

The photocatalytic activity of MWNTs/TiO_2 composite shown in Figure 4.26 and table 4.8, it can be seen that the photocatalytic activity of film calcined at the temperature of 500 ^{o}C was highest the photocatalytic activity and increases with an increase in MWNTs content from 0.1-1 wt% about 65-81%,respectively. Under UV light the photocatalytic activities of 1MWNTs/TiO_2 composites are lower than pure TiO_2 and Ag/TiO_2 film. It is due to its larger crystallite size compared with that of pure TiO_2 and 1Ag/TiO_2 film leading to a smaller specific surface area of 1MWNTs/TiO_2 film for photocatalytic reaction.

The photocatalytic degradation of methylene blue with 1Ag/1MWNTs/TiO_2 film calcined at the temperatures of 400 ^{o}C, 500 ^{o}C and 600 ^{o}C are illustrated in Figure 4.27 and Table 4.8. It can be seen that the 1Ag/1MWNTs/TiO_2 films calcined at at the temperatures of 400 ^{o}C, 500 ^{o}C and 600 ^{o}C, exhibit k = 0.29, 0.38 and 0.32, respectively. Since, from XRD pattern shown in Figure 4.12, the films calcined at the temperature range of 400 ^{o}C -600 ^{o}C , anatase single phase are formed and a degree of anatase crystallinity increase with an in crease calcinations temperature. Furthermore, the crystallite of film calcined at the temperature of 500 ^{o}C is smaller than that of 600 ^{o}C. It has seen that the photocatalytic activity of 1Ag/TiO_2 composites are higher than those of pure TiO_2 and 1Ag/1MWNTs/TiO_2 composites (Table 4.8) because the specific surface area and crystallite size are smaller than those of 1Ag/1MWNTs/TiO_2 and pureTiO_2 (Table4.5 and Table4.6). The photocatalytic reaction of the composite films calcined at the temperature of 500^{o}C are expressed in the following sequence as 1Ag/TiO_2>1Ag/1MWNTs/TiO_2> pureTiO_2 > 1MWNTs/TiO_2.

The photocatalytic activity determined by degradation methylene blue solution under the radiation of fluorescent light of 20 x 3 W powers in dark chamber. Are shown in Figure 4.28. It observes that 1Ag/TiO_2 films give the higher rate than those of 1Ag/1MWNTs/TiO_2, 1MWNTs/TiO_2 and pure TiO_2 films, respectively. The photocatalytic activity of pure TiO_2 is lower than that of 1MWNTs/TiO_2 film since MWNTs in 1MWNTs/TiO_2 composite film, can reduce band gap energy shown in Teble4.7. Therefore, for low energy activation condition (under fluorescent light), 1MWNTs/TiO_2 has a higher photocatalytic activity than pure TiO_2.

a) Ag/TiO_2_400°C

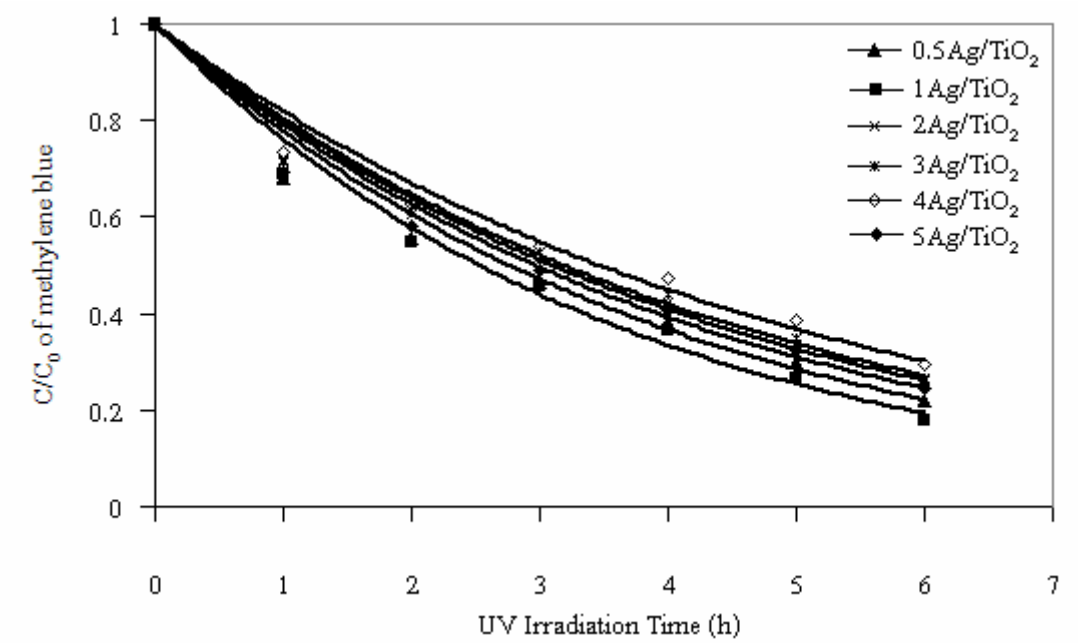

b) Ag/TiO_2_500°C

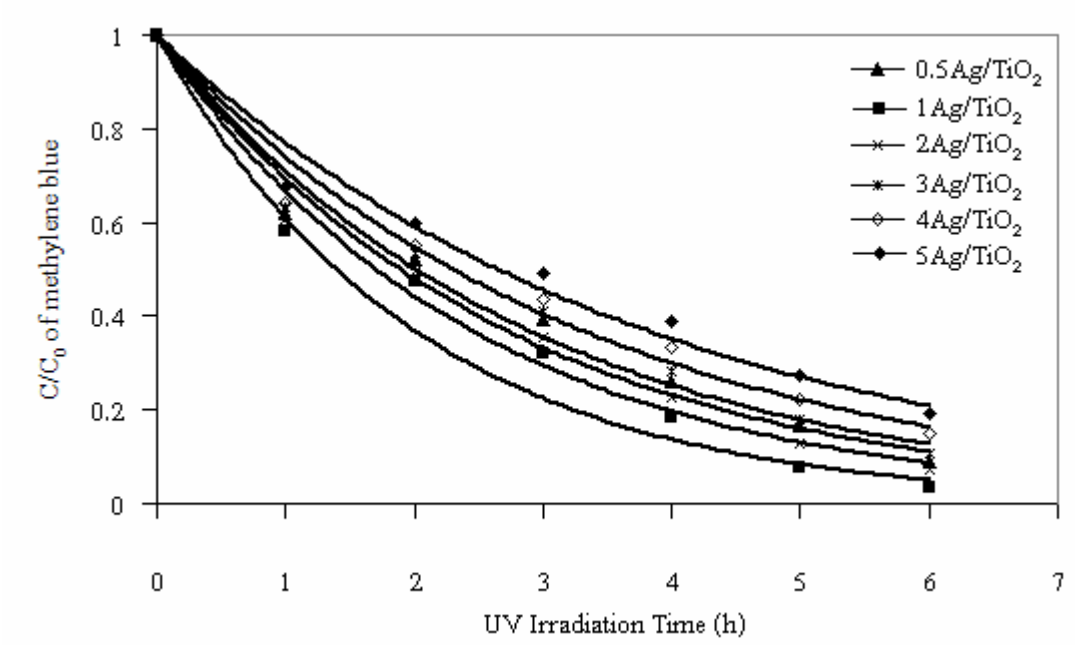

c) Ag/TiO_2_600°C

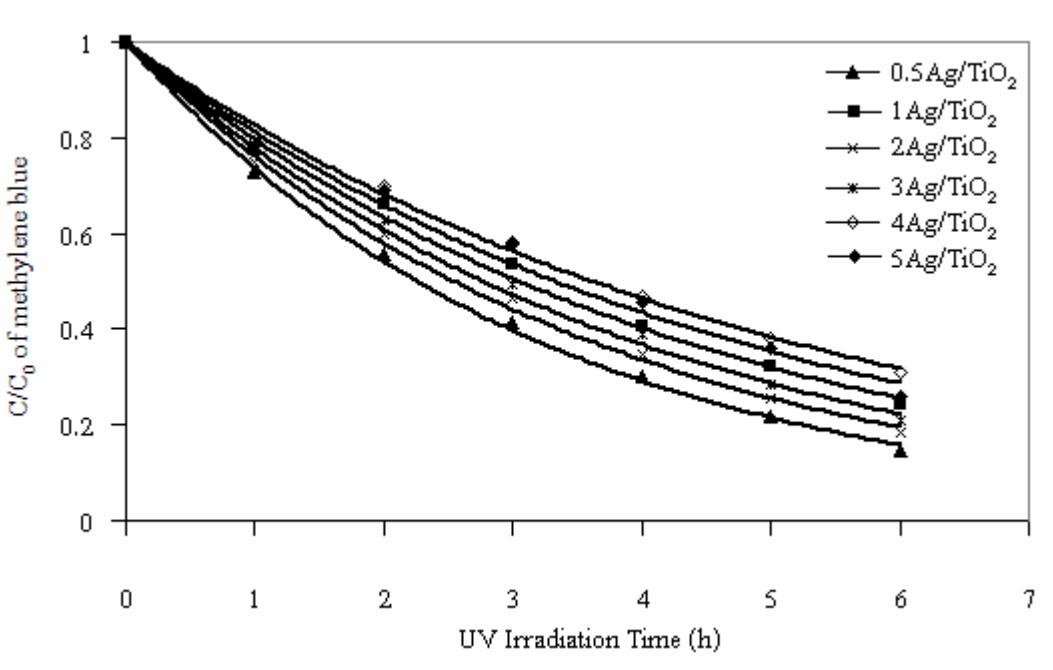

Figure 4.25 Photocatalytic degradation of methylene blue with Ag/TiO_2 catalysts calcined at the temperatures of a) 400 °C, b) 500 °C and c) 600 °C

a) $MWNTs/TiO_2$_400°C

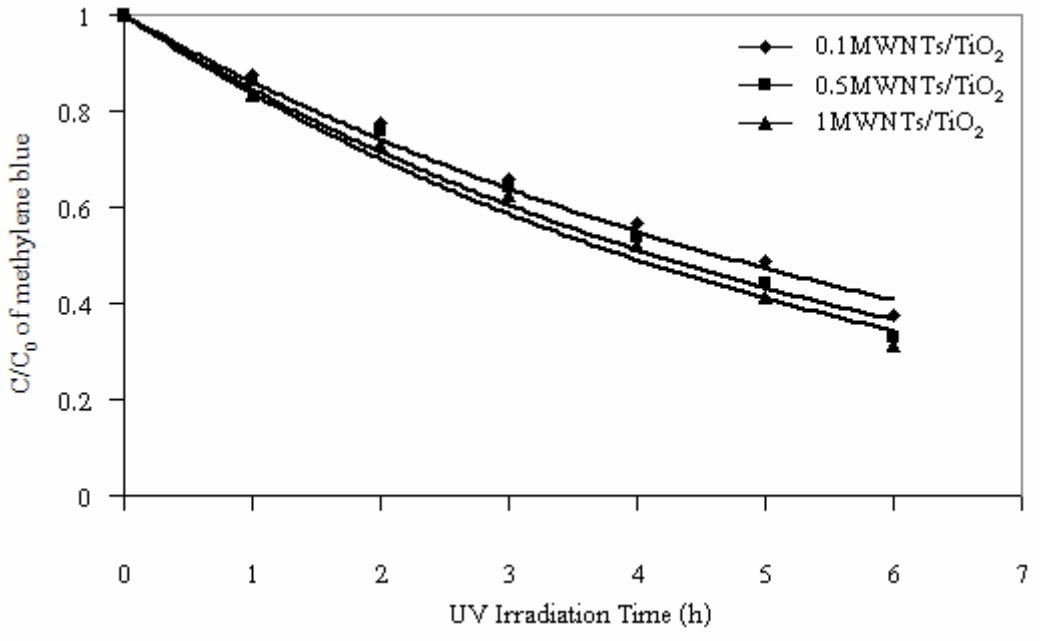

b) MWNTs/TiO_2_500°C

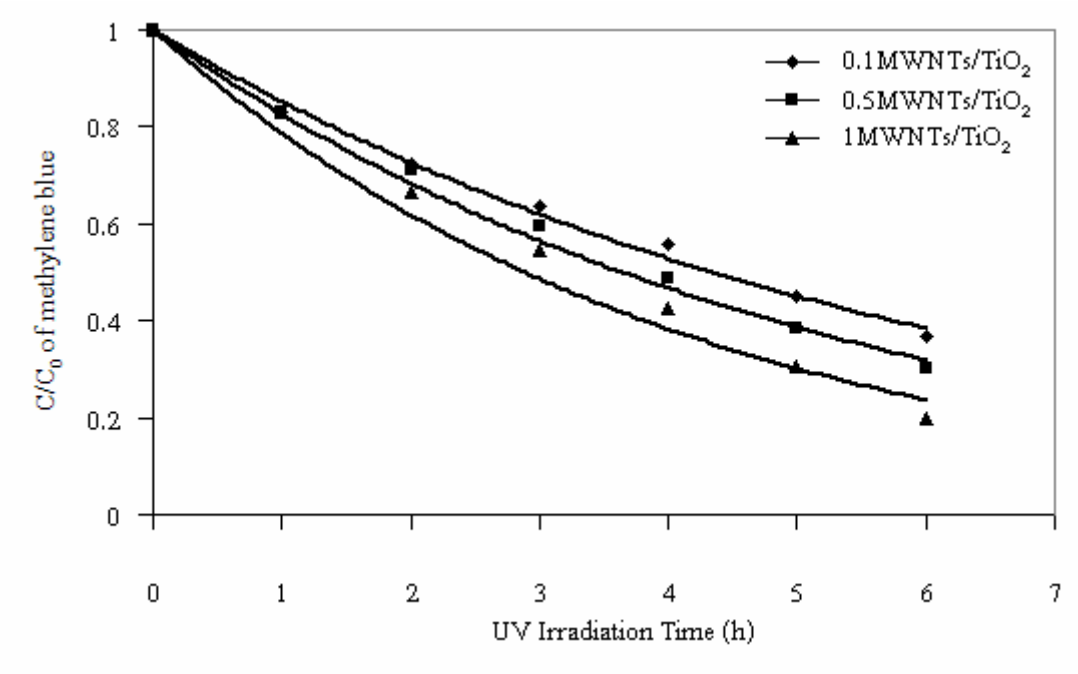

c) MWNTs/TiO_2_600°C

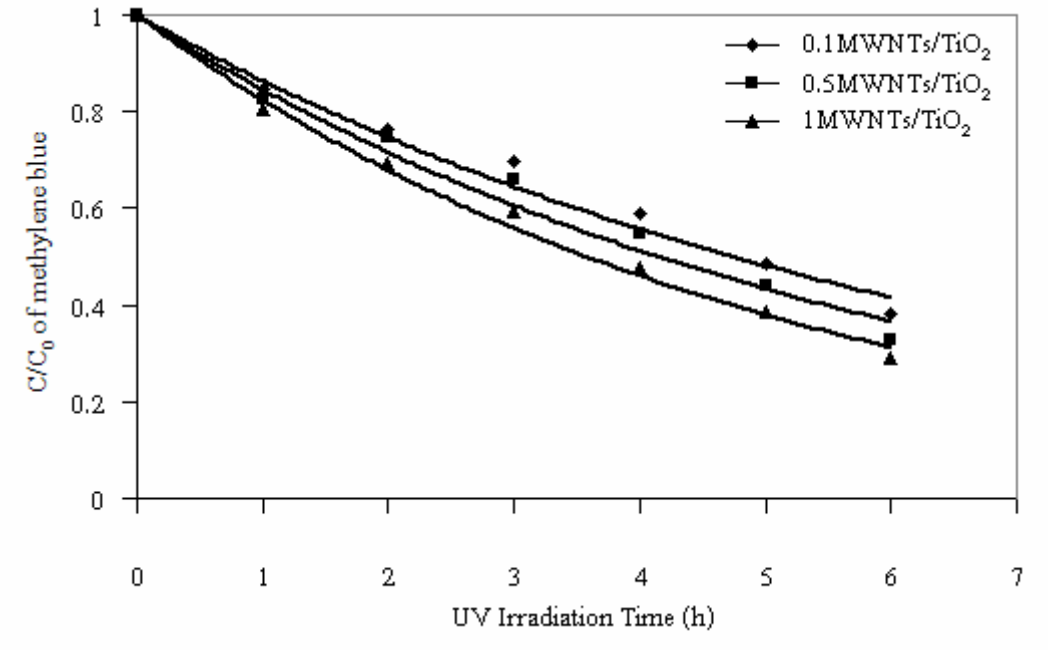

Figure 4.26 Photocatalytic degradation of methylene blue with MWNTs/TiO_2 catalysts calcined at the temperatures of a) 400 °C, b) 500 °C and c) 600 °C

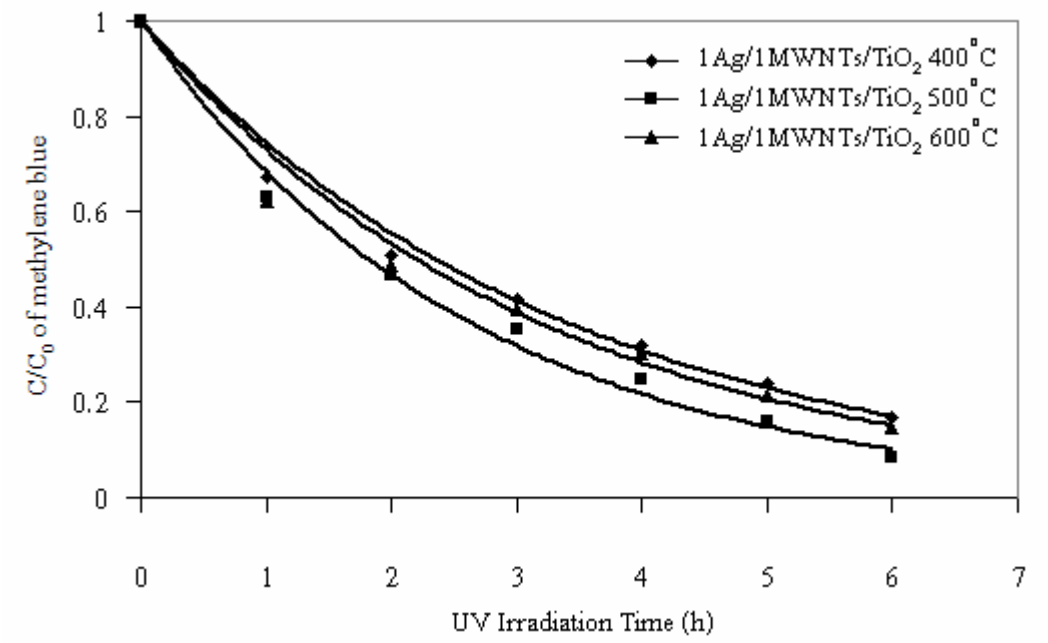

Figure 4.27 Photocatalytic degradation of methylene blue with 1Ag/1MWNTs/TiO_2 catalysts calcined at the temperatures of 400 °C, 500 °C and 600 °C

4.5 Effect of dopant on hydrophilic property

The contact angles of TiO_2 composite films are shown in Figure4.29 indicate the hydrophilic property unactivated and activated by photocatalytic reaction. It can be seen that pure TiO_2 has larger contact angle than the uncoated ceramic tile. It means that pure TiO_2 film has less hydrophilic property than uncoated ceramic tile surface. Because ceramic tile surface mainly contain SiO_2 or silicate which normally have higher hydropholic property than TiO_2. However, TiO_2 composite films seem to have smaller contact angle than uncoated surface and TiO_2 film. 1Ag/1MWNTs/TiO_2 has a super hydrophilic property shown in Figure 4.29 because its contact angle is zero after UV light irradiation for 10 min.

Table 4.8 Equation and rate constant of photocatalytic reaction under UV light

Samples	Rate Equation (R)	Rate constant (k)	R^2
Pure TiO_2			
Pure TiO_2_400°C	1.0000exp(-0.2197t)	0.2197	0.9862
Pure TiO_2_500°C	1.0000exp(-0.3051t)	0.3051	0.9729
Pure TiO_2_600°C	1.0000exp(-0.2597t)	0.2597	0.9898
Ag /TiO_2_400 °C			
0.5Ag/ TiO_2	1.0000exp(-0.2509t)	0.2509	0.9815
1Ag/ TiO_2	1.0000exp(-0.2737t)	0.2737	0.9850
2Ag/ TiO_2	1.0000exp(-0.2736t)	0.2536	0.9869
3Ag/ TiO_2	1.0000exp(-0.2173t)	0.2173	0.9828
4Ag/ TiO_2	1.0000exp(-0.2000t)	0.2000	0.9788
5Ag/ TiO_2	1.0000exp(-0.2339t)	0.2339	0.9801
Ag /TiO_2_500 °C			
0.5Ag/ TiO_2	1.0000exp(-0.3664t)	0.3664	0.9746
1Ag/ TiO_2	1.0000exp(-0.4973t)	0.4973	0.9500
2Ag/ TiO_2	1.0000exp(-0.4070t)	0.4070	0.9978
3Ag/ TiO_2	1.0000exp(-0.3444t)	0.3444	0.9788
4Ag/ TiO_2	1.0000exp(-0.3012t)	0.3012	0.9814
5Ag/ TiO_2	1.0000exp(-0.2615t)	0.2615	0.9777
Ag /TiO_2_600 °C			
0.5Ag/ TiO_2	1.0000exp(-0.3075t)	0.3075	0.9969
1Ag/ TiO_2	1.0000exp(-0.2276t)	0.2276	0.9944
2Ag/ TiO_2	1.0000exp(-0.2726t)	0.2726	0.9959
3Ag/ TiO_2	1.0000exp(-0.2501t)	0.2501	0.9947
4Ag/ TiO_2	1.0000exp(-0.1916t)	0.1916	0.9959
5Ag/ TiO_2	1.0000exp(-0.2083t)	0.2083	0.9846
MWNTs /TiO_2_400 °C			
0.1MWNTs/ TiO_2	1.0000exp(-0.1498t)	0.1498	0.9834
0.5MWNTs/ TiO_2	1.0000exp(-0.1677t)	0.1677	0.9785
1MWNTs/ TiO_2	1.0000exp(-0.1782t)	0.1782	0.9811
MWNTs /TiO_2_500 °C			
0.1MWNTs/ TiO_2	1.0000exp(-0.1595t)	0.1595	0.9907
0.5MWNTs/ TiO_2	1.0000exp(-0.1903t)	0.1903	0.9913
1MWNTs/ TiO_2	1.0000exp(-0.2400t)	0.2400	0.9671
MWNTs /TiO_2_600 °C			
0.1MWNTs/ TiO_2	1.0000exp(-0.1462t)	0.1462	0.9738
0.5MWNTs/ TiO_2	1.0000exp(-0.1673t)	0.1673	0.9704
1MWNTs/ TiO_2	1.0000exp(-0.1937t)	0.1937	0.9891
1Ag/MWNTs /TiO_2			
1Ag/MWNTs/TiO_2_400 °C	1.0000exp(-0.2943t)	0.2943	0.9900
1Ag/MWNTs/TiO_2_500 °C	1.0000exp(-0.3814t)	0.3817	0.9842
1Ag/MWNTs/TiO_2_600 °C	1.0000exp(-0.3152t)	0.3152	0.9847

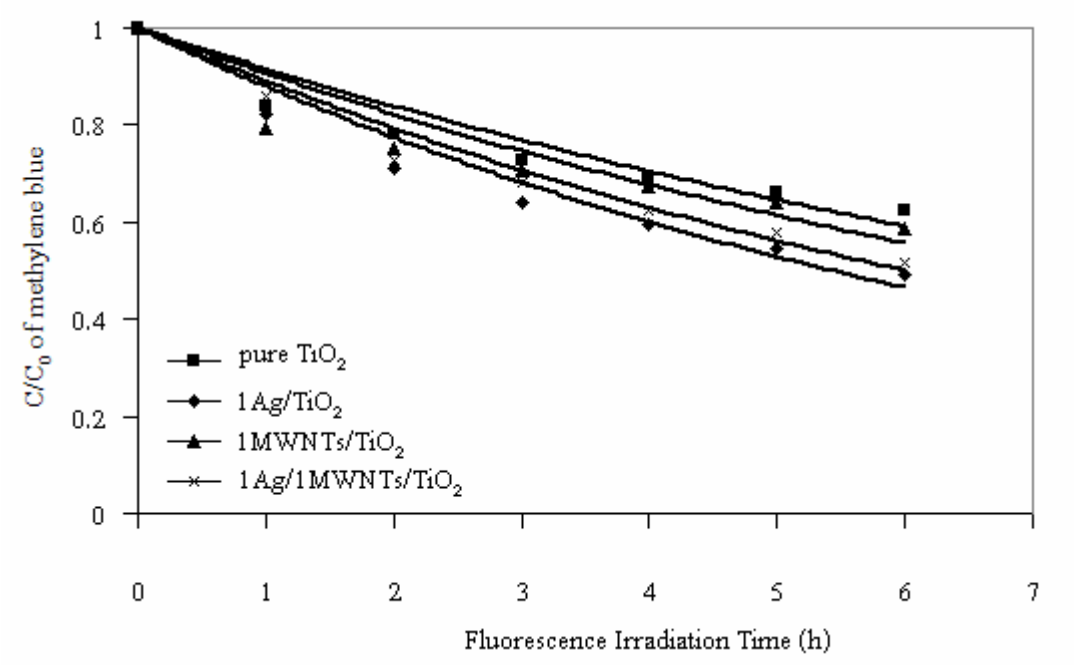

Figure 4.28 Photocatalytic degradation of Methylene blue under fluorescent light

Table 4.9 Equation and rate constant of photocatalytic reaction under fluorescent light

Samples	Rate Equation (C)	Rate constant (k)	R^2
pure TiO_2	1.0000exp(-0.0875t)	0.0875	0.8723
1Ag/TiO_2	1.0000exp(-0.2750t)	0.2750	0.9444
1MWNTs/TiO_2	1.0000exp(-0.0976t)	0.0976	0.8116
1Ag/1MWNTs/TiO_2	1.0000exp(-0.1155t)	0.1155	0.9601

Furthermore, the contact angle of 1Ag/TiO_2 and 1MWNTs/TiO_2 film because to be zero (super hydrophilic) after UV irradiation time of 15 min. It is due to their longer wavelength absorbed than pure TiO_2. The contact angle decrease as an increase photocatalytic time.

Figure 4.30 shows the contact angles of pure TiO_2, 1Ag/TiO_2, 1MWNTs/TiO_2 and 1Ag/1MWNTs/TiO_2 calcined at 500^{o}C under fluorescent light. It was observed that pure TiO_2 film has larger contact angle than TiO_2 composite film and uncoated ceramic tile surface. The trend of contact angles of the composite films under fluorescent are similar to those under UV light. However, the contact angle under fluorescent light are larger than those under UV due to higher energy activation of UV light. It believes that 1Ag/TiO_2, 1MWNTs/TiO_2 and

1Ag/1MWNTs/TiO_2 films will exhibit the superhydrophilic property as the irradiation un fluorescent light for longer period of time.

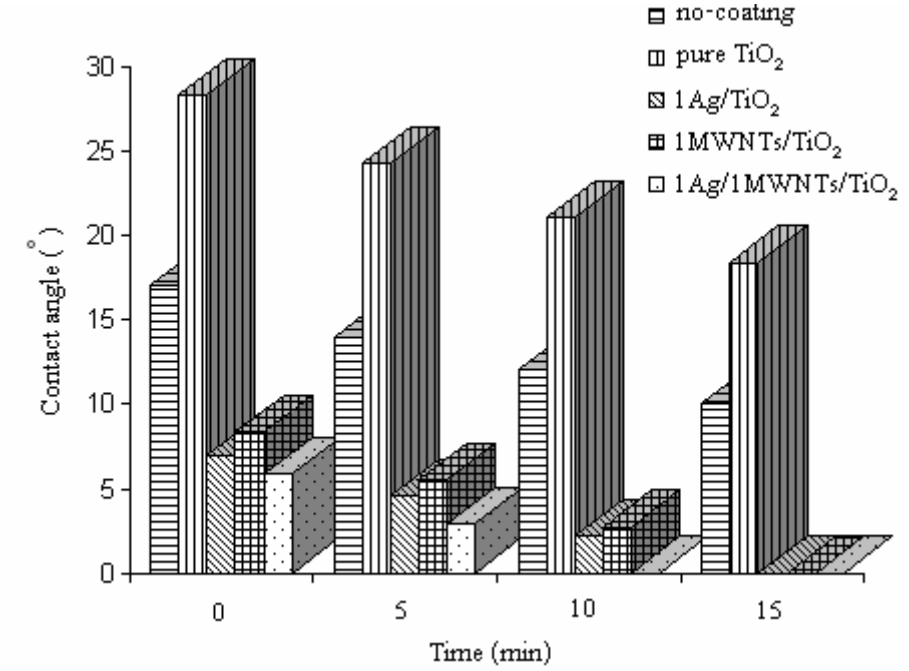

Figure4.29 Contact angle of pure TiO_2, 1Ag/TiO_2, 1MWNTs/TiO_2 and 1Ag/1MWNTs/TiO_2 calcined at the temperature of 500°C under UV light irradiation

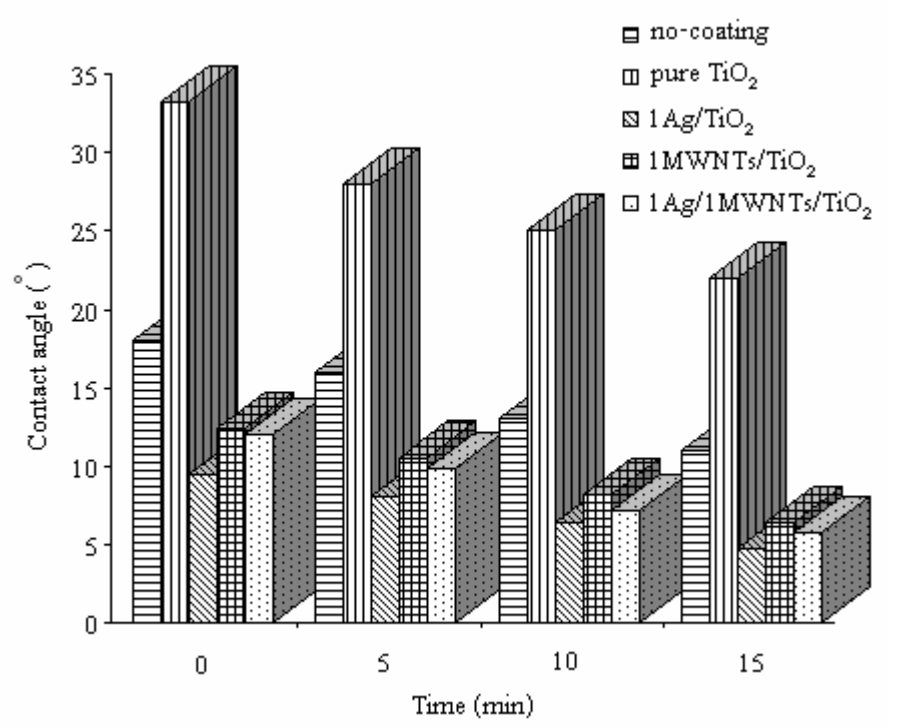

Figure4.30 Contact angle of pure TiO_2, 1Ag/TiO_2, 1MWNTs/TiO_2 and 1Ag/1MWNTs/TiO_2 calcined at the temperature of 500°C under fluorescent light

CHAPTER 5

Conclusion

In this work, pure TiO_2 and TiO_2 composite nanopowders and films were synthesized by sol-gel method. Ag ions and multiwalled carbon nanotubes (MWNTs) were used as dopants of the TiO_2 composite. The effect of calcinations temperature and dopant content on phase transformation, crystallite size, morphology, band gap energy, photocatalytic reaction and hydrophilic property were investigated and concluded as followings,

1) Both calcinations temperature and dopant content have an influence on the phase transformation and crystallite size of TiO_2 and TiO_2 composite powders and films. For pure TiO_2 the anatase single phase appears at the calcinations temperatures of 400 ^{o}C -500 ^{o}C and anatase phase partly transformed to rutile phase at above 500 ^{o}C. Therefore, the mixed phase of anatase and rutil were found at 600 ^{o}C -700 ^{o}C. At temperature of 800 ^{o}C, a rutile single phase was found. The crystallite sizes of pure TiO_2 increase with an increase in calcinations temperature. These trends were also found for Ag-doped TiO_2 or MWNTs doped TiO_2 or 1Ag/1MWNTa/TiO_2.

2) Dopant either Ag or MWNTs has an effect on the absorbed wavelength of light and band gap energy of the film. The more amount of Ag or MWNTs doped lead to shift the wavelength to be longer and the band gap energy to be narrower. Than that of pure TiO_2

3) The photocatalytic reaction of TiO_2 composite films were found to be highest at the calcinations temperature of 500 ^{o}C because the complete crystallinity of anatase phase appears at this temperature. The photocatalytic efficiency of pure TiO_2 and TiO_2 composite films in sequence were 1Ag/TiO_2 > 1Ag/1MWNTs/TiO_2 > pureTiO_2 ≥ 1MWNTs/TiO_2.

4) The photocatalytic reaction of pure TiO_2 and TiO_2 composite films may be expressed as an exponential rate equation of $R = 1.00\ e^{-kt}$, where k is a kinetic rate constant and t is irradiation time (h) under UV or fluorescent light.

5) The contact angles of 1Ag/TiO_2, 1MWNTs/TiO_2 and 1Ag/1MWNTs/TiO_2 calcined at 500^{o}C were found to be hydrophilicity (zero degree) after irradiation by UV light for 15 minutes, and less than 10 degree after irradiation by fluorescent light for 15 minute.

REFFERENCES

An, G., Ma, W., Sun, Z., Liu, Z., Han, B., Miao, S., Miao, Z. and Ding, K. (2007). "Preparation of titania/carbon nanotube composites using supercritical ethanol and their photocatalytic activity for phenol degradation under visible light irradiation." *Carbon* ,45, 1795–1801.

Arana, J. Garriga i Cabo,C., Dona-Rodryguez, J.M., Gonzalez-Dyaz, O. Herrera-Melian, J.A. and Perez-Pena, J. (2004). "FTIR study of formic acid interaction with TiO_2 and TiO_2 doped with Pd and Cu in photocatalytic processes." *Applied Surface Science*, 239, 60–71.

Brinker, C. J. and Scherer G.W. (1990) *Sol-Gel Science: The Physics and Chemistry of Sol-Gel Processing*, London, Academic Press, Inc.

Chang, C.C., Lin, C.K., Chan, C.C., Hsu, C.S. and Chen, C.Y. (2006). "Photocatalytic properties of nanocrystalline TiO_2 thin film with Ag additions." *Thin Solid Films*, 494, 274–278.

Chaoa, H.E., Yuna, Y.U. and Xingfanga, H.U. (2003). "Effect of silver doping on the phase transformation and grain growth of sol-gel titania powder." *Journal of the European Ceramic Society,* 23, 1457–1464.

Coleman, H.M., Chiang, K. and Amal, R. (2005). "Effects of Ag and Pt on photocatalytic degradation of endocrine disrupting chemicals in water." *Chemical Engineering Journal*, 113, 65–72.

Evans, P.and Sheel, D.W. (2007). "Photoactive and antibacterial TiO_2 thin films on stainless steel." *Surface & Coatings Technology*, 201, 9319–9324.

Eswaramoorthi, I.and Hwang L.P. (2007). "Anodic titanium oxide: A new template for the synthesis of larger diameter multi-walled carbon nanotubes." *Diamond & Related Materials,* doi:10.1016/j.diamond.2006.12.035.

Ghorai, T.K., Dhakb, D., Biswas, S.K., Dalai, S. and Pramanik, P. (2007). "Photocatalytic oxidation of organic dyes by nano-sized metal molybdate incorporated titanium dioxide ($M_xM_{ox}Ti_{1-x}O_6$) (M = Ni, Cu, Zn) photocatalysts." *Journal of Molecular Catalysis A: Chemica,.* 273, 224–229.

Guo, B., Liu, Z., Hong, L. and Jiang H. (2005). "Sol gel derived photocatalytic porous TiO_2 thin films." *Surface & Coatings Technology*, 198, 24–29.

Guan K. (2004). "Relationship between photocatalytic activity, hydrophilicity and self-cleaning effect of TiO_2/SiO_2." *films Surface & Coatings Technology*, 191, 155–160.

Harizanov, O., Ivanova, T. and Harizanova, A. (2001). "Study of sol–gel TiO_2 and TiO_2 –MnO obtained from a peptized Solution." *Materials Letters*, 49, 165–171.

Hoffmann, M. R., Martin, S.T., Choi, W. and Bahnemannt, D.W. (1995). "Environmental applications of semiconductor photocatalysis." *Chem. Rev*, 95, 69-96.

Hong, W.J. and Kang, M. (2006). "The super-hydrophilicities of Bi–TiO_2, V–TiO_2, and Bi–V–TiO_2 nano-sized particles and their benzene photodecompositions with H2O addition." *Materials Letters*, 60, 1296–1305.

Hou, X. G., Hao, F. H., Fan, B., Gu X. Y. and Liu, A. D. (2005). "Modification of TiO_2 Photocatalytic Films by V^+ Ion Implantation." *Nuclear Instruments and Methods in Physics Research B*, doi:10.1016/j.nimb.2005.07. 195.

Hsiang, H.-I. and Lin, S.-C. (2006). "Effects of aging on the kinetics of nanocrystalline anatase crystallite growth," *Materials Chemistry and Physics*, 95, 275–279.

Hu, Y., Tsai, H.L. and Huang, C.L. (2003). "Phase transformation of precipitated TiO_2 nanoparticles." *Materials Science and Engineerin,.* A344, 209-214.

Huang, D.G., Liao, S.J., Liu, J.M., Danga, Z. and Petrik, L. (2006). "Preparation of visible-light responsive N–F-codoped TiO_2 photocatalyst by a sol–gel-solvothermal method." *Journal of Photochemistry and Photobiology A: Che*mistry, 184, 282–288.

Jitianu, A,. Cacciaguerra, T., Berger, M.H., Benoit, R., Beguin, F. and Bonnamy, S. (2004). "New carbon multiwall nanotubes – TiO2 nanocomposites obtained by the sol–gel method." *Journal of Non-Crystalline Solids*, 345-346, 596–600.

Jung, K.Y. and Park, S.B. (2004). "Photoactivity of SiO_2/TiO_2 and ZrO_2/TiO_2 mixed oxides prepared by sol–gel method." *Materials Lette, .*58, 2897–2900.

Kim, K.D., Han, D.H., Lee, J.B. Hee and Kim, T. (2006). "Formation and characterization of Ag-deposited TiO_2 nanoparticles by chemical reduction method." *Scripta Materialia*, 54, 143–146.

Kuo, C.S., Tseng, Y.H., Huangb, C.H. and Li, Y.Y. (2007). "Carbon-containing nano-titania prepared by chemical vapor deposition and its visible-light-responsive photocatalytic activity." *Journal of Molecular Catalysis A: Chemical,* 270, 93–100.

Kwona, C.H., Kima, J.H., Junga, I.S., Shina, H. and Yoon, K.H. (2003). "Preparation and characterization of TiO2–SiO_2 nano-composite thin films." *Ceramics International*, 29, 851–856.

Langlet, M., Kima, A., Audiera, M., Guillar, C. and Herrmann J.M. (2003). "Transparent photocatalytic films deposited on polymer substrates from Sol–gel processed titania sols." *Thin Solid Fils,* 429, 13–21.

Lee, T.Y., Alegaonkar, P.S. and Yoo, J.B. (2007). "Fabrication of dye sensitized solar cell using TiO_2 coated carbon nanotubes." *Thin Solid Film*, 515, 5131–5135.

Liu, Y., Liu, C.Y. Rong, Q.H. and Zhang, Z. (2003). "Characteristics of The Silver-doped TiO_2 nanoparticles." *Applied Surface Science*, 220, 7–11.

Li, J.G. and Ishigaki T. (2004). "Brookite !rutile phase transformation of TiO_2 studied with monodispersed particles." *Acta Materialia*, 52, 5143–5150.

Li, Y., Hwang, D.S., Lee, N.H. and Kim, S.J. (2005). "Synthesis and characterization of carbon-doped titania as an artificial solar light sensitive photocatalyst." *Chemical Physics Letters,* 404, 25–29.

L.M.S. Colpini Alves, H.J., Santos, O.A.A. and Costa, C.M.M. (2008). "Discoloration and degradation of textile dye aqueous solutions with titanium oxide catalysts obtained by the solegel method." *Dyes and Pigment,* 76, 525-529.

Madaeni, S.S.and Ghaemi, N. (2007). "Characterization of self-cleaning RO membranes coated with TiO_2 particles under UV irradiation." *Journal of Membrane Science*, 303, 221–233.

Maness, P.C. Smolinski, S. Blake, D.M., Huang, Z., Wolfrum, E. J. and Jacob, W.A. (1999). "Bactericidal activity of photocatalytic TiO_2 reaction: toward an understanding of its killing mechanism." *Applied and environmental microbiology*, 4094–4098.

Mills, A., Davies, R.H. and Worsley, D. (1993). *Chem. Soc. Rev*. 22 (6) 417–425.

Muruganandham, M., Chen, S.H. and Wu, J.J. (2007). "Evaluation of water treatment sludge as a catalyst for aqueous ozone decomposition." *Catalysis Communications*, 8, 1609–1614.

Neppolian, B., Wang, Q., Jung, H. and Choi, H. (2008). "Ultrasonic-assisted sol-gel method of preparation of TiO_2 nano-particles: Characterization, properties and 4-chlorophenol removal application." *Ultrasonics Sonochemistry*, 15, 649–658.

Nguyen, V.N.H., Amal, R. and Beydoun D. (2005). "Photodeposition of CdSe using Se- TiO_2 Suspensions as Photocatalysts." *Journal of Photochemistry and Photobiology A: Chemistry*, doi:10.1016/j.jphotochem.2005.07.012.

Ou, Y., Lin, J., Fang, S. and Liao D. (2006). "MWNT–TiO_2: Ni composite catalyst: A new class of catalyst for photocatalytic H_2 evolution from water under visible light illumination.", *Chemical Physics Letters*, 429,199–203.

Priya, M.H. and Madras, G. (2005). " Kinetics of photocatalytic degradation of phenols with multiple substituent groups." *Journal of Photochemistryand PhotobiologyA: Chemistr*, doi:10.1016/j.jphotochem.2005.08.022.

Rengaraj, S. and Li, X.Z. (2006). "Enhanced photocatalytic activity of TiO_2 by doping with Ag for degradation of 2, 4, 6-trichlorophenol in aqueous suspension." *Journal of Molecular Catalysis A: Chemical,* 243, 60–67.

Sen, S., Mahantya, S., Roya, S., Heintzb, O., Bourgeoisb, S. and Chaumont, D. (2005). "Investigation on sol–gel synthesized Ag-doped TiO2 cermet thin films." *Thin Solid Film*, 474, 245– 249.

Shifu, C., Lei, C., Shen G., and Gengyu C. (2005). "The preparation of nitrogen-doped photocatalyst $TiO_{2-x}N_x$ by ball milling." *Chemical Physics Letters*, 413, 404–409.

Siddiquey, I.A., Furusawa, T., Sato, M., Honda, K., Suzuki,N. (2008). "Control of the photocatalytic activity of TiO_2 nanoparticles by silica coating with polydiethoxysiloxane." *Dyes and Pigments*, 76, 754-759.

Sonawane, R.S. and Dongare, M.K. (2006). "Sol–gel synthesis of Au/TiO_2 thin films for photocatalytic degradation of phenol in sunlight." *Journal of Molecular Catalysis A: Chemical*, 243, 68–76.

Sonawane, R.S., Kale, B.B and Dongare, M.K. (2004). "Preparation and photo-catalytic activity of Fe–TiO_2 thin films prepared by sol–gel dip coating." *Materials Chemistry and Physics,* 85, 52–57.

Sreethawong, T. and Yoshikawa S. (2005). "Enhanced photocatalytic hydrogen evolution over Pt supported on mesoporous TiO_2 prepared by single-step sol–gel process with surfactant template." *International Journalof Hydrogen Energy,* doi:10.1016/j.ijhydene.2005.06.015.

Su, P.-G. and Chang Y.-P. (2008). "Low-humidity sensor based on a quartz-crystal microbalance coated with polypyrrole/Ag/TiO_2 nanoparticles composite thin films." *Sensors and Actuators B*, 129, 915–920.

Sun, L., Lu, H. and Zhou, J. (2008). "The synergistic effect of two photosynthetic pigments in dye-sensitized mesoporous TiO_2 solar cells." *Dyes and Pigment*, 76, 327-331.

Suresh, C., Biju, V., Mukundan, P. and Warrier, K. G.K. (1998). "Anatase to rutile tranfromation in sol-gel titania by modification of precursor." *Polyhedro,* 17, 3131-135.

Tsuji, H., Sugahara, H., Gotoh, Y. and Ishikawa, J. (2003). "Improvement of photocatalytic efficiency of rutile titania by silver negative-ion implantation." *Nuclear Instruments and Methods in Physics Research*, B 206, 249–253.

Tsuji, H., Sakai, N., Sugahara, H., Gotoh, Y. and Ishikawa, J. (2005). "Silver negative-ion implantation to sol–gel TiO_2 film for improving photocatalytic property under fluorescent light." *Nuclear Instruments and Methods in Physics Research*, B 237, 433–437.

Tsuji, H., Sakai, N., Gotoh, Y. and Ishikawa, J. (2006). "Photocatalytic properties of sol–gel titania film under fluorescent-light irradiation improved by silver negative-ion implantation." *Nuclear Instruments and Methods in Physics Research,* 242, 129–132.

Usui, H., Matsui, H., Tanabe, N. and Yanagida, S. (2004). "Improved dye-sensitized solar cells using ionic nanocomposite gel electrolytes." *Journal of Photochemistry and PhotobiologyA: Chemistry*, 164, 97–101.

Venkatachalam, N. Palanichamy, M. Murugesan, V. (2007), "Sol–gel preparation and characterization of alkaline earth metal doped nano TiO_2: Efficient photocatalytic degradation of 4-chlorophenol." *Journal of Molecular Catalysis A: Chemical*, 273, 177–185.

Wang, W., Serp, P., Kalck, P. and Faria, J.L. (2005). "Visible light photo degradation of phenol on MWNT-TiO_2 composite catalysts prepared by a modified sol–gel method." *Journal of Molecular Catalysis A: Chemical,* 235, 194–199.

Wang, W., Serp, P., Kalck, P. C.G. Silva, and Faria, J.L. (2007). "Preparation and characterization of nanostructured MWCNT-TiO_2 composite materials for photocatalytic water treatment applications." *Materials Research Bulletin,* doi:10.1016/j. materresbull. 2007.04.032.

Wang, Z.C., Chen, J.F. and Hu, X.F. (2000). "Preparation of nanocrystalline TiO_2 powders at near room temperature from peroxo-polytitanic acid gel." *Materials Letters*, 43, 87–90.

Wei, C., Lin, W.Y., Zaina1, Z., Williams, N.E., Zhu, K., Krurlc, A.P., Smith, R.L. and Rajeshwar, K. (1994). "Bactericidal activity of $Ti0_2$ photocatalyst in aqueous media: toward a solar- assisted water disinfection system." *Environ. Sci. Technol*, 28, 934- 938.

Wells, AF., (1975). *Structural inorganic chemistry*. Oxford: Clarendon Press.

Wu, X., Wei, Q. and Zhaohua J. (2006). "Influence of Fe^{3+} ions on the photocatalytic activity of TiO_2 films prepared by micro-plasma oxidation method." *Thin Solid Films,* 496, 288–292.

Xia, X.H., Jia, Z.J., Yu, Y., Liang, Y., Wang, Z., and Ma, L.L. (2007). "Preparation of multi-walled carbon nanotube supported TiO_2 and its photocatalytic activity in the reduction of CO_2 with H_2O." *Carbon*, 45, 717–721.

Xiaodan, Y., Qingyin, W., Shicheng, J. and Yihang, G. (2006). "Nanoscale ZnS/TiO_2 composites: Preparation, characterization, and visible-light photocatalytic activity." *Materials Characterization*, 57, 333–341.

Xin, B., Ren, Z., Hu, H., Zhang, X., Dong,C., Shi, K., Jing, L. and Fu, H. (2005). "Photocatalytic activity and interfacial carrier transfer of Ag–TiO_2 nanoparticle films." Applied Surface Science, 252, 2050–2055.

Xua, M.W., Baob, S.J. and Zhang, X.G. (2005), "Enhanced photocatalytic activity of magnetic TiO_2 photocatalyst by silver deposition," *Materials Letters,* 59, 2194–2198.

Yang, J. ,Bai, H., Tan, X. and Lian, J. (2006). "IR and XPS investigation of visible-light photocatalysis: nitrogen–carbon-doped TiO_2 film." *Applied Surface Science*, 253, 1988–1994.

Yoon, K.H., Noha, J.S., Kwon, C.H. and Muhammed M. (2006). "Photocatalytic behavior of TiO_2 thin films prepared by sol–gel process." *Materials Chemistry and Physics,* 95, 79–83.

Yu, J., Yu, H., Ao, C.H., Lee, S.C., Yu, J.C. and Ho, W. (2006). "Preparation, characterization and photocatalytic activity of in situ Fe-doped TiO_2 thin films." *Thin Solid Films*, 496, 273– 280.

Yu, Y., Yu, J.C., Chan, C.Y., Che,Y.K., Zhao, J.C., Ding, L., Ge, W.K. and Wong, P.K. (2005). "Enhancement of adsorption and photocatalytic activity of TiO_2 by using carbon nanotubes for the treatment of azo dye." *Applied Catalysis B: Environmental*, 61, 1–11.

Yuan, R., Guana, R., Liu, P. and Zheng, J. (2007). "Photocatalytic treatment of wastewater from paper mill by TiO_2 loaded on activated carbon fibers." *Colloids and Surfaces A: Physicochem. Eng. Aspects,* 293, 80–86.

Zhang, Q., Gao, L. and Guo, J. (2000). "Effect of hydrolysis conditions on morphology and crystallization of nanosized TiO2 powder." *Journal of the European Ceramic Society*, 20, 2153-2158.

Zhang, X., Yang, H., Zhang, F. and Chan, K.Y. (2007). "Preparation and characterization of Pt–TiO_2– SiO_2 mesoporous materials and visible-light photocatalytic performance." *Materials Letters*, 61, 2231–2234.

Zhang, X., Zhang, F. and Chanb, K.Y. (2005). "The Synthesis of Pt-modified titanium dioxide thin films by micro emulsion templating their characterization and visible-light photocatalytic." *Materials Chemistry and Physics,* doi:10.1016/j.matchemphys.2005.08.060.

Zhu, K.R., Zhang, M.S., Hong, J.M. and, Yin, Z. (2005). "Size Effect on phase transition sequence of TiO_2 nanocrystal." *Materials Science and Engineering A,* 403, 87–93.

Zhu, J., Zheng, W., Hea, B. Zhang, J. and Anpo, M. (2004). "Characterization of Fe–TiO_2 photocatalysts synthesized by hydrothermal method and their photocatalytic reactivity for photodegradation of XRG dye diluted in water." *Journal of Molecular Catalysis A: Chemical,* 216, 35–43.

APPENDIX A

Photocatalytic activity test

Appendices A

Table A1 Photocatalytic activity of ceramic tile uncoated TiO_2

Sample	UV Irradiation Time (h)					
	1	2	3	4	5	6
Repeat 1	0.83	0.83	0.82	0.79	0.78	0.76
Repeat2	0.80	0.80	0.79	0.77	0.77	0.75
Repeat3	0.79	0.78	0.77	0.76	0.75	0.75
Avg.	0.81	0.80	0.80	0.78	0.77	0.75
S.D	0.02	0.02	0.03	0.02	0.01	0.01

Table A2 Photocatalytic activity of pure TiO_2 calcined at temperature of 400 ^{o}C

Sample	UV Irradiation Time (h)					
	1	2	3	4	5	6
Repeat 1	0.76	0.71	0.62	0.55	0.44	0.34
Repeat2	0.68	0.60	0.43	0.28	0.17	0.13
Repeat3	0.74	0.68	0.55	0.47	0.38	0.27
Avg.	0.73	0.66	0.54	0.43	0.33	0.25
S.D	0.04	0.06	0.09	0.14	0.14	0.11

Table A3 Photocatalytic activity of pure TiO_2 calcined at temperature of 500 ^{o}C

Sample	UV Irradiation Time (h)					
	1	2	3	4	5	6
Repeat 1	0.52	0.54	0.44	0.32	0.20	0.11
Repeat2	0.65	0.54	0.48	0.36	0.24	0.15
Repeat3	0.64	0.54	0.42	0.31	0.21	0.14
Avg.	0.63	0.54	0.45	0.33	0.22	0.13
S.D	0.02	0.00	0.03	0.02	0.02	0.02

Table A4 Photocatalytic activity of pure TiO_2 calcined at temperature of 600 ^{o}C

Sample	UV Irradiation Time (h)					
	1	2	3	4	5	6
Repeat1	0.67	0.60	0.53	0.47	0.36	0.21
Repeat2	0.71	0.58	0.45	0.32	0.25	0.19
Repeat3	0.72	0.60	0.46	0.31	0.22	0.17
Avg.	0.70	0.59	0.48	0.37	0.27	0.19
S.D	0.02	0.01	0.04	0.09	0.07	0.02

Table A5 Photocatalytic activity of Ag/TiO_2 calcined at temperature of 400 ^{o}C

Sample	Repeat	UV Irradiation Time (h)					
		1	2	3	4	5	6
$0.5Ag/TiO_2$	1	0.61	0.48	0.41	0.36	0.20	0.15
	2	0.75	0.59	0.50	0.38	0.31	0.23
	3	0.68	0.59	0.48	0.41	0.38	0.29
	Avg.	0.68	0.56	0.46	0.38	0.30	0.22
	S.D	0.07	0.06	0.05	0.03	0.09	0.07
$1Ag/TiO_2$	1	0.70	0.55	0.46	0.36	0.23	0.17
	2	0.70	0.56	0.46	0.33	0.21	0.18
	3	0.67	0.54	0.45	0.40	0.35	0.19
	Avg.	0.69	0.55	0.46	0.37	0.26	0.18
	S.D	0.02	0.01	0.01	0.04	0.07	0.01
$2Ag/TiO_2$	1	0.72	0.60	0.49	0.40	0.31	0.19
	2	0.75	0.61	0.56	0.43	0.33	0.31
	3	0.69	0.59	0.48	0.44	0.36	0.28
	Avg.	0.72	0.60	0.51	0.42	0.33	0.26
	S.D	0.03	0.01	0.04	0.02	0.03	0.06
$3Ag/TiO_2$	1	0.69	0.62	0.55	0.48	0.41	0.30
	2	0.74	0.62	0.52	0.40	0.31	0.24
	3	0.71	0.61	0.51	0.43	0.32	0.26
	Avg.	0.71	0.62	0.53	0.44	0.35	0.27
	S.D	0.02	0.01	0.02	0.04	0.05	0.03
$4Ag/TiO_2$	1	0.75	0.63	0.53	0.48	0.35	0.26
	2	0.76	0.61	0.55	0.43	0.37	0.26
	3	0.69	0.64	0.54	0.51	0.43	0.36
	Avg.	0.73	0.63	0.54	0.47	0.39	0.29
	S.D	0.04	0.02	0.01	0.04	0.04	0.06
$5Ag/TiO_2$	1	0.67	0.55	0.45	0.37	0.31	0.21
	2	0.73	0.60	0.50	0.37	0.24	0.20
	3	0.68	0.59	0.52	0.49	0.42	0.32
	Avg.	0.69	0.58	0.49	0.41	0.32	0.24
	S.D	0.03	0.02	0.03	0.07	0.09	0.07

Table A6 Photocatalytic activity of Ag/TiO_2 calcined at temperature of 500 ^{o}C

Sample	Repeat	UV Irradiation Time (h)					
		1	2	3	4	5	6
$0.5Ag/TiO_2$	1	0.61	0.52	0.36	0.25	0.16	0.09
	2	0.62	0.53	0.41	0.27	0.16	0.09
	3	0.63	0.52	0.40	0.26	0.18	0.09
	Avg.	0.62	0.52	0.39	0.26	0.17	0.09
	S.D	0.01	0.00	0.03	0.01	0.01	0.00
$1Ag/TiO_2$	1	0.62	0.47	0.31	0.18	0.10	0.06
	2	0.59	0.47	0.33	0.18	0.07	0.02
	3	0.53	0.48	0.33	0.18	0.07	0.02
	Avg.	0.58	0.47	0.32	0.18	0.08	0.03
	S.D	0.05	0.01	0.01	0.00	0.02	0.02
$2Ag/TiO_2$	1	0.60	0.49	0.36	0.25	0.16	0.11
	2	0.61	0.51	0.35	0.21	0.12	0.05
	3	0.61	0.50	0.35	0.22	0.11	0.05
	Avg.	0.61	0.50	0.36	0.23	0.13	0.07
	S.D	0.00	0.01	0.00	0.02	0.03	0.03
$3Ag/TiO_2$	1	0.64	0.54	0.39	0.27	0.18	0.10
	2	0.63	0.53	0.42	0.29	0.18	0.11
	3	0.62	0.54	0.42	0.30	0.17	0.10
	Avg.	0.63	0.54	0.41	0.29	0.18	0.11
	S.D	0.01	0.00	0.02	0.01	0.00	0.01
$4Ag/TiO_2$	1	0.66	0.54	0.44	0.34	0.25	0.18
	2	0.64	0.56	0.44	0.34	0.22	0.15
	3	0.63	0.55	0.44	0.32	0.21	0.13
	Avg.	0.64	0.55	0.44	0.34	0.23	0.16
	S.D	0.02	0.01	0.00	0.34	0.02	0.02
$5Ag/TiO_2$	1	0.67	0.56	0.47	0.39	0.30	0.21
	2	0.67	0.60	0.50	0.39	0.27	0.18
	3	0.68	0.62	0.50	0.37	0.26	0.20
	Avg.	0.67	0.59	0.49	0.38	0.28	0.19
	S.D	0.00	0.03	0.02	0.01	0.02	0.02

Table A7 Photocatalytic activity of Ag/TiO_2 calcined at temperature of 600 ^{o}C

Sample	Repeat	UV Irradiation Time (h)					
		1	2	3	4	5	6
$0.5Ag/TiO_2$	1	0.73	0.55	0.44	0.32	0.23	0.15
	2	0.75	0.57	0.45	0.36	0.28	0.19
	3	0.70	0.54	0.35	0.23	0.14	0.10
	Avg.	0.73	0.55	0.41	0.30	0.22	0.15
	S.D	0.02	0.02	0.05	0.07	0.07	0.05
$1Ag/TiO_2$	1	0.77	0.66	0.53	0.39	0.31	0.22
	2	0.73	0.60	0.46	0.33	0.27	0.18
	3	0.83	0.72	0.61	0.51	0.39	0.32
	Avg.	0.78	0.66	0.53	0.41	0.32	0.24
	S.D	0.05	0.06	0.07	0.09	0.06	0.07
$2Ag/TiO_2$	1	0.76	0.59	0.46	0.34	0.24	0.17
	2	0.70	0.59	0.45	0.34	0.26	0.18
	3	0.79	0.61	0.48	0.37	0.27	0.21
	Avg.	0.75	0.60	0.47	0.35	0.26	0.18
	S.D	0.04	0.01	0.01	0.02	0.02	0.02
$3Ag/TiO_2$	1	0.77	0.64	0.48	0.38	0.26	0.19
	2	0.73	0.54	0.41	0.28	0.18	0.12
	3	0.83	0.71	0.59	0.51	0.40	0.32
	Avg.	0.77	0.63	0.50	0.39	0.28	0.21
	S.D	0.05	0.08	0.09	0.12	0.11	0.10
$4Ag/TiO_2$	1	0.78	0.70	0.58	0.46	0.37	0.30
	2	0.77	0.67	0.55	0.44	0.35	0.28
	3	0.82	0.73	0.61	0.50	0.43	0.36
	Avg.	0.79	0.70	0.58	0.47	0.38	0.31
	S.D	0.03	0.03	0.03	0.03	0.04	0.05
$5Ag/TiO_2$	1	0.78	0.72	0.61	0.51	0.41	0.27
	2	0.74	0.60	0.47	0.31	0.22	0.19
	3	0.83	0.75	0.65	0.55	0.46	0.32
	Avg.	0.78	0.69	0.58	0.46	0.36	0.26
	S.D	0.04	0.08	0.09	0.13	0.13	0.07

Table A8 Photocatalytic activity of MWNTs/TiO_2 calcined at temperature of 400 ^oC

Sample	Repeat	UV Irradiation Time (h)					
		1	2	3	4	5	6
0.1MWNTs	1	0.87	0.77	0.66	0.57	0.50	0.38
/TiO_2	2	0.82	0.71	0.66	0.59	0.50	0.38
	3	0.92	0.84	0.66	0.54	0.47	0.37
	Avg.	0.87	0.77	0.66	0.57	0.49	0.38
	S.D	0.05	0.06	0.00	0.02	0.01	0.00
0.5MWNTs	1	0.93	0.79	0.61	0.51	0.38	0.28
/TiO_2	2	0.80	0.72	0.67	0.57	0.50	0.38
	3	0.86	0.76	0.64	0.53	0.44	0.33
	Avg.	0.86	0.76	0.64	0.54	0.44	0.33
	S.D	0.07	0.03	0.03	0.03	0.06	0.05
1MWNTs/	1	0.85	0.71	0.59	0.47	0.35	0.26
TiO_2	2	0.82	0.75	0.66	0.57	0.47	0.36
	3	0.84	0.73	0.63	0.52	0.41	0.31
	Avg.	0.84	0.73	0.63	0.52	0.41	0.31
	S.D	0.02	0.02	0.03	0.05	0.06	0.05

Table A9 Photocatalytic activity of MWNTs/TiO_2 calcined at temperature of 500 ^oC

Sample	Repeat	UV Irradiation Time (h)					
		1	2	3	4	5	6
0.1MWNTs	1	0.82	0.75	0.64	0.57	0.49	0.36
/TiO_2	2	0.84	0.72	0.64	0.57	0.44	0.39
	3	0.81	0.67	0.59	0.50	0.43	0.35
	Avg.	0.82	0.71	0.62	0.55	0.46	0.36
	S.D	0.02	0.04	0.03	0.04	0.03	0.03
0.5MWNTs	1	0.84	0.71	0.61	0.52	0.40	0.31
/TiO_2	2	0.82	0.71	0.57	0.45	0.37	0.29
	3	0.81	0.74	0.60	0.51	0.41	0.30
	Avg.	0.82	0.72	0.60	0.50	0.39	0.30
	S.D	0.02	0.02	0.02	0.04	0.02	0.01
1MWNTs/	1	0.84	0.67	0.53	0.41	0.26	0.16
TiO_2	2	0.85	0.70	0.56	0.44	0.32	0.20
	3	0.78	0.66	0.54	0.39	0.25	0.14
	Avg.	0.82	0.68	0.54	0.41	0.28	0.17
	S.D	0.03	0.02	0.01	0.03	0.04	0.03

Table A10 Photocatalytic activity of MWNTs/TiO_2 calcined at temperature of 600 ^oC

Sample	Repeat	UV Irradiation Time (h)					
		1	2	3	4	5	6
0.1MWNTs	1	0.84	0.76	0.71	0.59	0.49	0.38
/TiO_2	2	0.85	0.81	0.75	0.74	0.64	0.48
	3	0.85	0.72	0.62	0.44	0.33	0.28
	Avg.	0.85	0.76	0.70	0.59	0.49	0.38
	S.D	0.00	0.04	0.06	0.15	0.16	0.10
0.5MWNTs	1	0.83	0.75	0.67	0.55	0.44	0.32
/TiO_2	2	0.89	0.82	0.75	0.70	0.59	0.44
	3	0.77	0.67	0.56	0.40	0.29	0.22
	Avg.	0.83	0.75	0.66	0.55	0.44	0.33
	S.D	0.06	0.07	0.10	0.15	0.15	0.11
1MWNTs/	1	0.72	0.62	0.48	0.32	0.23	0.17
TiO_2	2	0.89	0.77	0.69	0.63	0.55	0.38
	3	0.80	0.69	0.61	0.49	0.39	0.31
	Avg.	0.80	0.69	0.59	0.48	0.39	0.29
	S.D	0.08	0.07	0.11	0.16	0.16	0.11

Table A11 Photocatalytic activity of 1Ag/1MWNTs/TiO_2 calcined at temperature of 400 ^oC

Sample	UV Irradiation Time (h)					
	1	2	3	4	5	6
Repeat 1	0.68	0.52	0.45	0.36	0.27	0.20
Repeat2	0.69	0.51	0.42	0.32	0.25	0.17
Repeat3	0.65	0.49	0.39	0.27	0.20	0.14
Avg.	0.67	0.51	0.42	0.32	0.24	0.17
S.D	0.02	0.02	0.03	0.05	0.04	0.03

Table A12 Photocatalytic activity of 1Ag/1MWNTs/TiO_2 calcined at temperature of 500 ^oC

Sample	UV Irradiation Time (h)					
	1	2	3	4	5	6
Repeat 1	0.62	0.47	0.35	0.25	0.16	0.09
Repeat2	0.59	0.45	0.35	0.24	0.15	0.08
Repeat3	0.69	0.48	0.36	0.26	0.16	0.09
Avg.	0.63	0.47	0.35	0.25	0.16	0.09
S.D	0.05	0.02	0.00	0.01	0.01	0.00

Table A13 Photocatalytic activity of 1Ag/1MWNTs/TiO_2 calcined at temperature of 600 ^{o}C

Sample	UV Irradiation Time (h)					
	1	2	3	4	5	6
Repeat 1	0.65	0.53	0.45	0.35	0.25	0.18
Repeat2	0.62	0.51	0.40	0.31	0.23	0.15
Repeat3	0.62	0.46	0.38	0.27	0.20	0.13
Avg.	0.62	0.49	0.39	0.29	0.21	0.14
S.D	0.02	0.04	0.03	0.04	0.03	0.03

Table A14 Photocatalytic activity of pure TiO_2 irradiation under fluorescent light calcined at temperature of 500 ^{o}C

Sample	Fluorescent Irradiation Time (h)					
	1	2	3	4	5	6
Repeat 1	0.86	0.79	0.74	0.71	0.69	0.65
Repeat2	0.85	0.80	0.74	0.69	0.67	0.64
Repeat3	0.81	0.76	0.71	0.68	0.63	0.59
Avg.	0.84	0.78	0.73	0.69	0.66	0.63
S.D	0.03	0.02	0.01	0.02	0.03	0.04

Table A15 Photocatalytic activity of 1Ag/TiO_2 irradiation under fluorescent light calcined at temperature of 500 ^{o}C

Sample	Fluorescent Irradiation Time (h)					
	1	2	3	4	5	6
Repeat 1	0.82	0.71	0.64	0.59	0.55	0.49
Repeat2	0.83	0.72	0.65	0.61	0.56	0.51
Repeat3	0.82	0.70	0.63	0.58	0.53	0.47
Avg.	0.82	0.71	0.64	0.59	0.55	0.49
S.D	0.01	0.01	0.01	0.02	0.02	0.02

Table A16 Photocatalytic activity of 1MWNTs/TiO_2 irradiation under fluorescent light calcined at temperature of 500 ^{o}C

Sample	Fluorescent Irradiation Time (h)					
	1	2	3	4	5	6
Repeat 1	0.77	0.71	0.68	0.66	0.64	0.60
Repeat2	0.81	0.78	0.72	0.68	0.64	0.58
Repeat3	0.79	0.76	0.72	0.68	0.64	0.58
Avg.	0.79	0.75	0.71	0.67	0.64	0.59
S.D	0.02	0.04	0.02	0.01	0.00	0.01

Table A17 Photocatalytic activity of 1Ag/1MWNTs/TiO_2 irradiation under fluorescent light calcined at temperature of 500 ^{o}C

Sample	Fluorescent Irradiation Time (h)					
	1	2	3	4	5	6
Repeat 1	0.86	0.71	0.69	0.61	0.57	0.51
Repeat2	0.85	0.72	0.66	0.61	0.57	0.51
Repeat3	0.87	0.75	0.70	0.65	0.60	0.53
Avg.	0.86	0.73	0.68	0.62	0.58	0.52
S.D	0.01	0.02	0.02	0.02	0.02	0.01